



POLITECNICO DI TORINO

FACULTY OF ENGINEERING

Master of Science in Biomedical Engineering

**Combined Use of Pattern Recognition and Proportional
Control Methods for sEMG Based Control of a Lower Limb
Exoskeleton**

Supervisors:

Prof. **Marco Gazzoni**

Prof. **Dario Farina**

Candidate:

Antonio De Benedictis



**Imperial College
London**

Academic Year 2017 – 2018

*Dedicated to my family,
the only support when everything is going wrong*

Contents

Abstract	10
1 Introduction	12
1.1 Electromiographic Signal (EMG)	14
1.1.1 EMG Signal Detection	17
1.2 sEMG Electrode configuration	18
1.3 Control strategies based on Myoelectric Control	20
1.3.1 Pattern recognition based control	21
1.3.2 Non pattern recogniton based control	23
1.4 Lower Limb Exoskeletons	24
2 Aim of the study	26
3 Experimental Protocol	27
3.1 Movement Description	27
3.2 Muscle Selection	28
3.3 Technical Specifications	30
3.3.1 EMG recording system	30
3.3.2 Electrogoniometers	31
3.4 Electrode placement	32
3.5 Electrogoniometer placement	33
3.6 Final Setup	35
3.7 Test Subjects	36
4 Algorithm Description	37
4.1 Data Preparation	37
4.1.1 Emg and angle signals digital filtering	37
4.1.2 Angle calibration	38
4.2 Trial Segmentation	39
4.2.1 Standing-Sitting trials segmentation	39
4.2.2 Gait trials segmentation	42

4.2.3	Stair Ascending and Stair descending trials segmentation	44
4.2.4	Rest trials segmentation	47
4.3	Feature Extraction and Selection	48
4.3.1	Feature scaling	52
4.4	Support Vector Machines (SVM)	53
4.4.1	Multiclass SVMs	55
4.4.2	SVM Parameter Tuning	56
4.5	K-Nearest Neighbor Classifier (KNN)	57
4.5.1	KNN Parameter Tuning	59
4.6	Multiple Linear Regressor (MLR)	60
4.7	Generalized Regression Neural Networks (GRNN)	62
4.8	Training and testing	64
4.8.1	Classifiers	64
4.8.2	Regressors	65
4.9	Validation phase	65
5	Results and Discussion	67
5.1	Performance Metrics Definitions	67
5.1.1	Classifier Performances Evaluation Metrics	67
5.1.2	Regressor Performances Evaluation Metrics	68
5.2	Classifiers Cross-Validation	70
5.2.1	Knn LOOCV results	70
5.2.2	SVM LOOCV results	73
5.3	Regressors Cross-Validation	76
5.3.1	GRNN LOOCV results for ankle joint	76
5.3.2	GRNN LOOCV results for knee joint	78
5.3.3	MLR LOOCV results for ankle joint	80
5.3.4	MLR LOOCV results for knee joint	82
5.4	Validation - First method	84
5.4.1	Classification	84
5.4.2	Ankle angle predictions	86

5.4.3	Knee angle predictions	90
5.5	Validation - Second method	94
5.5.1	Classification	94
5.5.2	Ankle angle predictions	96
5.5.3	Knee angle predictions	100
5.6	Processing Time Analysis	104
6	Conclusions and Future Work	105
6.1	Conclusion	105
6.2	Future work	107

List of Figures

1	Propagation of a nerve impulse from motor cortex to the muscle. Taken from [1]	14
2	Physiological structure of a motor unit. Taken from [2]	15
3	Representation of generation of a motor unit action potential. Taken from [3]	15
4	Physiological and mathematical model for the composition of a detected EMG signal. Taken from [4]	16
5	Schematic representation of monopolar acquisition. Taken from [3]	18
6	Schematic representation of bipolar acquisition. Taken from [3]	19
7	Different types of Myoelectric control systems. Taken from [5]	20
8	Pattern recognition flow. Taken from [6]	21
9	Lokomat [7], LOPES [8] and ALEX [9] exoskeletons	25
10	H2 [10] and HAL [11] exoskeletons	25
11	Channels and muscles	29
12	Left: DuePro system. Right: Technical specifications of the system.	30
13	Left: Disposable adhesive bipolar electrode. Right: Due probe connected with 2 bipolar electrodes, one for each channel.	31
14	Left: SG150 and SG110 electrogoniometers. Right: Sensors plugged into DueBio probe	31
15	Anterior and Posterior view of electrodes placement on a test subject.	33
16	Left: Knee Goniometer Placement. Right: Ankle Goniometer Placement	34
17	Anterior, Sagittal and Posterior views of the final setup.	35
18	EMG, Knee and Ankle angle signals of a subject during gait.	37
19	EMG and Knee angle signals of a subject during standing-sitting task.	39
20	Signals of knee angle and its derivative	40
21	Movement Activation interval signal	41
22	Example of segmented Standing-Sitting task for a subject. In red, EMG portions corresponding to a segmented trial	41
23	EMG and Knee angle signals of a subject during gait task	42
24	Knee angle signal with highlighted local maxima	43

25	Example of segmented gait task for a subject. In red, EMG portions corresponding to a segmented trial	44
26	EMG and Knee angle signals of a subject during stair ascending task.	45
27	Angle signal and filtered angle signal	45
28	Zoom on a single trial in the interval [M1;M2].	46
29	Example of segmented stair ascending task for a subject	47
30	Left: Adjacent windowing of an EMG signal; Right: Overlapped windowing. τ represents the computational delay [12].	48
31	Linear separating hyperplanes with maximum margin. The support vectors are circled (taken from [13])	53
32	Mapping data into feature space F with kernel function (taken from [14]). In the normal space data are nonlinearly separable, so SVM is not able to find the best separating hyperplane. With the mapping in the feature space, data becomes linearly separable and so SVM is effective.	54
33	Tuning of SVM parameters for a test subject	57
34	Example of KNN classification. The test sample (green circle) should be classified either to the first class of blue squares or to the second class of red triangles. If $k = 3$ (solid line circle) it is assigned to the second class because there are 2 triangles and only 1 square inside the inner circle. If $k = 5$ (dashed line circle) it is assigned to the first class (3 squares vs. 2 triangles inside the outer circle). Taken from [15]	58
35	Tuning of KNN parameters for a test subject	59
36	Left: Example of simple linear regression with one independent variable [16]; Right: In a three-dimensional setting, with two predictors and one response, the least squares regression line becomes a plane (taken from [17])	60
37	The basic GRNN architecture, taken from [18]	63
38	Example of multiclass confusion matrix. Taken from [19]	67
39	Boxplot containing Knn Cross-Validation Accuracy values evaluated for each class in test subjects	70
40	Boxplot containing Knn Cross-Validation Accuracy values evaluated for each class in test subjects	71

41	Confusion Matrices of Subject 1 (top left), 3 (top right), 5 (bottom left) and 7 (bottom right). The average Accuracy of the KNN classifier is indicated on the top of the matrix	72
42	Boxplot containing Knn Cross-Validation Accuracy values evaluated for each class in test subjects	73
43	Boxplot containing Knn Cross-Validation Accuracy values evaluated for each class in test subjects	74
44	Confusion Matrices of Subject 1 (top left), 3 (top right), 5 (bottom left) and 7 (bottom right). The average Accuracy of the SVM classifier is indicated on the top of the matrix	75
45	Boxplot containing GRNN Cross-Validation R^2 values evaluated for each class in test subjects for Ankle joint	76
46	Boxplot containing GRNN Cross-Validation NRMSE values evaluated for each class in test subjects for Ankle joint	77
47	Boxplot containing GRNN Cross-Validation R^2 values evaluated for each class in test subjects for Knee joint	78
48	Boxplot containing GRNN Cross-Validation NRMSE values evaluated for each class in test subjects for Knee joint	79
49	Boxplot containing MLR Cross-Validation R^2 values evaluated for each class in test subjects for Ankle joint	80
50	Boxplot containing MLR Cross-Validation $NRMSE$ values evaluated for each class in test subjects for Ankle joint	81
51	Boxplot containing MLR Cross-Validation R^2 values evaluated for each class in test subjects for Knee joint	82
52	Boxplot containing MLR Cross-Validation $NRMSE$ values evaluated for each class in test subjects for Knee joint	83
53	Bar diagram with KNN validation accuracy values for each class in 8 subjects	84
54	Bar diagram with KNN validation accuracy values for each class in 8 subjects	85
55	R^2 value trend for different models in 8 subjects, Ankle Joint	86
56	NRMSE value trend for different models in 8 subjects, Ankle Joint	87

57	Ankle angle reconstruction in subjects 7 with different models. From top to bottom: SVM-GRNN, KNN-GRNN, SVM-MLR, KNN-MLR, MLR and GRNN	88
58	R^2 value trend for different models in 8 subjects, Ankle Joint	90
59	NRMSE value trend for different models in 8 subjects, Ankle Joint	91
60	Knee angle reconstruction in subjects 7 with different models. From top to bottom: SVM-GRNN, KNN-GRNN, SVM-MLR, KNN-MLR, MLR and GRNN	92
61	Bar diagram with KNN validation accuracy values for each class in 8 subjects	94
62	Bar diagram with KNN validation accuracy values for each class in 8 subjects	95
63	R^2 value trend for different models in 8 subjects, Ankle Joint	96
64	NRMSE value trend for different models in 8 subjects, Ankle Joint	97
65	Ankle angle reconstruction in subjects 7 with different models. From top to bottom: SVM-GRNN, KNN-GRNN, SVM-MLR, KNN-MLR, MLR and GRNN	98
66	R^2 value trend for different models in 8 subjects, Ankle Joint	100
67	NRMSE value trend for different models in 8 subjects, Ankle Joint	101
68	Knee angle reconstruction in subjects 7 with different models. From top to bottom: SVM-GRNN, KNN-GRNN, SVM-MLR, KNN-MLR, MLR and GRNN	102

List of Tables

1	Channels, Muscles and abbreviations	29
2	Electrodes sites positioning from SENIAM guidelines [20]	32
3	First Method, Ankle joint: Tukey-Kramer multiple comparison test. p-values of the pairwise comparison between combined methods and general regressors	89
4	First Method, Ankle joint: R^2 Mean and Standard deviation values of the six methods predictions	89
5	First Method, Knee joint: Tukey-Kramer multiple comparison test. p-values of the pairwise comparison between combined methods and general regressors	93
6	First Method, Knee joint: R^2 Mean and Standard deviation values of the six methods predictions	93
7	Second Method, Ankle joint: Tukey-Kramer multiple comparison test. p- values of the pairwise comparison between combined methods and general regressors	99
8	Second Method, Ankle joint: R^2 Mean and Standard deviation values of the six methods predictions	99
9	Second Method, Knee joint: Tukey-Kramer multiple comparison test. p- values of the pairwise comparison between combined methods and general regressors	103
10	Second Method, Knee joint: R^2 Mean and Standard deviation values of the six methods predictions	103
11	Processing delays for angle prediction from an EMG epoch.	104

Abstract

It has been demonstrated that robotic assisted rehabilitation has many advantages over conventional strategies. Nevertheless lot of studies have been performed in this field, still a significant work is required to find an optimal strategy to control a robotic device. In this study, an sEMG based control strategy that exploits combined information from pattern recognition and proportional myoelectric control methods for a lower limb exoskeleton control has been developed and tested in order to improve the drawbacks deriving from the use of this two control methods separately. sEMG signals are recorded using adhesive disposable bipolar electrodes, while two electrogoniometers are used in order to record ankle signal from knee and ankle joint. Seven different movements of activities of daily living (ADL) are taken into account: *gait, sitting down, standing up, stair ascending, stair descending, rest (standing position) and rest (sitting position)*. Eight lower limbs muscles are selected: Tibialis Anterior, Gastrocnemius Lateralis and Medialis are mainly responsible to actuate the ankle joint movements, while Rectus Femoris, Vastus Lateralis and Medialis, Biceps Femoris and Semitendinosus are associated to knee joint activity. Eight able-bodied male subjects participated for the data collection procedure. Two classifiers and two regressor are studied in this work: Support Vector Machines (SVM) and K-Nearest Neighbour (KNN) classifiers, Multiple Linear Regressor (MLR) and Generalized Regression Neural Networks (GRNN). Four different combined model were tested: SVM-GRNN, KNN-GRNN, SVM-MLR and KNN-MLR. The performances in prediction of these models are then compared to two standard techniques of regression, i.e. only GRNN and MLR.

Two processes were conducted: a training and testing phase in order to find the best classifier and regressor models and a validation phase in order to analyze the performances of the different systems. The EMG signal is segmented using 250ms windows with 75% of overlap and a subset of six features (Root Mean Square, Zero Crossing, Integrated EMG, Willison Amplitude, Number of Turns, Waveform Length) is used to characterize each window. This way constructed feature vector is used as input for SVM, KNN and GRNN models, while

for the MLR only the Logarithm of Variance feature is used. In order to find the best classifier parameters for each subject a tuning process is executed on both SVM and KNN classifiers. For the training and testing phase, the subject is asked to perform different repetition of the 7 movements.

A Leave One Out Cross-Validation is performed on 10 trials of the different movements and the classifier model that has the highest average accuracy on a cycle of the Cross-Validation is selected for performing the validation phase. This process is repeated for both KNN and SVM classifiers. Similarly, for the two models of regressors a LOOCV on the same 10 trials is performed and the model that has the highest R^2 value for each class reconstruction in a cycle of the cross-validation is selected for performing the validation phase. This process is repeated for both ankle and knee joints. The standard regressor models are instead trained using all the 10 trials. Two different validation approaches are examined.

The first validation method consisted on comparing the performances of the combined and standard models using two previously segmented trials for each movement. For both ankle and knee joints the quality of angle prediction is improved ($p < 0.05$) using a the combined approach, in particular the best performances are registered with KNN-GRNN ($R^2 = 0.8459 \pm 0.1127$ and $NRMSE = 0.1231 \pm 0.0385$ for knee joint and $R^2 = 0.6066 \pm 0.1184$ and $NRMSE = 0.1178 \pm 0.0201$ for ankle joint).

In the second validation method, the subject was asked to perform a sequence of movements in order to simulate a daily scenario. In this phase there is evidence of a decreasing in the performances for both the classification and the prediction of the angles due to the different modality of movement execution. Also in this case the combined approach has better prediction performances ($p < 0.05$) with respect to the standard one, in particular KNN-GRNN model has demonstrated the highest quality of prediction ($R^2 = 0.5296 \pm 0.2133$ and $NRMSE = 0.2237 \pm 0.0514$ for knee joint and $R^2 = 0.2888 \pm 0.1060$ and $NRMSE = 0.1600 \pm 0.0188$ for ankle joint).

1 Introduction

Nowadays Stroke and Spinal cord Injuries is one of the main causes of serious long-term disability [21]. The majority of victims suffers from neurological and sensory-motor deficits, so that they need a period of rehabilitation in order to achieve functional independence. This type of neurological injury results in an important lower limb muscles weakness with a substantial impairment in motor control. This kind of patients often have significant limitations in performing a normal movement. Physical therapy and rehabilitation surely are a mean to improve the motor functions and to recover the ability to perform daily living activities. This rehabilitation strategy requires that a patient have to perform repetitive motion, specifically using the muscles affected by the neurological injury [9]. With this view, robotic assisted rehabilitation has many advantages over conventional strategies, in particular: reduced dependence on clinical staff, (ii) measured forces and torques with sensors can quantitatively assess the level of motor recovery, (iii) robotics can help in empowering the patient independence and self-consciousness.

Due to physical disability, assistance through an automated technical system may potentially enhance the physical activities of a patient during rehabilitation, as discovered by Moshier in the 1960s. He introduced the Human Machine Interface (HMI) as a control system and effectively demonstrated the system's use in the mechanism of lower-limb orthoses.

In addition, the usage of robotic interventions in training tasks is expected to improve the recovery at a faster rate, and to resume daily activities sooner; this is the reason why different kind of technologies have been designed. Many disabled people have difficulty to access current assistive robotic systems and rehabilitation devices, which have a traditional user interface (such as joysticks and keyboards), and for that reason more advanced hands-free human-machine interfaces are necessary. A lot of studies have been performed in order to find an intuitive control strategy that uses the EMG signal in order to control the robotic device using only the user intention in the form of a muscular contraction. It is clear that impaired people are able to generate repeatable activation patterns during different lower limb common activities. These patterns can be used in a control system, known as a myoelectric control system, to control rehabilitation devices or assistive robots.

The most important advantage of myoelectric control over other types of control system, such as body-powered mechanical systems, is its hands-free control. The signal is non-invasively detected from the surface of the skin, and can be adapted for proportional speed control. Myoelectric control is now a competent alternative for mechanical body-powered systems and has potential in different applications fields of research. Although several studies are conducted in order to find the best control strategy for controlling a lower limb rehabilitation exoskeleton, still a lot of work has to be performed. The aim of this study is indeed to develop a control strategy for myoelectric-driven lower limb exoskeletons that are applicable in a daily-living condition and can have the potential to increase the quality of life for the user.

1.1 Electromyographic Signal (EMG)

In this chapter the nature of the EMG signal origin and the main techniques of detection are briefly presented.

Electromyographic signals are electrical potentials that are generated in skeletal muscles during contraction. All body movements are driven by muscles that apply forces to the skeleton when contracting. The principal function of the skeletal muscles is to produce the movement of the different parts of the body such as locomotion, standing posture, and a lot of actions throughout the daily live. These movements generated first in the nervous system which consist of two parts: central nervous system (CNS) and peripheral nervous system (PNS) [22].

Motor intention takes origin in the premotor and motor cortex. Inside the motor cortex, the pyramidal tract spreads impulses (in the form of nerve action potentials) that control the execution of determined voluntary movements. These impulses move from motor cortex to the lower motoneurons, located into the ventral horn of the spinal cord (which is the lower part of the central nervous system). Spinal cord gives rise to the peripheral nerves that reach out into muscles, where a Neuromuscular Junction is formed [1]. Figure 1 shows how a nerve impulse is generated by the CNS and propagated to the muscle, in order to perform a voluntary movement.

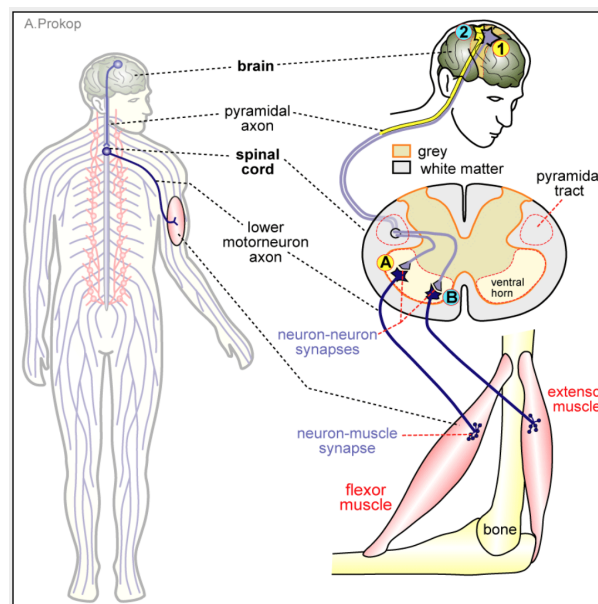


Figure 1: Propagation of a nerve impulse from motor cortex to the muscle. Taken from [1]

The fundamental functional unit of a muscle is the Motor Unit (MU), that is made up of a motor neuron and the skeletal muscle fibers innervated by that motor neuron's axonal terminals [23] (Figure 2).

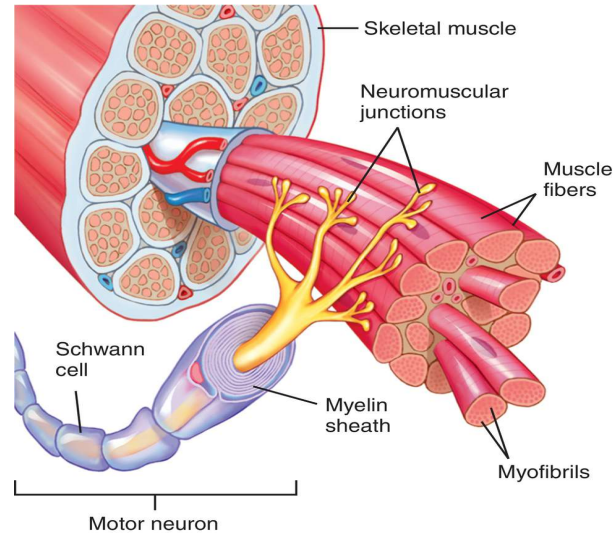


Figure 2: Physiological structure of a motor unit. Taken from [2]

Each muscle contains a certain number of motor units basing on its size: from 100 for small hand muscle to 1000 for the largest muscles in the lower limb [24]. The number of motor unit is proportional to the force needed. Fine force requires small numbers of motor unit while course motion needs large force as well as large number of motor units.

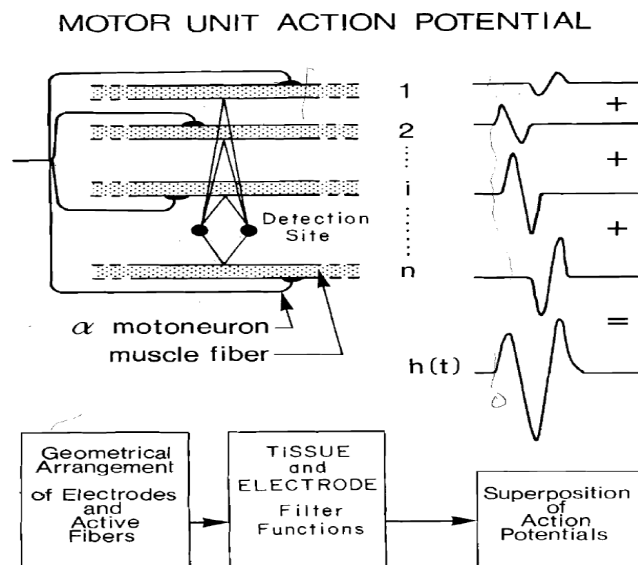


Figure 3: Representation of generation of a motor unit action potential. Taken from [3]

The depolarizations of the muscle fibers of one MU overlap in time and the resultant signal present at the detection site will constitute a both spatial and temporal superposition of the contributions of individual action potentials. The resultant signal (Figure 3) is known as Motor Unit Action Potential (**MUAP**). Motor units must fire repeatedly to maintain or increase the force generated by a muscle. In this way, during a sustained contraction each motor unit generates multiple MUAPs. The collection of MUAPs generated by one motor unit is called a motor unit action potential train (**MUAPT**) [4]. An electrode in a conducting medium measures the electric potential field. Due to the property of superposition of electric fields, the electrode will measure the total electric potential, which is the spatial and temporal sum of potential contributions from all excited muscle fibres of any motor unit. Therefore, the composite EMG signal is simply the summation of the MUAPTs of all recruited motor units (Figure 4):

$$EMG(t) = \sum_{i=1}^{N_m} MUAPT_j(t) + n(t)$$

where: $MUAPT_j(t)$ is the j^{th} MUAPT; N_m is the number of active motor units; $n(t)$ is the background noise.

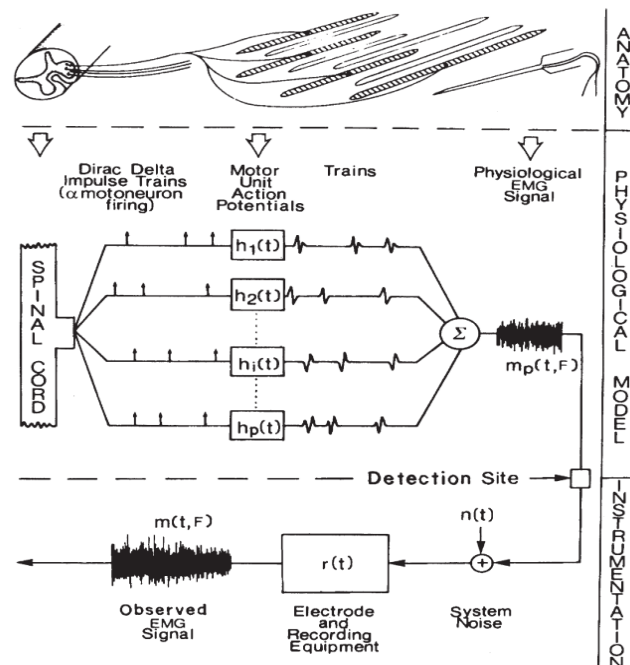


Figure 4: Physiological and mathematical model for the composition of a detected EMG signal. Taken from [4]

1.1.1 EMG Signal Detection

Basically, two techniques are used to detect the motor unit action potential (MUAP) generated by muscle contraction; intramuscular EMG (iEMG) and surface EMG electrodes (sEMG). The signals detected by those two techniques are not similar due to the difference in the recording sites and the amount of the biological tissues that separate the muscle and the recording sites. These amounts of biological tissues are known as volume conductor. The volume conductor characteristics mainly determine the properties of the recorded signal, regarding to the frequency content and to the distance that limits the signal detection.

- **Intramuscular EMG (iEMG).** In the iEMG detecting approach, the needle electrodes are inserted directly into the muscle. In this technique, the measured signal is detected near to the source and contains the local action potential of a few muscle fibers that belongs to tens of MUs. The volume detected by the (iEMG) is very specific and this makes this technique robust to crosstalk. With this invasive method it is easier to identify the contributions of the single MUAP, as the filtering effect (Low-Pass) of the skin, subcutaneous layer and fat layer is reduced. In this way the morphology of the signal is preserved. The potential of using iEMG recording technique to record the electrical activity of muscles is to examine the physiology and pathology of the motor unit. The current clinical use of intramuscular EMG signals relates to the diagnosis of myopathies, of diseases of the alpha-motor neuron and of the neuromuscular junction. [25]. However, this methodology can only be performed by a doctor and therefore not practicable in the rehabilitation field (that requires dynamic condition of movement).
- **Surface EMG (sEMG).** The sEMG signal consists of the muscle activity of several numbers of MUAP, and contains global information about muscle. Facile applicazione e riposizionamento. The use of surface electromyography (SEMG) is having a notable diffusion both for the characteristics of non-invasivity and for the potential offered by modern techniques of numerical analysis of the electromyographic signal which can provide useful quantitative information on conditions of activity of the examined muscular district. Recently, sEMG has been used for different types of ap-

plications: evaluation of muscular strength, isometric tests, muscular fatigue studies, performance analysis in sports medicine, biofeedback of muscle contraction, and, obviously, for robotic myoelectric control.

1.2 sEMG Electrode configuration

There are basically two type of recording configuration: *Monopolar* and *Bipolar* detection configurations. In *Monopolar* configuration, the electrical activity using surface electrodes can be acquired by placing an electrode on the muscle that we want to analyze and a "reference" electrode located in an point which is either electrically quiet (like a bone prominence) or contains electrical signals that are not correlated (in the sense that there is a weak physiological or anatomical relation) with the signals that are being detected [3]. A schematic representation of this recordind technique can be seen in Figure 5.

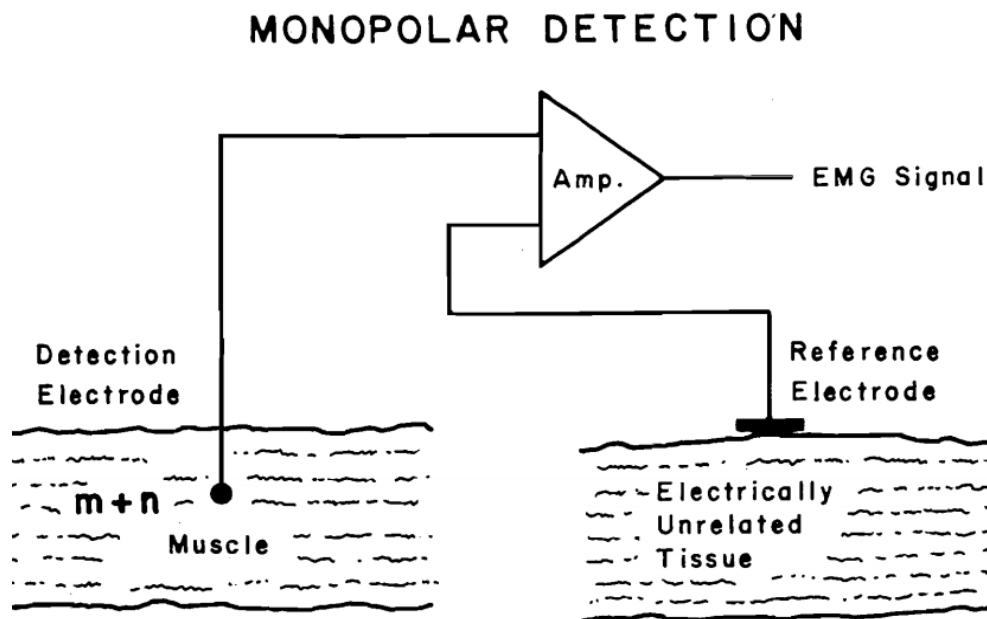


Figure 5: Schematic representation of monopolar acquisition. Taken from [3]

The monopolar configuration allows to record a wide volume conductor, it preserves all the informations contained in the EMG signal but it has the drawback of high sensibility to interferences and noise.

In *Bipolar* detection configuration (Figure 6) two detection electrodes are used in order to detect the difference of two potentials in the muscle tissue of interest, with respect to

the reference electrode. The differential amplifier then amplifies the recorded signal.

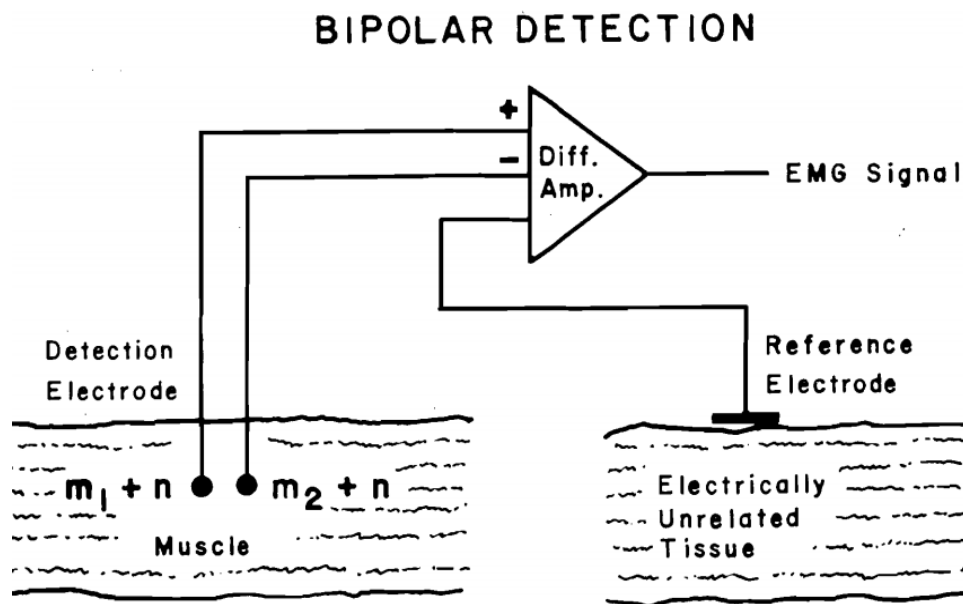


Figure 6: Schematic representation of bipolar acquisition. Taken from [3]

Bipolar configuration offers better immunity to interference because it filters out Common Mode components that has external origin. For the same reasons it is also robust to crosstalk because it is a more selective technique. These are the main reasons that lead to the use of this specific configuration strategy in order to analyze EMG signal in this work.

1.3 Control strategies based on Myoelectric Control

Electromyographic (EMG) signal contains different informations about the force of a muscle contraction or even the type of a movement made by a subject. These important features of the signal could be used to build an EMG based control system that employs the EMG signal recorded from different muscles to control exoskeleton, active orthoses and prostheses. This approach is known as myoelectric control. It is developed basing on the signals recorded from the human body in order to catch the human movement intention directly.

Not able-bodied subjects, like amputees or post-stroke patients, are able to generate repeatable myoelectric signal patterns during different muscle contractions or dynamic limb motion [26]. These patterns can be used with the aim of controlling rehabilitation devices or assistive robots. The most important advantage of myoelectric control with respect to other types of control system, such as body-powered mechanical systems, is its hands-free control [27] and it is only actuated according to user's intention.

Myoelectric control systems can be divided into two macro groups: pattern recognition (PR) and non-pattern recognition based approaches (Figure 7).

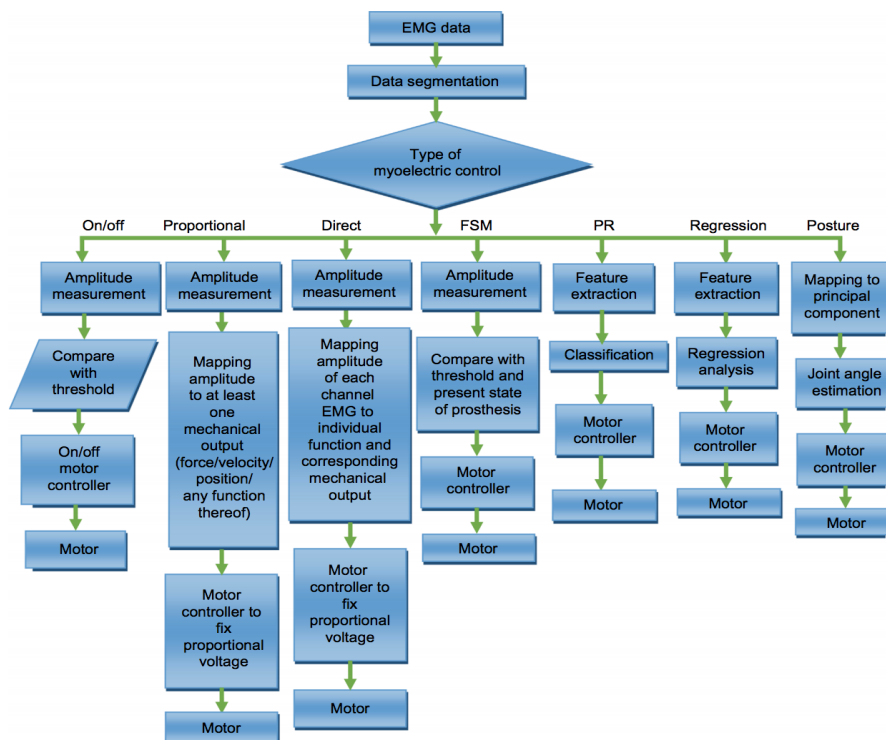


Figure 7: Different types of Myoelectric control systems. Taken from [5]

For what concerns the first group, the desired classes of movements are discriminated by classifiers that are able to identify a task basing on EMG set of features, and the performances of the system depend directly on classification accuracy. In contrast, non-pattern recognition based controllers, which are mainly constructed on threshold control or proportional control, uses EMG informations (principally its amplitude) in order to create a relation between muscular activity and electrical or mechanical information to actuate a motor (like torque, position or angles). In the next subsection, an overview of these systems is presented.

1.3.1 Pattern recognition based control

Pattern recognition-based EMG control techniques aim to discriminate different classes of motions by using time or frequency relevant informations contained in the EMG signal. These techniques are base on the hypotesis that the set of features representing a particular muscular activation's pattern is repeatable under specific electrode place [28]. Using a pattern classification technique, different patterns can be obtained from EMG signals and used to identify the intended movements. Therefore, once a pattern has been detected, the robotic system is activated and the desired movement is performed. In general, an EMG pattern recognition-based prosthetic control approach consists of EMG measurements, feature extraction (eventually feature reduction) and classification (Figure 8).

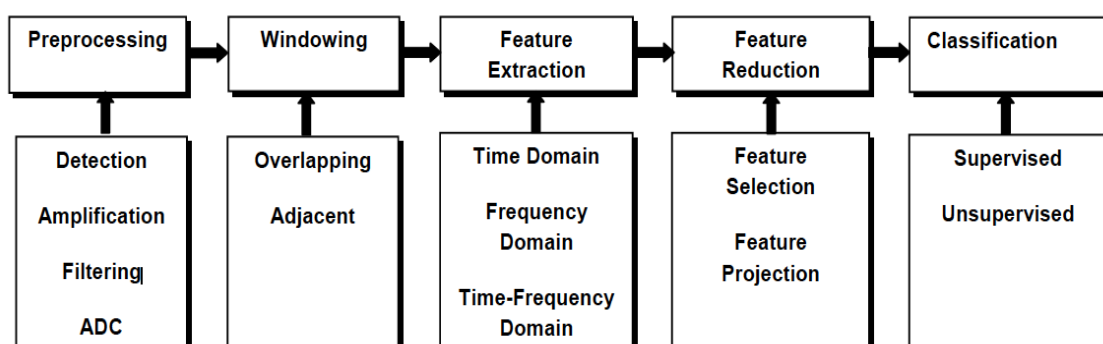


Figure 8: Pattern recognition flow. Taken from [6]

At first, EMG measurements are performed in order to capture more and reliable myoelectric signals, and to create a robust dataset in order to train and validate the classifier. Then the EMG signal is segmented in windows with length in the range 50-250 ms [12] and

for each window a set of features is extracted. The explored features include: *time-domain (TD)*, *frequency-domain (FD)* and *time-frequency domain (TFD)* features.

The most common *time-domain* features, such as the mean absolute value (MAV), variance (VAR), root mean square (RMS), number of zero crossings (ZC), number of slope sign changes (SSC) and wavelength (WL), are used in order to investigate the information content in the transient burst of myoelectric activity. One of TD features major advantage is that they are easy and fast to be calculated because there is no presence of mathematical transformations. However, because TD features are based on signal amplitude, they are relatively sensitive to noise and artifacts.

Frequency domain (FD) features are used in order to extract information about muscle fatigue, force production, changes in motor-unit recruitment and firing patterns [27]. FD features are more difficult and time-consuming to be calculated because they require first the evaluation of the power spectral density (PSD) of the signal. Among the most common FD features it is possible to include Mean Frequency (MNF) and Median Frequency (MDF).

Time-frequency domain (TFD) features used in sEMG classification include features that are calculated from time-frequency analysis of the EMG signal in order to find information of how the frequency content of the signal changes in the time. Among the most used TFD features it is possible to find short time Fourier transform (STFT), continuous Wavelet transform (CWT) and other wavelet transformations.

If the extracted feature vector results too high dimensional, it could be necessary to perform feature reduction algorithms (dimensionality reduction with PCA or LDA) in order to select only the most significant features and to reduce the effect of overfitting, when limited amount of training data is available.

In the final classification stage, the mapping between feature vectors into specific classes of movements is performed. Different type of classifiers are used in the state of the art applications, from linear models like Linear Discriminant Analysis (LDA), Support Vector Machines (SVM), to more complex systems like Artificial Neural Networks (ANN), Multi Layer Perceptron (MLP), Fuzzy Logic (FL) and Neuro-Fuzzy models [29].

One of the most important drawbacks of this control scheme is that the classifier provides only the estimation of the executed movement but not directly the level of contraction that is needed to control velocity or force of a robotic device, since the classification output

is a discrete value. Furthermore, it does not allow for a simultaneous control of several DOFs and smooth transitions from one movement to another, that are required for a natural scenario, are not possible with PR approach.

1.3.2 Non pattern recognition based control

Contrary to pattern recognition, this type of strategy estimates, instead, continuous multivariate outputs comprising all DOFs simultaneously. This allows for an independent simultaneous and proportional estimation since the output of this strategy is a continuous variable. Among with different non pattern recognition based control methods it is possible to mention the followings:

- **On-off myoelectric control:** The conventional on-off control is suitable for maximum 2 DOFs. The simplest strategy consists of a threshold on EMG signal amplitude in order to make a selection of the DOF to be actuated (for example flexion if flexors muscles activity is above the threshold and extension if extensors muscle activity is above the threshold). With this scheme the velocity of the movement is kept constant.
- **Proportional myoelectric control:** in this control scheme, the control signal (voltage or current) applied to the motor of the robotic device, is proportional to the amplitude of EMG signals. In this way also the velocity of the movement can be controlled proportionally to the level of contraction or activity of the muscle.
- **Regression myoelectric control:** this strategy is one of the most recent developed control strategies in order to provide both simultaneous an proportional control. In this control scheme, the prediction is made not basing only the EMG amplitude, but on different features of the signal. The aim of the regression is to approximate the function that relate the chosen features to the biomechanical information (like joint angle). There are different types of regression methods, from linear models (where the approximation function is linear) to non-linear methods.

1.4 Lower Limb Exoskeletons

Exoskeletons are defined as wearable systems created to help the wearers to perform a task. Among the different exoskeletons applications we can find: picking and placing heavy objects, carrying heavy loads, reducing the effort in physically demanding tasks and apply rehabilitation treatments to patients who suffers of trauma like strokes. Lower limbs Exoskeletons can also be implied in assisting the patient for carrying out normal activities of daily living such as, in particular, walking, ascending/descending stairs, perform sit-to-stand transitions and generally moving in daily life when the physical ability is decreased [30]. In this paragraph only exoskeletons with rehabilitation purposed are discussed.

Rehabilitation is needed for persons with movement disorders, which can derive from a different medical conditions such as cerebrovascular accidents, cerebral palsy and stroke. These condition force the patient to depend on wheelchairs for mobility reducing their independence during daily living activities. A lower limb rehabilitation exoskeleton could be a possible solution t.o perform therapy in order to recover the limbs activity. It has been studied that task-oriented repetitive movements can improve muscular strength and coordination in patients with physical impairments [10]. For that reason, different treadmill-based exoskeletons have been designed in order to train the patient to relearn the motion function by applying forces to the joint when the user does not follow the ideal trajectory of the movement.

Among this type of exoskeletons it is possible to mention Lokomat [7], LOPES [8] and ALEX [9] exoskeletons (Figure 9). Other types of lower limb exoskeletons can be found in [30].

Nevertheless, this type of exosketons requires the constant supervision of the clinical staff and does not empower the user independence or to help him to perform activities of daily living. Furthermore, it is known that patient's involvement in voluntary task is important to improve results in rehabilitation process.



Figure 9: Lokomat [7], LOPES [8] and ALEX [9] exoskeletons

For this reason, ambulatory exoskeletons with control strategies based on Emg signals such as H2 [10] or HAL (Hybrid Assistive Limb) [11] (Figure 10) can be more effective to reinstate neuroplasticity and improve motor functions.



Figure 10: H2 [10] and HAL [11] exoskeletons

These exoskeletons are designed to be driven with myoelectric control: different studies are carried out in order to find the best control strategies to improve the quality of the rehabilitation with myoelectric control, but there is still the need to do some work in this field.

2 Aim of the study

In nowadays literature, both pattern recognition and non pattern recognition methods presents some drawbacks: with using only PR there is not the possibility to finely and simultaneously control multiple DOFs, while with the other class of methods there is no information about a specific movement and the control is based only on the EMG informations that make the robotic movement less intuitive to be performed. To overcome this problem, a new method is proposed in order to incorporate both simultaneous control of multiple degrees of freedom (DoFs) and pattern recognition methods. Ankle flexion/extension and knee flexion/extension) are considered in this study in order to extract a control for a lower limb exoskeleton that has the possibility to actuate this 2 DOFs. In particular two classifier are first trained and tested: Support Vector Machine (SVM) and K Nearest Neighbour (KNN) classifiers. Then the classifier is associated to a regressor in order to create a continuous and simultaneous control command to both ankle and knee joint. In this case, Multiple Linear Regressor (MLR) and Generalized Regression Neural Network (GRNN) are used. This choice is motivated by the fact that there was the intention to study the performances of angle prediction with both a linear and non linear model. Both this two regressor are trained for each DoF and each class of movement in order to associate EMG features to their corresponding angle outputs. Basing on the output of the classifier, only the class-specialized model or regressor is selected in order to make the angle prediction. The aim of the study is to demonstrate that with this approach, the performances of angle estimation are improved with respect to the standard regression technique.

3 Experimental Protocol

In this section the experimental protocol established for the recording of electromyographic signals and used for acquiring suitable data sets for training, validation and testing of pattern recognition and regression methods is described in details. In particular in the following sections it has been analyzed what concerns the technical specifications of the equipment used for recording EMG and angle signals from the selected muscles, the electrodes and goniometers placement procedure, the movements involved in the study and the subjects choice

3.1 Movement Description

The purpose of this work is to study movements that each individual normally perform during common activities. This type of actions are the so called activities of daily living (ADLs) and these are the most important movements to be restored with a view to a neurorehabilitation expected scenario for a post-stroke patient.

For that reason and for what concerns lower limbs rehabilitation, 5 movements are selected in this study: *Gait*, *Sitting down*, *Standing up*, *Stair ascending*, *Stair descending*. Moreover, in order to achieve a complete perspective on the final control of the exoskeleton, also two rest conditions are included in the study, in particular *Rest in standing position* and *Rest in sitting position*. For the Stair ascending and descending movements, a custom-made step of 18cm of height is used in order to simulate a conventional step of a staircase. The planned experimental protocol foresees that this movement have to be performed as it is described below:

- **Gait** : the subject, in rest position, must start with his feet together, then he starts the gait cycle with the swing of the dominant leg and performs a natural walk along the laboratory space. The movements ends with the subject putting his feet together again.
- **Stair ascending** : the subject must start to climb the step with his dominant leg. Then, when the subject has completed the task, after 1.5 s of rest, he has to return back to his initial position moving first the contralateral leg.

- **Stair descending** : similarly to the stair ascending movement, the subject must start to descend the step with his dominant leg. Then, when the subject has completed the task, he has to return back to his initial position starting the movement with the contralateral leg.
- **Sitting down** and **Standing up** : starting in standing position, the subject must sit on a normal chair, rest for about 1.5 seconds and then stands up to the initial position and resting again.
- **Rest in sitting/standing position** : the subject is asked to rest in the required position for 30s.

All this movement are meant to be repeated cyclically in order to achieve enough data for training, testing and validating the system. Each repetition of a movement is from now on called a *trial*.

3.2 Muscle Selection

To evaluate the selected Activities of Daily living (ADLs), 8 lower limb muscles are selected: Vastus Medialis (VM), Vastus Lateralis (VL), Rectus Femoris (RF), Biceps Femoris (BF), Semitendinosus (ST), Tibialis Anterior (TA), Gastrocnemius medialis (GM) and Gastrocnemius Lateralis (GL). In fact all this muscles play an important role in the considered ADLs: Knee flexion/extension and ankle flexion/extension. In particular, Biceps Femoris and Semitendinosus play a crucial role in stretching the hips, flexing the legs and rotating the knee joints externally, especially when a person is standing up from a chair. Gastrocnemius Medialis and Lateralis are mainly concerned with standing and walking activities [31]. Rectus femoris, Vastus Medialis and Lateralis are powerful knee extensors, which has a role in flexing the hips, and the Tibialis Anterior muscle activity is mainly regarding to the flexion of the ankle and enabling the foot eversion [32].

A bipolar electrode is associated to each muscle. The configuration of the acquisition setup is shown in Figure 11 and summarized in Table 1. For the electrodes placement procedure, see section 3.4

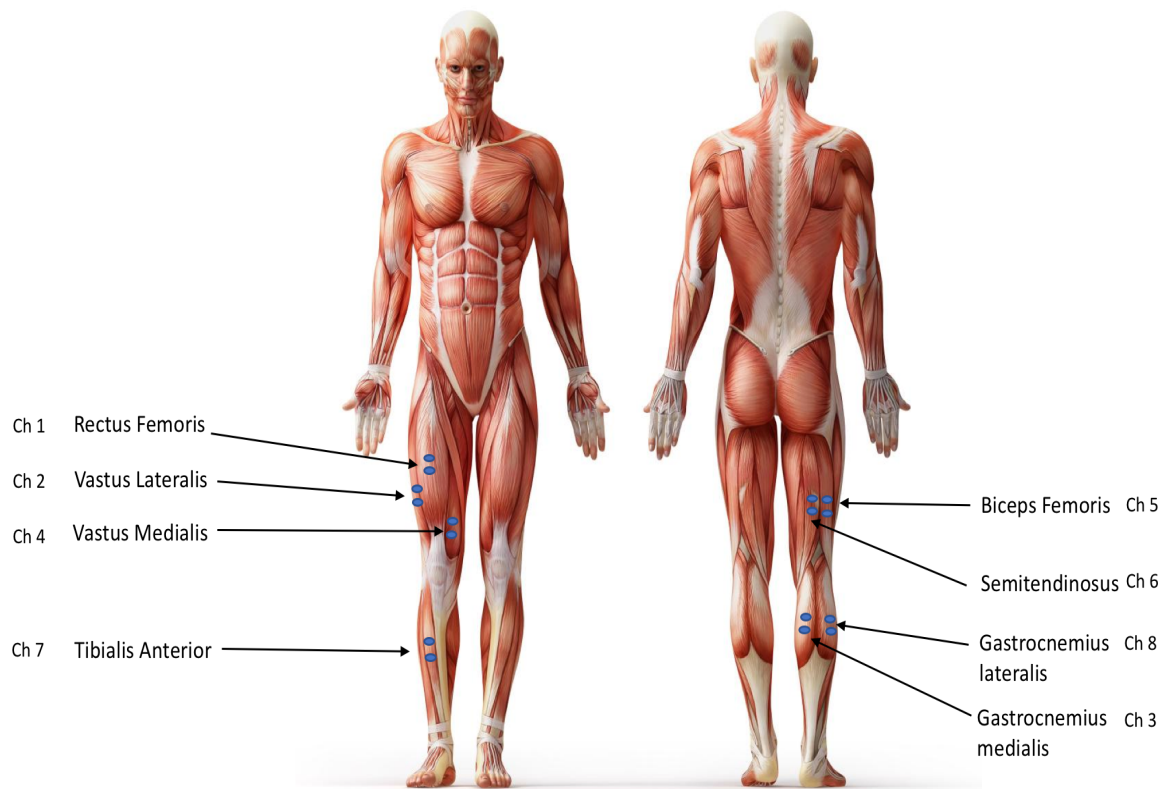


Figure 11: Channels and muscles

CHANNEL	MUSCLE	ABRREVIATION
1	Rectus Femoris	RF
2	Vastus Lateralis	VL
3	Gastrocnemius Medialis	GM
4	Vastus Medialis	VM
5	Biceps Femoris	BF
6	Semitendinosus	ST
7	Tibialis Anterior	TA
8	Gastrocnemius Medialis	GM

Table 1: Channels, Muscles and abbreviations

3.3 Technical Specifications

3.3.1 EMG recording system

EMG was sampled using the OT Bioelettronica DuePro device (Figure 12), a wearable EMG device designed for having the possibility to record up to 14 EMG signals and 2 auxiliary signals (e.g. force, angle) with a total of 8 wireless probes. In this particular case of study, only 4 EMG probes are used to record the signals from 8 muscles and 1 DueBio probe, configured in Load Cell mode, is used to acquire signals from the electrogoniometers.



Class	II BF
Number of probes	7
Number of EMG channels for each probe	2
Number of auxiliary signals	2
Gain	200 V/V – 100V/V for DueBio
Bandwidth	10Hz - 500 Hz
CMRR	> 100 dB
Sampling frequency	2048 Hz
Communication	Bluetooth 4.0
Receiver	PC, Smartphone, Tablet (Android)
Resolution	16 bits
Dimension	47 x 11 mm
Life time	11 h
Power supply	Li-Po battery
Charging mode	wireless

Figure 12: Left: DuePro system. Right: Technical specifications of the system.

EMG signals normally have a bandwidth of 500Hz. DuePro does the EMG sampling at 2048 Hz, which is a common sampling frequency for surface EMG signals according to the Nyquist criterion. In this project the EMG data acquisition system is designed to be used with sEMG technique using bipolar electrodes in order to suppress the common signal in the detection sites. The electrodes used to acquire signals, compatible with DuePro probes and distributed by the same producer of the device, are disposable adhesive surface electrodes (24mm of diameter) with a bipolar connector (Figure 13).



Figure 13: Left: Disposable adhesive bipolar electrode. Right: Due probe connected with 2 bipolar electrodes, one for each channel.

3.3.2 Electrogoniometers

Biometrics LTD's "SG" series twin axes Goniometers permit the simultaneous measurement of angle in two planes, but in this work only the rotation in flexion/extension degree of freedom is considered. In particular models SG110 (ankle flexion/extension) and SG150 (knee flexion/extension) are used in combination with the DueBio probe that records the output of the goniometers. (Figure 14)

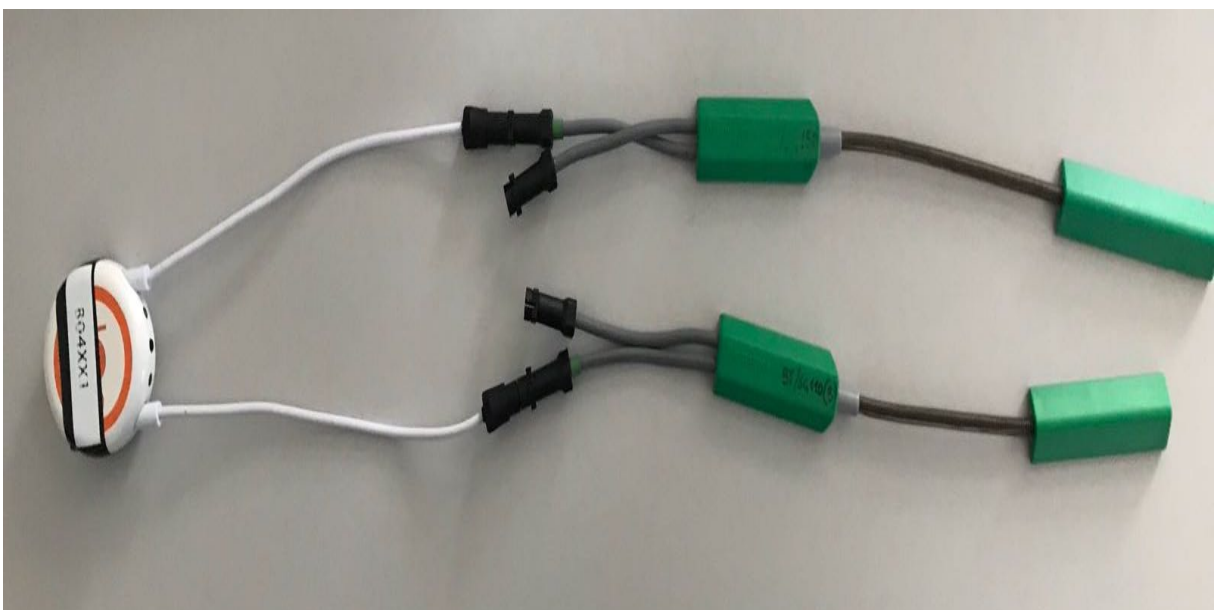


Figure 14: Left: SG150 and SG110 electrogoniometers. Right: Sensors plugged into DueBio probe

The working mechanism of this two sensors is the same. Between the two endblocks inside the protective spring, there is a composite wire that has a series of strain gauges mounted around the circumference. As the angle between the two endblocks changes, the change in the strain along the length of the wire is measured using a Wheatston bridge circuit.

3.4 Electrode placement

Surface Electromyography for the Non-Invasive Assessment of Muscle project (SE-NIAM) has defined some recommendations for sensor locations [20] that are used in this work in order to obtain measure repeatability. In particular, for the muscles involved in this case of study, the correct position for bipolar electrodes is summarized in Table 2. For each subject only the dominant leg is sensorized, and therefore only the muscles of this leg are studied in this work. The selected Inter Electrode Distance in this work is 25mm. In order to optimize skin-electrode impedance, the skin area where the electrodes must be positioned is shaved and then cleaned using an abrasive paste. An important concern is that for each subject the electrodes should be placed correctly and at the same place every time, so that the classification procedure and the signal processing is done under the hypothesis of repeatability.

Muscle	Electrode Position
Rectus Femoris	The electrodes need to be placed at 50% on the line from the anterior spina iliaca superior to the superior part of the patella
Vastus Medialis	Electrodes need to be placed at 80% on the line between the anterior spina iliaca superior and the joint space in front of the anterior border of the medial ligam
Vastus Lateralis	Electrodes need to be placed at 2/3 on the line from the anterior spina iliaca superior to the lateral side of the patella
Biceps Femoris	The electrodes need to be placed at 50% on the line between the ischial tuberosity and the lateral epicondyle of the tibia.
Semitendinosus	The electrodes need to be placed at 1/3 on the line between the tip of the fibula and the tip of the medial malleolus.
Tibialis Anterior	The electrodes need to be placed at 1/3 on the line between the tip of the fibula and the tip of the medial malleolus.
Gastrocnemius Medialis	Electrodes need to be placed on the most prominent bulge of the muscle.
Gastrocnemius Lateralis	Electrodes need to be placed at 1/3 of the line between the head of the fibula and the heel.

Table 2: Electrodes sites positioning from SENIAM guidelines [20]

After positioning the electrodes as shown in Figure 15, for the final configuration a further reinforcement is applied by using an adhesive tap on the connectors in order to

avoid electrodes displacement and movement artifacts.

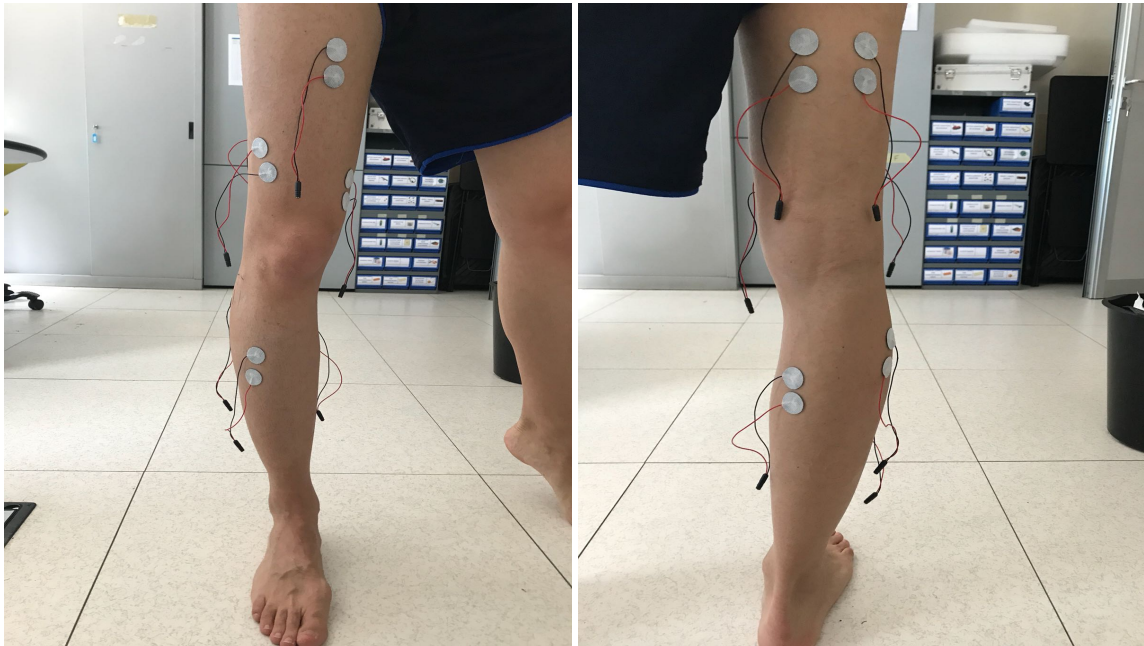


Figure 15: Anterior and Posterior view of electrodes placement on a test subject.

3.5 Electrogoniometer placement

For the electrogoniometer placement, the recommendations in Biometrics Goniometers Operating manual are followed. In order to properly attach the endblocks of the sensors to the leg or foot segment, a medical bi-adhesive foam is used.

- Ankle (sensor SG110): starting with the subject in standing neutral position with the foot on a flat surface, the proximal block of the sensor is aligned with the leg axis while the distal enblock is fixed on the lateral side of the foot after alignment with the foot axis. The spring have to pass near a landmark that can be assumed as the center of the rotation, i.e. the malleolus(Figure 16 on the right)
- Knee (sensor SG150): starting with the subject in standing neutral position with the foot on a flat surface and with the leg fully extended, the proximal block of the sensor is aligned with the leg axis and laterally attached, while the distal enblock is fixed laterally on the thigh after alignment with the thigh axis. The sensor must be in position of maximum extension of the spring (Figure 16 on the left)

In order to avoid sensor detachment during the movements, an additional adhesive tape is applied on the top of the sensors enblocks.



Figure 16: Left: Knee Goniometer Placement. Right: Ankle Goniometer Placement

3.6 Final Setup

After having applied the goniometers and the electrodes, also the Due and DueBio probed has been connected and fixed on the subject with adhesive tape. In this way we have a final setup configuration that allows the subject to perform all the movements in the most natural and repeatable way. Some examples of the final setup on a subject are presented in the Figure 17



Figure 17: Anterior, Sagittal and Posterior views of the final setup.

3.7 Test Subjects

The entire experimental protocol was carried out on a total of 8 able-bodied male volunteers. To have a more generally valid result, the chosen subjects have different age and antropometric characteristics. For the same purpose, it is also worth noting that 2 subjects on the total of 8 are left footed, and coherently on what had been said in the previous sections, always the dominant leg is selected. The age of the subject is in the range 22-27 years and the weights in the range 65-86 Kg.

4 Algorithm Description

In this chapter all the main points that are involved in the proposed strategy flow (see Section 2) are presented, starting from the recording and filtering of the EMG and angle signals, the segmentation of the different tasks through the biomechanical information given by the goniometers, the detailed explanation of pattern recognition and regression tools used in this work and the proposed validation strategy.

4.1 Data Preparation

4.1.1 Emg and angle signals digital filtering

The purpose of this filtering procedure is to make a smooth representation of the signals amplitude and to remove eventual movement artifacts or high frequency noise.

The EMG signal is filtered with a Butterworth band-pass filter of order 4 with the technique of zero-phase digital filtering in order to avoid EMG morphology distortion. The chosen band has cut-off frequencies $f_{HP} = 20 \text{ Hz}$ and $f_{LP} = 500 \text{ Hz}$.

The Angle signal is filtered with a Butterworth low-pass filter of order 4 with the technique of zero-phase digital filtering with a cut-off frequency of $f_{LP} = 10 \text{ Hz}$.

An example of EMG and signals during a gait is presented in Figure 18

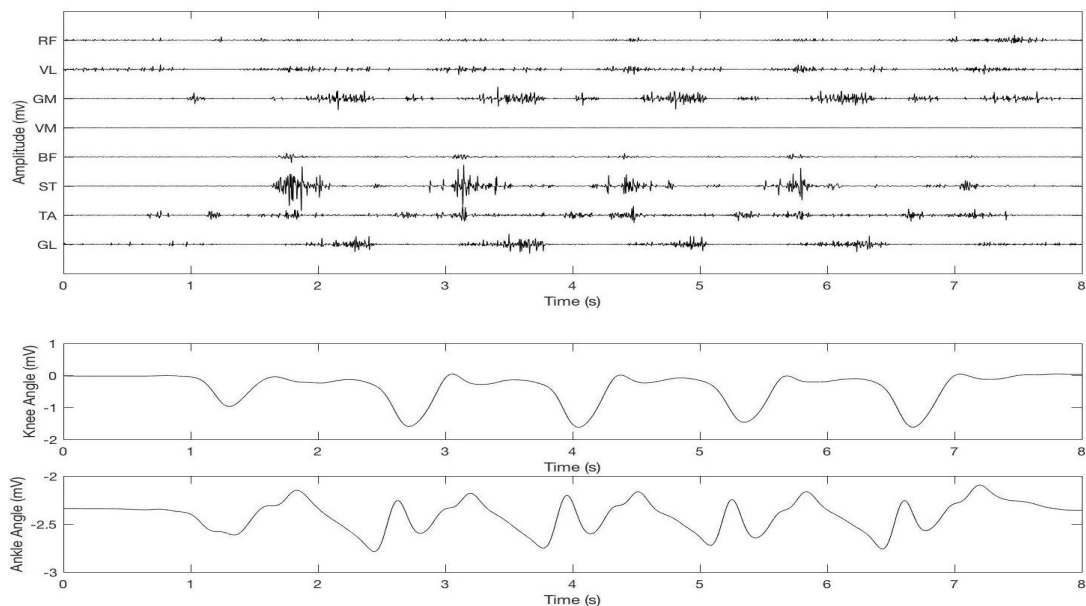


Figure 18: EMG, Knee and Ankle angle signals of a subject during gait.

4.1.2 Angle calibration

Since the output signal from the electrogoniometer is still a voltage signal, there is the need to find the relation between voltage and angle. This relation, that is the calibration curve of the sensor, can be found by two calibration movements:

- Knee angle calibration : the subject is asked to stay in standing position with the leg in total extension (180°). Then he is asked to sit down on a chair in order to have 90° of knee flexion. The relation between voltage and angle is linear, due to the design characteristics of the electrogoniometer. In this way we can find the calibration curve as the line that passes between the two points $[mV_{90}, 90]$ and $[mV_{180}, 180]$, where mV_{90} and mV_{180} are the value in mV (averaged on a time interval chosen by the operator) corresponding to an angle of respectively 90° and 180° .
- Ankle angle calibration : the subject is asked to stay in sitting position with the foot in total plantar flexion (30°). He is asked to reach the neutral position and then to maximally extend the foot to -50° in our reference system. The calibration can be calculated curve as the line that passes between the two points $[mV_{30}, 30]$ and $[mV_{(-50)}, -50]$, where mV_{30} and $mV_{(-50)}$ are the value in mV (averaged on a time interval chosen by the operator) corresponding to an angle of respectively 30° and -50° .

This calibration procedure is repeated for each subject.

4.2 Trial Segmentation

Recorded EMG signals were processed to isolate the epochs corresponding to the task execution (trials) in order to create a proper dataset for the classifiers and regressors training and testing.

The task epoch identification was performed using the knee angle signal in order to find the starting and ending point of a trial. In the following sections, it is described the implemented algorithm for the different movements.

4.2.1 Standing-Sitting trials segmentation

The task requires that the subject alternately perform a sitting movement and a standing movement interspersed with phases of rest (Figure 19), so we have to discriminate between the two movements and to cut off the rest phases.

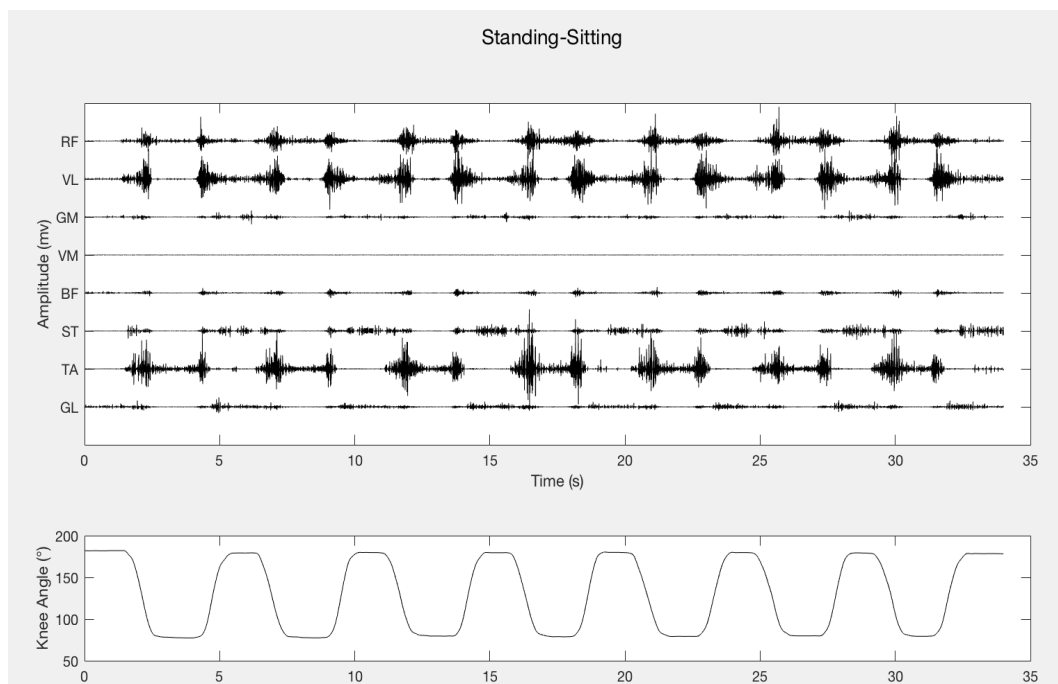


Figure 19: EMG and Knee angle signals of a subject during standing-sitting task.

The algorithm follows this steps:

- First, the derivative of the angle signal with a step of 256 samples is calculated (as the difference between the signal and itself delayed by 256 samples), in order to find the variation of the slopes during time. The derivative signal ($angle_{der}$) has

positive values when a standing movement is performed, and negative when a sitting movement occurs (Figure 20).

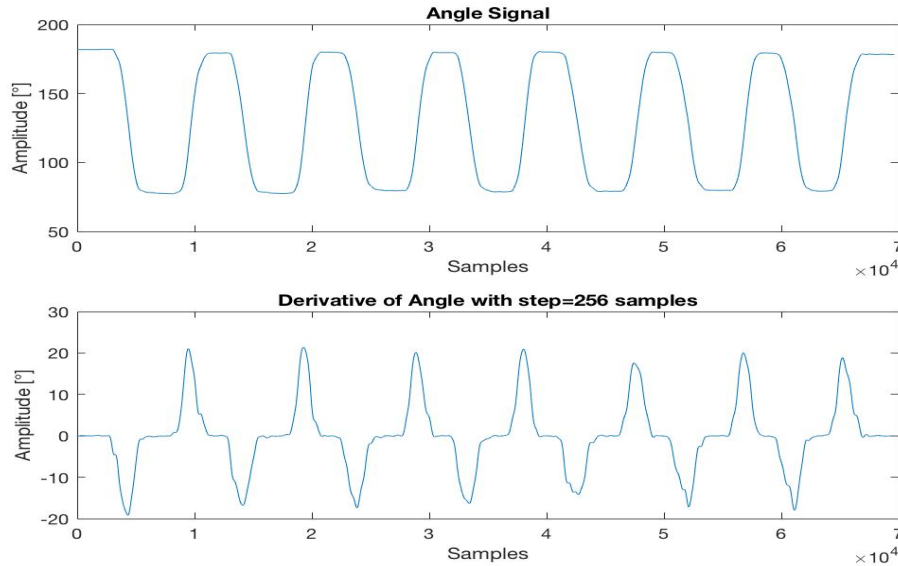


Figure 20: Signals of knee angle and its derivative

- Then a threshold value is set to $thr = 0.05 \max(|angle_{der}|)$, in order to transform the derivative signal into a rectangular signal ($angle_{rect}$) through thresholding. In particular, the thresholding was done putting :

$$angle_{rect} = \begin{cases} +1, & \text{if } angle_{der} \geq thr \\ -2, & \text{if } angle_{der} \leq -thr \end{cases}$$

- In this way we have a signal that describes the onset and offset of the two interested movements, in fact when $angle_{rect} = 1$ we have the activation interval of standing movement and when $angle_{rect} = -2$ we have the onset of the sitting movement (Figure 21). Moreover, an additional control is added in order to eliminate eventual onsets that lasts less than 1024 samples (0.5s) due to noise artifacts. From this signal it is easy to find the starting and ending points of each trial for both the movements.

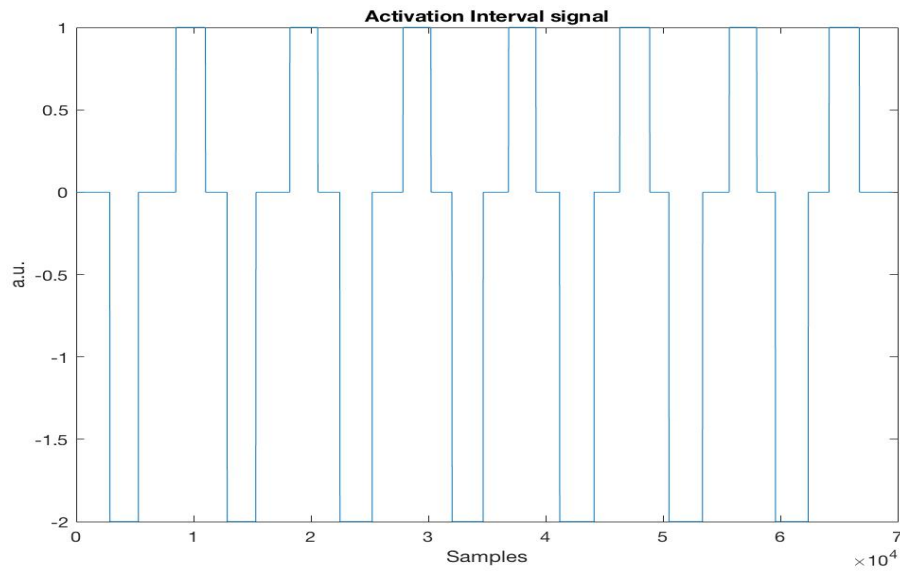


Figure 21: Movement Activation interval signal

The result of the final segmentation can be seen in Figure 22, in which the portion of signal that is highlighted in red corresponds to the segmented trials.

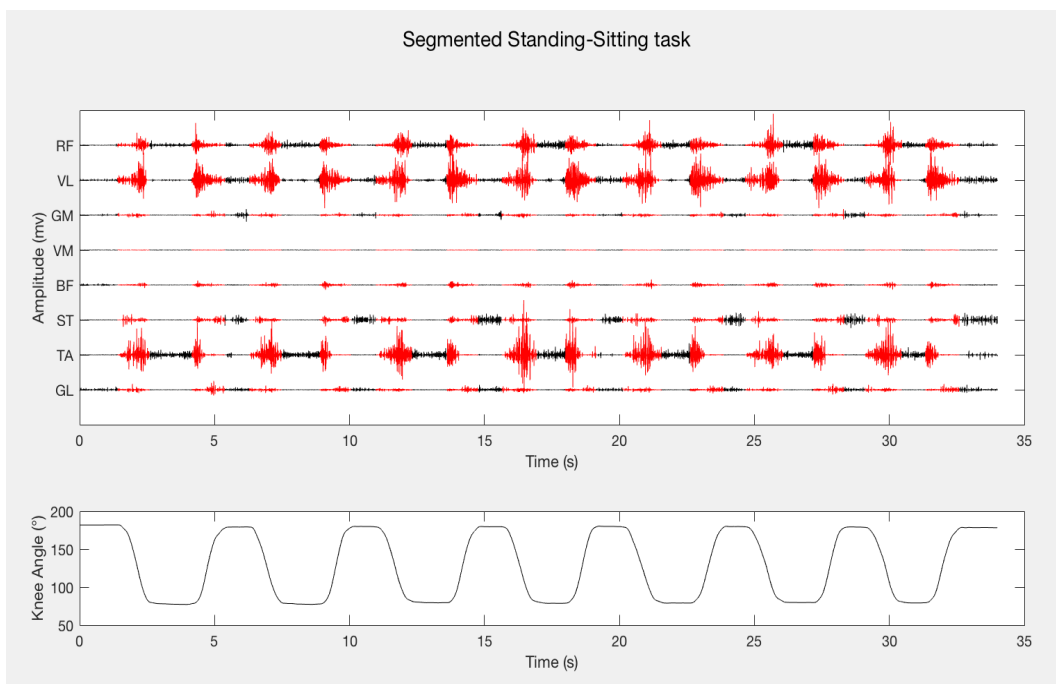


Figure 22: Example of segmented Standing-Sitting task for a subject. In red, EMG portions corresponding to a segmented trial

4.2.2 Gait trials segmentation

For this task, basing on the knee angle information, the aim is to find the starting and ending point of a single gait during a walk (Figure 23).

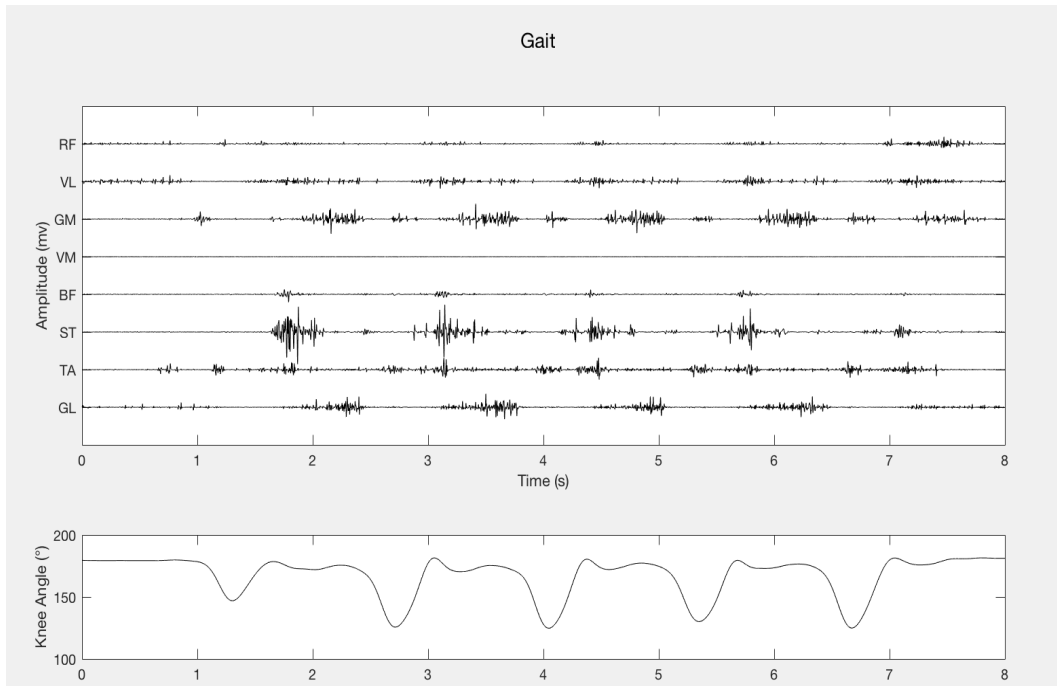


Figure 23: EMG and Knee angle signals of a subject during gait task

It is chosen to consider as segmented trial a cycle of gait that starts from the point of maximum extension of the knee to the subsequent point of maximum extension (Heel-Off to Heel-Off cycle). The first and last cycles are not considered for avoiding the transition phases.

The algorithm follows this steps:

- First of all, the local maxima of the angle signal ($angle_{sig}$) are found, and sorted in amplitude ascending order.
- The total number of steps ($nsteps$) made in the task, can be found by counting the number of local minima (maximum knee flexion) that exceeds a threshold set to $thr = 0.9(mean(angle_{rect}))$. The local maxima before the first minimum and after the last one are not considered (Figure 24) .

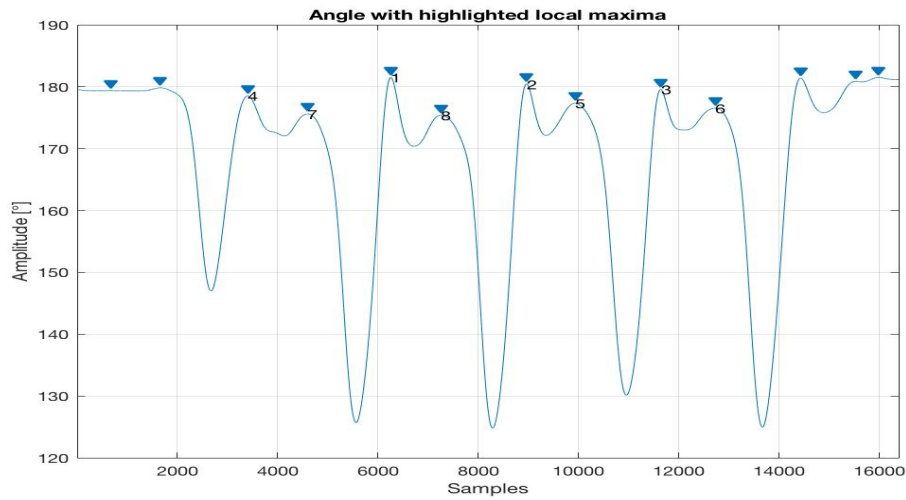


Figure 24: Knee angle signal with highlighted local maxima

- The starting and ending points of a gait cycle could be found as the first ($nsteps - 1$) local maxima, sorted in ascending order of position on the x-axis. Since we don't consider the first and last steps, the total number of segmented trials in this task is $nsteps - 2$.

The result of the final segmentation can be seen in Figure 25, in which the portion of signal that is highlighted in red corresponds to the segmented trials.

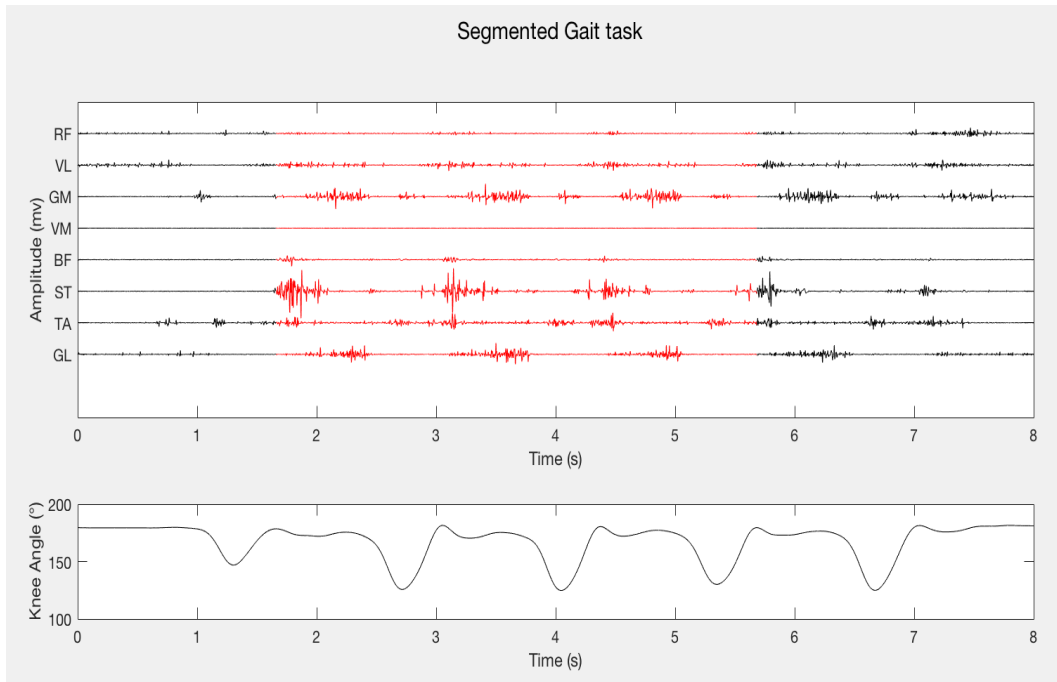


Figure 25: Example of segmented gait task for a subject. In red, EMG portions corresponding to a segmented trial

4.2.3 Stair Ascending and Stair descending trials segmentation

The algorithm used to segment this two tasks is the same because also the trend of the angle signal during the movements is similar. Moreover, both the two task require to perform the movement and then to recover the initial position after a rest phase (Figure 26). For the sake of simplicity, only an example of Stair ascending trial segmentation is shown. In this case the aim of the algorithm is to isolate the trial of the movement from the rest phases and the recover movements.

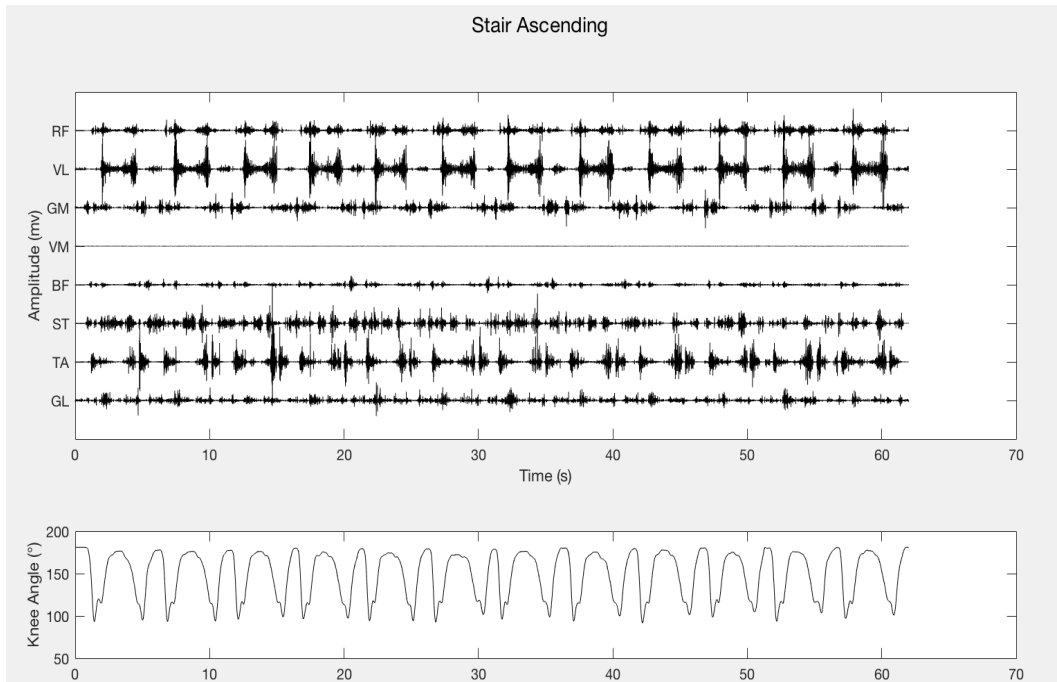


Figure 26: EMG and Knee angle signals of a subject during stair ascending task.

In order to do make what was said earlier, the subsequent steps are followed:

- First of all, the angle signal is low-pass filtered with a Butterworth filter of order 4 and $f_{cut} = 1Hz$ in order to suppress all the variation of the signal and to take into account only its envelope (Figure 27).

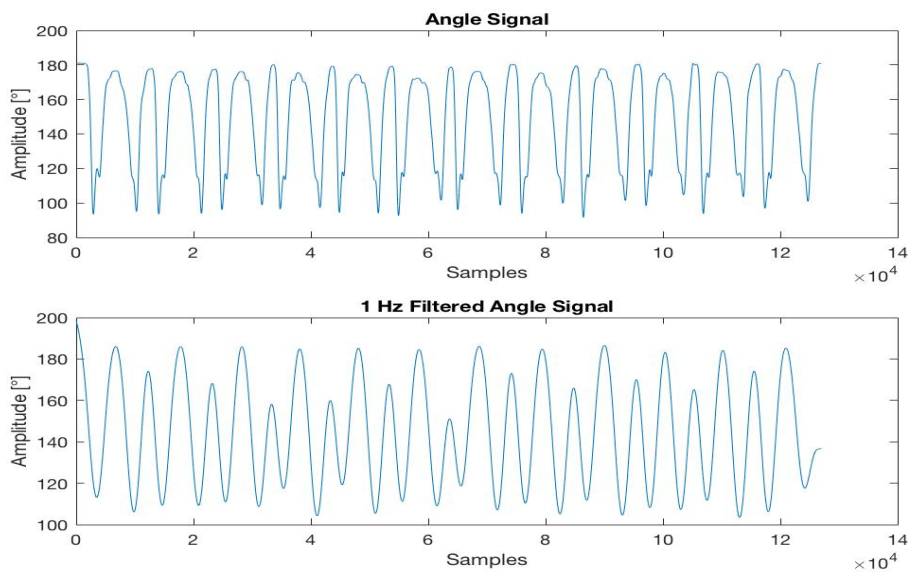


Figure 27: Angle signal and filtered angle signal

- On the filtered signal, the local maxima and minima are evaluated. Since it is known that the subject always start the exercise with a stair ascending (or descending) movement, we can say that the interested trials correspond to the odd patterns while the recover movements corresponds to the even patterns. A pattern occurs in correspondance of a local minima, therefore only the odd minima are considered from now on (the first trial is not taken into account).
- For each minima we know that the task is completed between the two adjacent local maxima (one before and one after the minimum) where the rest phase occurs. So, after evaluating the two adjacent maxima for each minnum point, the signal is isolated in the intervals defined by these three points. In particular we know that the starting point of the trial is contained in the interval between the first maximum (M1) and the minimum (m), while the ending point is cointained between the minimum and the second maximum (M2) (Figure 28)

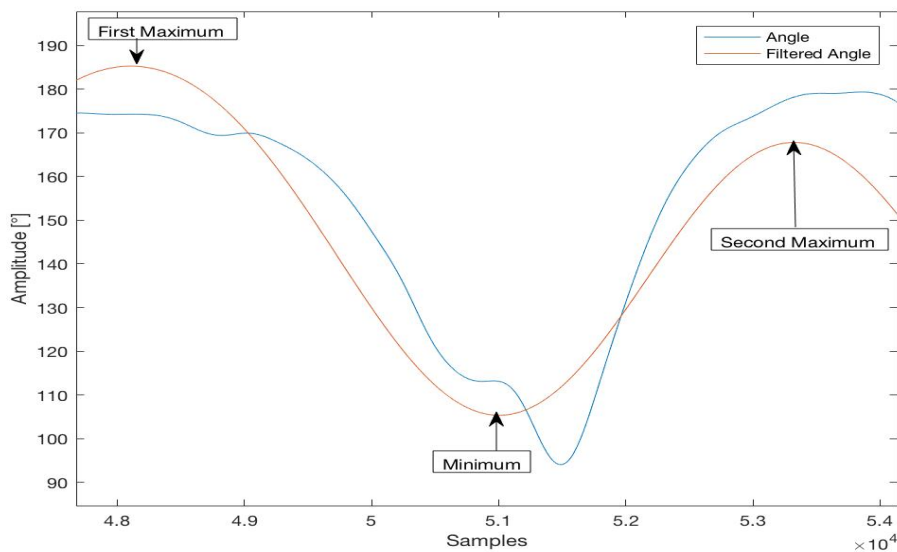


Figure 28: Zoom on a single trial in the interval [M1;M2].

- Two threshold are calculated in order to find the exact starting and ending points of a trial: $thr1$ is the mean value on 1024 samples of the angle signal in the rest interval $[M1-512;M1+512]$ and $thr2$ is the mean value of the angle signal in the rest interval $[M2-512;M2+512]$. This thresholds define the amplitude of the angle signal respectively before and after the subject has completed the movement.

- The starting point of a trial is calculated as the first point in which the angle amplitude in the interval $[M1;m]$ is less than or equal to 98% of $thr1$. Similarly, the ending point of a trial is calculated as the first point in which the angle amplitude in the interval $[m;M2]$ is greater than or equal to 98% of $thr1$.

The result of the final segmentation can be seen in Figure 29, in which the portion of signal that is highlighted in red corresponds to the segmented trials.

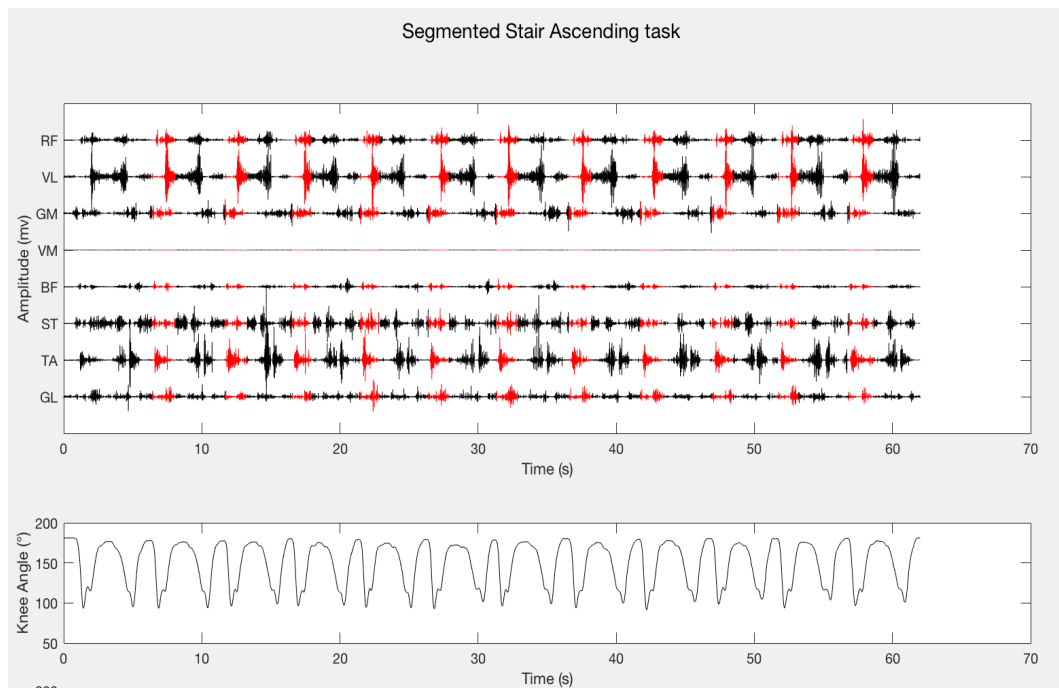


Figure 29: Example of segmented stair ascending task for a subject

4.2.4 Rest trials segmentation

For what concerns the two Rest tasks, there is no need to use the biomechanical information to segment the trials because the subject is always in the same position for about 30s. Having said that, it is chosen to simply segment the whole signal in epochs of 1.4s, that is an average duration compared to the other tasks.

4.3 Feature Extraction and Selection

It is agreed that the analysis window length with the processing delay time should be less than 300ms [12]. Smith et al. [33] proved that the optimal window length should be in the range of 150 to 250ms for real-time myoelectric control. There are basically two different methods of data windowing: overlapped and adjacent windowing (Figure 30).

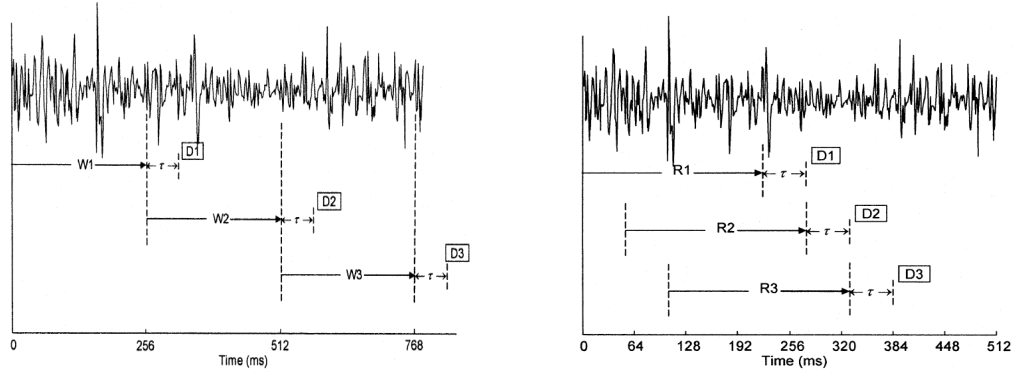


Figure 30: Left: Adjacent windowing of an EMG signal; Right: Overlapped windowing. τ represents the computational delay [12].

In order to find the best windowing strategy and the best feature to extract and select, two Pilot studies have been performed: different types of window length and overlapping sizes have been tested, and the parameter choice was based on the combination that gave the best performances in terms of classification accuracy.

Having said that, after the Pilot studies, windows of 250ms (512 samples with $f_s = 2048 \text{ Hz}$) with overlap of 75% are chosen in this work. Moreover, using the overlapped windowing strategy, it is possible to have a more dense control commands with respect to adjacent windowing: if adjacent windows of 250ms are selected, it means that a command is sent to the actuator in $(250 + \tau)$ ms (where τ is the computational time) after a subject starts a movement, and so we don't have too much margin on the computational time to stay within the real-time maximum delay; differently, with 75% of overlap we send a command every $(62.5 + \tau)$ ms and so we have enough time to do the processing.

With the same pilot studies, different time-domain features, and also different combinations of them, have been taken into account in order to find the best subset that maximize the performances of the classifier.

In total, 6 features are used. As each of the 8 channels has its own set of features, this

gives a 48 feature vector for each selected window. It is worth noting that no frequency-domain or time-frequency domain features have been tested due to an excessive computational complexity, and consequently an excessive computational time, required from their calculation.

The features taken into account in this study and both their definition and mathematical formulations are presented in the following lines (taken and adapted from [34]). Note that in this formulas x_i represents the i^{th} signal sample in a segment and N denotes the length of the EMG window.

- **Root Mean Square (RMS)**

Root mean square (RMS) is another popular feature in analysis of the EMG signal [35]. It is modeled as amplitude modulated Gaussian random process whose relates to constant force and non-fatiguing contraction. It is also similar to standard deviation method. The mathematical definition of RMS feature can be expressed as:

$$RMS = \sqrt{\frac{1}{N} \sum_{i=1}^N x_i^2} \quad (1)$$

- **Zero Crossing (ZC)**

Zero crossing (ZC) is a measure of frequency information of the EMG signal that is defined in time domain [36]. It is a number of times that amplitude values of the EMG signal cross zero level. It is defined as:

$$ZC = \sum_{i=1}^{N-1} u(x_i x_{i+1}) \quad (2)$$

$$u(x) = \begin{cases} 1, & \text{if } x \geq 0 \\ 0, & \text{otherwise} \end{cases}$$

- **Integrated EMG (IEMG)**

Integrated EMG (IEMG) is normally used as an onset detection index in EMG non-pattern recognition and in clinical application [37]. It is related to the EMG signal sequence firing point. Definition of IEMG feature is defined as a summation of

absolute values of the EMG signal amplitude, which can be expressed as

$$IAV = \sum_{i=1}^N |x_i| \quad (3)$$

- **Willison Amplitude (WA)**

Willison amplitude (WAMP) is a measure of frequency information of the EMG signal. This is the number of times that the difference between two consecutive EMG amplitudes exceeds a certain predefined threshold T that is dependent on the setting of gain value of instrument (in this work $T=0.5 \mu V$). Moreover, it is related to the firing of motor unit action potentials (MUAP) and muscle contraction force.

$$WAMP = \sum_{i=1}^N f(|x_{i+1} - x_i|) \quad (4)$$

$$f(x) = \begin{cases} 1, & \text{if } x \geq T \\ 0, & \text{otherwise} \end{cases}$$

- **Number of Turns (NT)**

NT is a number of times that slope of the EMG signal changes sign, or rather, the number of signal peaks. The count of changes between the positive and negative slopes among three sequential segments is performed with the step function. This can be mathematically expressed as:

$$NT = \sum_{i=1}^{N-2} u[(x_{i+1} - x_i)(x_{i+1} - x_{i+2})] \quad (5)$$

$$u(x) = \begin{cases} 1, & \text{if } x \geq 0 \\ 0, & \text{otherwise} \end{cases}$$

- **Waveform Length (WL)**

Waveform length (WL) is a measure of complexity of the EMG signal. It is defined as cumulative length of the EMG waveform over the time segment. Some literatures

called this feature as wavelength (WAVE). It can be calculated by:

$$WL = \sum_{i=1}^{N-1} |x_{i+1} - x_i| \quad (6)$$

For what it concerns the Linear Regressor, we have to use a set of features that can guarantee a linearity relationship between angles and EMG. It is studied by Hahne et al. [38] that a feature of the EMG that satisfies this hypothesis is the logarithm of the variance (LOG(VAR)) of the EMG, that is mathematically defined as it follows.

- **Logarithm of Variance of EMG (LOG(VAR))**

Variance of EMG (VAR) is a power index. Generally, variance is defined as an average of square values of the deviation of that variable; since the mean value of EMG signal is close to zero, variance of the EMG signal can also be defined as

$$VAR = \frac{1}{N-1} \sum_{i=1}^N x_i^2 \quad (7)$$

But, as it has been said before, the logarithmic value of this feature is used:

$$LOG(VAR) = \log\left(\frac{1}{N-1} \sum_{i=1}^N x_i^2\right) \quad (8)$$

4.3.1 Feature scaling

Scaling a feature matrix before applying a classification method is very important. The main advantage of scaling is to avoid attributes in greater numeric ranges dominating those in smaller numeric ranges. Another advantage is to avoid numerical difficulties during the calculation. In particular since kernel values in SVMs usually depend on the inner products of feature vectors and KNN distances depend on exponentiation of the vector, large attribute values might cause numerical problems and to govern on the smaller values. Having a bounded range of features values assures that all the features will equally contribute. For that reasons, it is recommended to linearly scale each feature to the range $[-1; +1]$ or $[0; 1]$ [39]. Furthermore, it is mandatory to use the same scaling method to scale both training and testing data, and in particular to scale the test set with the same scaling values used to scale the training set. Otherwise it can easily happen a drastic reduction of the classifier performances that is not due to a wrong modelling of the problem but rather to an improper use of the scaling method.

In this work the Min-Max scaling is used to scale the features in the range $[0;1]$:

$$x'_i = \frac{x_i - \min(x_i)}{\max(x_i) - \min(x_i)} \quad (9)$$

where x_i is the i^{th} column of the feature matrix, i.e. the vector that contains all the values of a specific feature for the dataset samples, and $[\min(x_i); \max(x_i)]$ represents the range in which the feature values span.

4.4 Support Vector Machines (SVM)

Support Vector Machines are a useful technique for data classification. A classification task usually involves separating data into training and testing sets. Each instance in the training set contains one target value (i.e. the class labels) and several attributes (i.e. the features or observed variables). The goal of SVM is to produce a supervised model (based on the training data) which predicts the target values of the test data given only the test data attributes [39].

The basic idea of the SVMs is to construct a hyperplane as the decision plane, which separates the positive and negative classes with the largest margin, where the margin is the sum of the distances from the hyperplane to the closest data points of each of the two classes (Figure 31). These closest data points are called Support Vectors (SVs) [40].

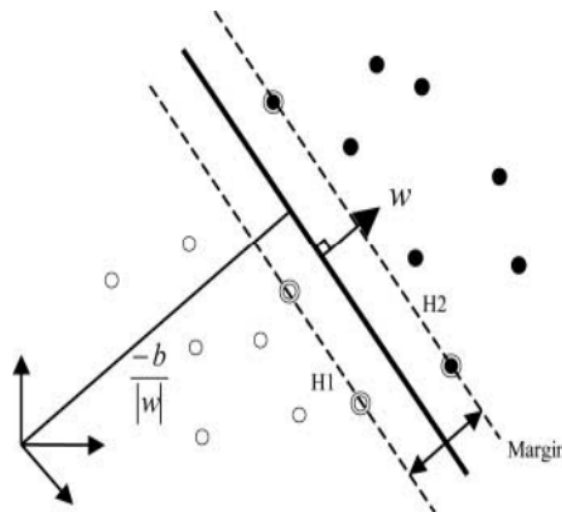


Figure 31: Linear separating hyperplanes with maximum margin. The support vectors are circled (taken from [13])

Given a training set of instance-label pairs (x_i, y_i) with $i = 1, \dots, l$ where $x_i \in \mathbb{R}^n$ and $y \in \{1, -1\}^l$ the support vector machines (SVM) require the solution of the following optimization problem:

$$\min_{w,b,\xi} \frac{1}{2} \mathbf{w}^T \mathbf{w} + C \sum_{i=1}^l \xi_i$$

$$\text{subject to } y_i(\mathbf{w}^T \phi(x_i) + b) \geq 1 - \xi_i, \quad \xi_i \geq 0$$

where $\mathbf{w} \in \mathfrak{R}^n$ is the weight vector, $C \in \mathfrak{R}^+$ is the regularization constant, and the mapping function ϕ projects the training data into a suitable feature space so as to allow for nonlinear decision surfaces. SVM, in fact, is normally able to classify data that are linearly separable. But, defining the *Kernel Function* as $K(x_i, x_j) \equiv \phi(x_i)^T \phi(x_j)$, it is possible to map the data in a higher dimensional with a nonlinear transformation where it is possible to find the optimal separating hyperplane (Figure 32).

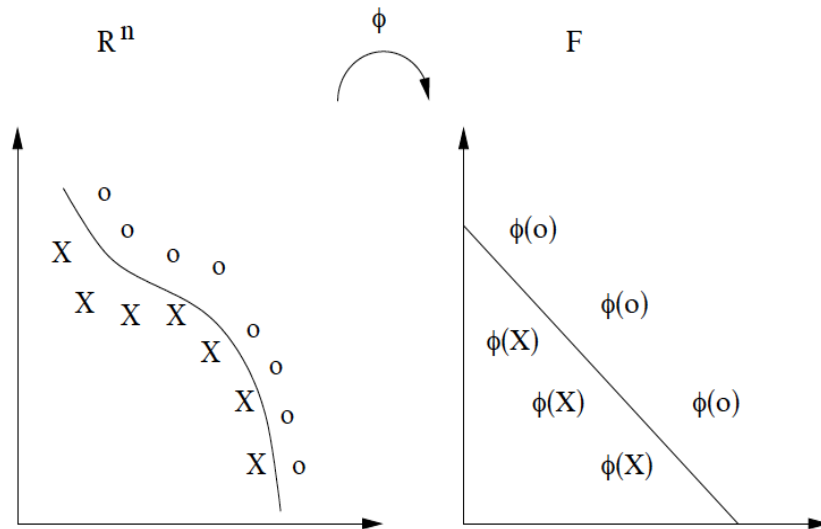


Figure 32: Mapping data into feature space F with kernel function (taken from [14]). In the normal space data are nonlinearly separable, so SVM is not able to find the best separating hyperplane. With the mapping in the feature space, data becomes linearly separable and so SVM is effective.

The most common basic Kernel that can be found in the literature are the following:

- **Linear** : $K(x_i, x_j) = x_i^T x_j$
- **Polynomial** : $K(x_i, x_j) = (\gamma x_i^T x_j + r)^d, \gamma > 0$
- **Radial Basis Function (RBF)** : $K(x_i, x_j) = \exp(\gamma \|x_i - x_j\|^2), \gamma > 0$

- **Sigmoid** : $K(x_i, x_j) = \tanh(\gamma x_i^T x_j + r)$, $\gamma > 0$

where γ, r, d are the hyperparameters of the Kernel functions.

In this work RBF kernel is used. The choice of Radial Basis Function is based on the fact that it nonlinearly maps samples into higher dimensional space and could be efficient in classifying nonlinearly separable data. Furthermore, RBF has lower model complexity and fewer hyperparameters to tune than most other kernels. Finally, RBF is ideally suited for cases where the number of features is not very large with the data, as is the case of sEMG signal classification.

4.4.1 Multiclass SVMs

Support vector machine (SVM) originally separates the binary classes with a maximized margin criterion. However, real-world problems often require the discrimination for more than two categories. In practice, the multi-class classification problems are commonly decomposed into a series of binary problems such that the standard SVM can be directly applied. Two representative ensemble schemes are one-versus-rest (1VR) and one-versus-one (1V1) approaches [41]:

- **One-versus-rest (1VR) approach**: constructs k separate binary classifiers for k -class classification. The m -th binary classifier is trained using the data from the m -th class as positive examples and the remaining $k - 1$ classes as negative examples. During test, the class label is determined by the binary classifier that gives maximum output value. One of the common problem of the one-versus-rest approach is the imbalanced training set. Suppose that all classes have an equal size of training examples, the ratio of positive to negative examples in each individual classifier is $\frac{1}{k-1}$. In this case, the symmetry of the original problem is lost [42].
- **One-versus-one (1V1) approach**: Another classical approach for multi-class classification is the one-versus-one (1V1) or pairwise decomposition. It evaluates all possible pairwise classifiers and thus induces $\frac{k(k-1)}{2}$ individual binary classifiers. Applying each classifier to a test example would give one vote to the winning class. A

test example is labeled to the class with the most votes. The size of classifiers created by the one-versus-one approach is much larger than that of the one-versus-rest. However, with 1V1 approach the computational effort is smaller and so it makes possible to train faster the classifiers. Moreover, compared with the one-versus-rest approach, the one-versus-one method is more symmetric [42].

For the aim of this study, all the classification processing with SVM are performed using the software LIBSVM (Chang and Lin, 2011 [43]) and its extension for Matlab that has already included the possibility of studying multiclass problems using 1V1 approach.

4.4.2 SVM Parameter Tuning

To determine the value of the parameters for the RBF kernel (γ) and the penalty parameter of the error term (C), cross validation was used along with grid search. In a k -fold cross-validation, a data set is divided into k groups of equal size. A group is sequentially left out while the rest of the data is used to train the classifier. The accuracy of the classifier is then tested on the left out group. This process is continued such that each group of the whole training data set is predicted once and the cross validation accuracy is the average of all the testing accuracies achieved. Thus cross-validation accuracy is the percentage of data which are correctly classified. In this study, a particular case of k -fold cross-validation is used : the Leave-One-Out cross validation, where only a trial is used as test set and the remaining as training set (in this particular case, 9 trials for training and 1 for test). Different pairs of (C, γ) were tried for cross validation and the one with highest accuracy was chosen. The process was started with a course grid search with the two Pilot studies and, after identifying a region of better accuracy, a finer grid search was performed on that region for each subject. In particular it is found from the Pilot studies that the region in which the better results are seen is $[2^{-3}, 2^3]$ for both C and γ parameters.

Therefore the parameters are chosen by performing a grid search in that region where C and γ vary from 2^{-3} to 2^3 in a logarithmic scale with a step size of 0.5.

The algorithm has 2 stopping condition, one on the maximum number of iteration to perform, set to 300 cycles, and another on the maximum number of times that the best accuracy doesn't change, set to 50 times (this is a strategy to avoid unnecessary cycles

and to speed up the tuning if we are close to the asymptotic value). An example of this procedure can be seen in Figure 33.

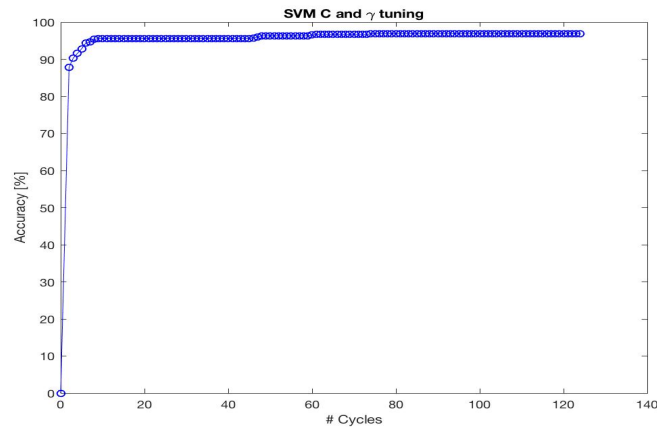


Figure 33: Tuning of SVM parameters for a test subject

4.5 K-Nearest Neighbor Classifier (KNN)

k – Nearest Neighbor (kNN) is one of the instance-based supervised learning approaches, that is widely used in classifying the objects based on the closest or nearest neighbor training examples. The classification rules are generated by the training samples themselves without any additional data. The KNN classification algorithm predicts the test sample's category according to the K training samples which are the nearest neighbors to the test sample, and judge it to that category which has the largest category probability.

The training examples are vectors in a multidimensional feature space, each with a class label. The training phase of the algorithm consists only of storing the feature vectors and class labels of the training samples. In the classification phase an unlabeled vector (a query or test point) is classified following this steps (Figure 34):

- An integer k is chosen;
- All the distances between the query point and training samples are calculated and sorted in ascending order;
- The query point is assigned to the class C if it is the most frequent class label among the k nearest training samples;

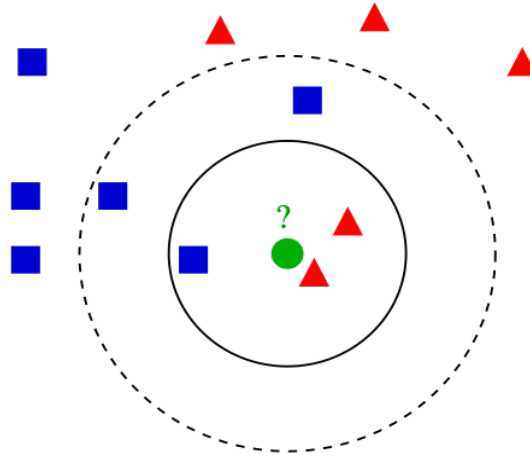


Figure 34: Example of KNN classification. The test sample (green circle) should be classified either to the first class of blue squares or to the second class of red triangles. If $k = 3$ (solid line circle) it is assigned to the second class because there are 2 triangles and only 1 square inside the inner circle. If $k = 5$ (dashed line circle) it is assigned to the first class (3 squares vs. 2 triangles inside the outer circle). Taken from [15]

The commonly used metrics to find the distance between the query point and the training samples are:

- **Minkowsky** : $d(\mathbf{x}, \mathbf{y}) = \sqrt[p]{\sum_{i=1}^n (x_i - y_i)^p}$
- **Euclidean** : $d(\mathbf{x}, \mathbf{y}) = \sqrt{\sum_{i=1}^n |x_i - y_i|^2}$
- **Cityblock** : $d(\mathbf{x}, \mathbf{y}) = \sum_{i=1}^p |x_i - y_i|$
- **Mahalanobis** : $d(\mathbf{x}, \mathbf{y}) = \sqrt{(\mathbf{x} - \mathbf{y})^T \Sigma^{-1} (\mathbf{x} - \mathbf{y})}$, where Σ is the covariance matrix

In order to find the best k parameter and distance for each subject, a tuning process was performed.

4.5.1 KNN Parameter Tuning

Likewise the SVMs case, also for the KNN classifier two design choices must be taken: the first on the value of k parameter and the second on the type of similarity metrics ($d(x,y)$) that can be used for the classifier. Also in this case a Leave-One-Out cross-validation is used to measure the classifier performances, and the pair of k and d that leads to the maximum accuracy is chosen. In this tuning process k values from 1 to 20 are tested, and, for what concerns the distance metric, Mahalanobis, Euclidean, Minkowsky and Cityblock distances are chosen to be tested. This choice is derived from the results of the Pilot studies. The algorithm has 2 stopping condition, one on the maximum number of iteration to perform, set to 200 cycles, and another on the maximum number of times that the best accuracy doesn't change, set to 30 times.

An example of this procedure can be seen in the Figure 35.

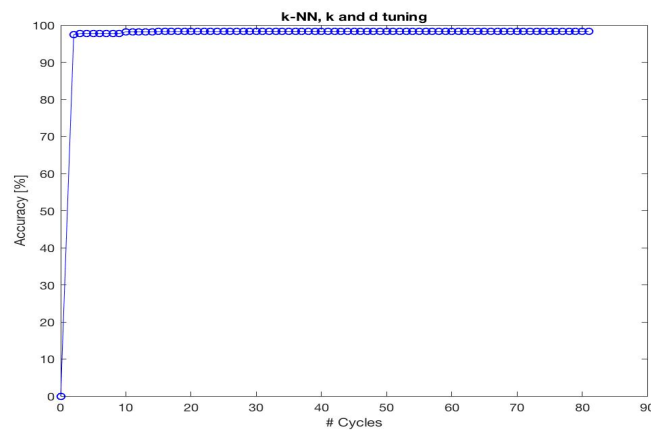


Figure 35: Tuning of KNN parameters for a test subject

4.6 Multiple Linear Regressor (MLR)

In statistics, linear regression is a linear approach to modelling the relationship between a dependent variable and one or more explanatory variables (or independent variables). If we have more than one independent variable, the model is called Multiple linear regression. This term is distinct from multivariate linear regression, where multiple correlated dependent variables are predicted, rather than a single scalar variable [44].

If the goal is prediction (like in this case where we want to predict angles from EMG) linear regression can be used to fit a predictive model to an observed data set of values of the response and explanatory variables. After developing this model, if additional values of the explanatory variables are collected without a response value, the fitted model can be used to make a prediction of the response [16]. The final aim of linear regression is to find the line (or the hyperplane in higher dimensional cases) that minimizes the squared error between each observation and the model itself (Figure 36).

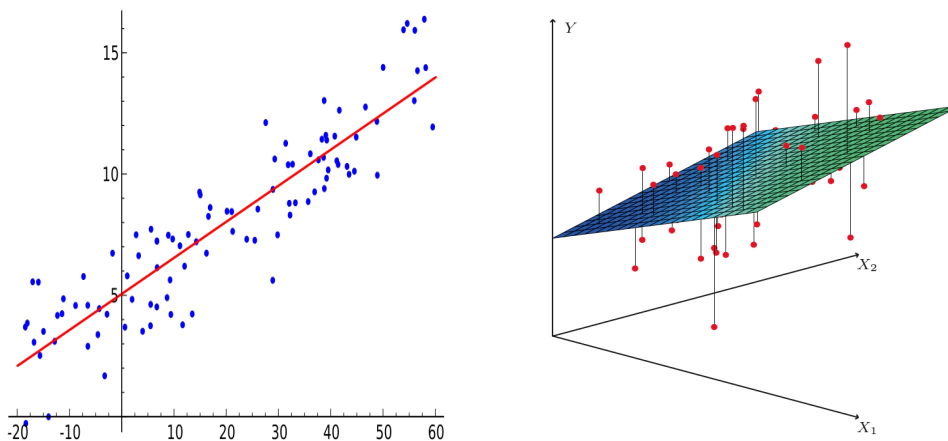


Figure 36: Left: Example of simple linear regression with one independent variable [16];
Right: In a three-dimensional setting, with two predictors and one response, the least squares regression line becomes a plane (taken from [17])

In multiple linear regression, there are p explanatory variables (features) for T time instances, and the relationship between the dependent variable and the explanatory variables is represented by the following equation:

$$y_i = w_0 + w_1x_{1i} + w_2x_{2i} + \dots + w_px_{pi} \quad (10)$$

or, in general, with the matricial form :

$$\mathbf{Y} = \mathbf{W}^T \mathbf{X} + \mathbf{w}_0 \quad (11)$$

where \mathbf{w}_0 is the intercept value, $\mathbf{W} \in \mathbb{R}^{p \times 1}$ is the Weight matrix, $\mathbf{X} \in \mathbb{R}^{p \times T}$ is the feature matrix and $\mathbf{Y} \in \mathbb{R}^{1 \times T}$ contains the observed angle data. The least mean squares solution for finding \mathbf{W} is obtained by minimizing the following error (or cost) function:

$$J(\mathbf{w}) = \frac{1}{2} \sum_t (\mathbf{y}(t) - \mathbf{w}^T \mathbf{x}(t))^2 \quad (12)$$

This minimization problem could be solved through Gradient Descent method, that is an iterative process to find a global minimum, or using the closed form solution known as Normal Equation:

$$\mathbf{W} = (\mathbf{X}\mathbf{X}^T)^{-1} \mathbf{X}\mathbf{Y}^T \quad (13)$$

By adding a column of 1 values inside \mathbf{X} , also the intercept value \mathbf{w}_0 is calculated with this formula that basically constitutes the training of the regressor. To evaluate the prediction of angles ($\hat{\mathbf{Y}}$) using a new test data \mathbf{X}_{test} , we have to use the weight matrix \mathbf{W} found from the training as it follows:

$$\hat{\mathbf{Y}} = \mathbf{W}^T \mathbf{X}_{test} \quad (14)$$

4.7 Generalized Regression Neural Networks (GRNN)

GRNN is a type of supervised Feed-Forward NN and is one of the most popular neural networks. Donald F. Specht first introduced it in 1991 [45]. GRNNs are known for their ability to train quickly on sparse data sets. Rather than categorizing data, GRNN applications are able to produce continuous valued outputs. One of the main advantages of the GRNN, with respect to other Back Propagation based NNs, is that the training of the network is faster because data only needs to propagate forward once.

GRNNs work well on interpolation problems and are suitable for estimation of continuous variables, as in standard regression techniques. This type of network uses a single common radial basis function kernel to do the estimation.

The regression performed by a GRNN is the conditional expectation of Y; in other words, its output is the most probable scalar Y given specified input vector x.

Hereinafter the mathematical and structural fundamentals of GRNN are shortly reported. More details can be found in chapter 3 of Artificial Neural Networks (Joao Luis Garcia Rosa, 2016) [18]. Assume $f(x, y)$ as the joint continuous probability density function of a vector random variable X, and a scalar random variable Y. Let x be a particular measured value of the random X. The regression of Y given x (also called conditional mean of Y given x) is given by:

$$E\{Y/x\} = \frac{\int_{-\infty}^{\infty} Y f(x, Y) dy}{\int_{-\infty}^{\infty} f(x, Y) dy} \quad (15)$$

For a nonparametric estimate of $f(x, y)$, one of the most common consistent estimators is used, i.e. a Gaussian function (or Radial Basis Function (RBF)). The good choice for probability estimator $\hat{f}(x, y)$ is based on sample values x_i and y_i of the random variables X and Y is given by:

$$\hat{f}(x, y) = \frac{1}{(2\pi)^{\frac{(p+1)}{2\sigma^{(p+1)}}}} \cdot \frac{1}{n} \sum_{i=1}^n e^{-\frac{(x-x_i)^T(x-x_i)}{2\sigma^2}} e^{-\frac{(y-y_i)^2}{2\sigma^2}} \quad (16)$$

where p : is the dimension of the vector variable.

n : is the number of training pairs $(x_i \rightarrow y_i)$.

σ : is the single learning or smoothing parameter chosen during network training.

y_i : is desired scalar output given the observed input x_i .

The topology of a common GRNN presented in Figure 37 consists of four layers.

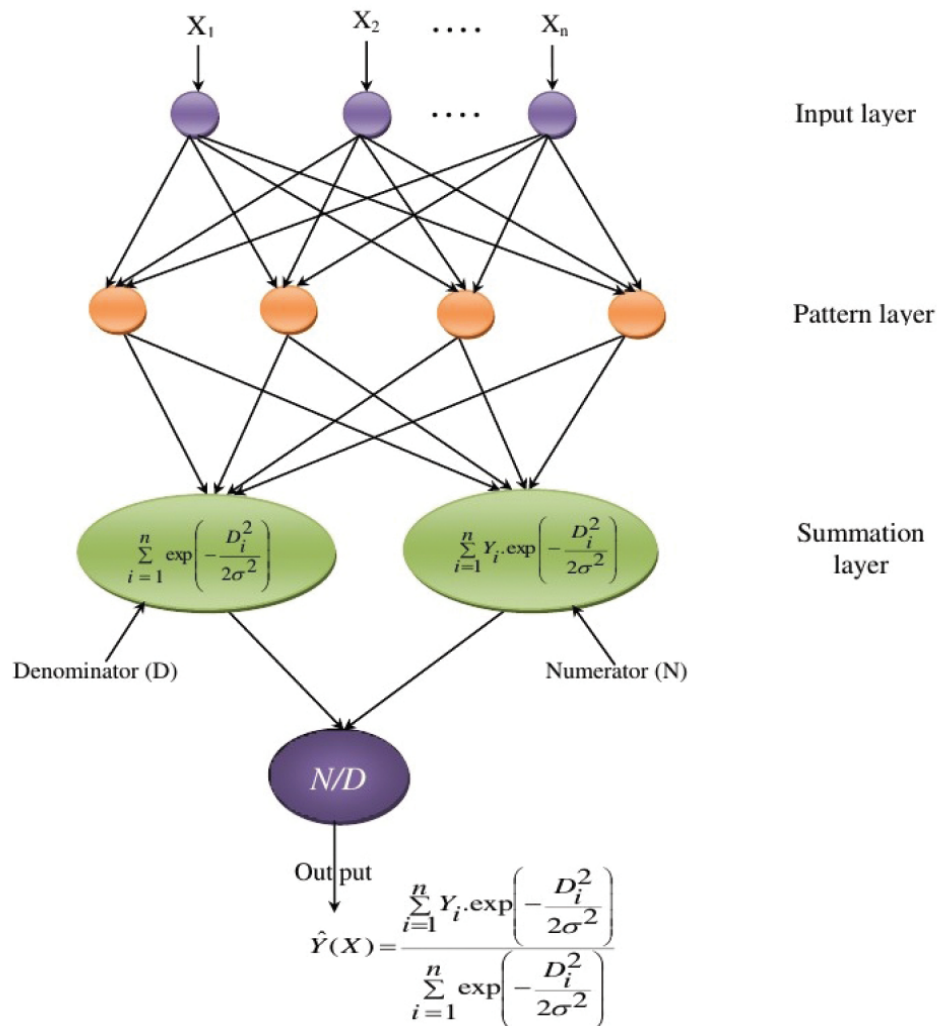


Figure 37: The basic GRNN architecture, taken from [18]

The first layer of the network is the input layer. The input units provide all of the scaled measurement variables X to the neurons that constitute the second layer.

The second layer represents the first hidden layer (also called Pattern layer). It consists of N processing elements or nodes, where N is the number of sample within a training data set and each node represents the input vector, X_i . Each input vector is associated with the

vector assigned with the j^{th} sample in training data and, inside the node, it is subtracted from the vector assigned to the node itself, i.e. X_j . This difference is then squared and the result is given into the RBF kernel. The outputs of the pattern layer are then passed to the summation units. It is worth noting that the second hidden layer always has exactly one more node than the output layer.

The third layer represents the second hidden layer (also called Summation layer) which consists of two nodes. The input to the first node is the sum of the first hidden layer outputs, weighted by the observed output y_j corresponding to X_j . Instead, the input of the second node is the summation of the first hidden layer activations.

Finally, the fourth layer is the output layer. It receives the two outputs from the hidden layers and divides them in order to provide the prediction result.

4.8 Training and testing

In this section it is described how both the classifiers and regressors are trained and tested, and the design choices for selecting the best models to perform the validation phase of the system. In this phase 10 trials for each of the 7 movements are taken into account.

4.8.1 Classifiers

First of all, the Feature Matrix and the label Vector are evaluated for the dataset. After finding the best parameters for each subject, as explained in sections 4.4.2 and 4.5.1, for both the SVM and KNN classifiers the training and testing is performed with a Leave-One-Out cross validation (LOOCV) in order to prevent overfitting. In particular, 9 trials for each class are given to the classifier for training and 1 trial for test in repetition such that each trial of the dataset is predicted once, and so for a total of 10 cycles. For each cycle of the cross validation, the related classifier accuracy on the prediction of the test set is calculated from the confusion matrix (see Results).

The model of classifier, for both KNN and SVM, chosen for the validation phase is the one related to the cycle of LOOCV that had the best performance in terms of average accuracy on the 7 classes. This choice is supported by the fact that it is possible that a not well segmented or performed trial in the training or in the test set could negatively polarize the performances of the classifier during the validation phase. Instead, with this strategy

we have the reasonable certainty that only the best trials are taken into account inside the trained model.

4.8.2 Regressors

It is worth noting that two different regressors are constructed, one for ankle joint and one for knee joint: this is motivated by the fact that different muscles are involved in this two different joints, and it is a mistake to predict an angle of a joint with muscles that interest the other joint. In particular, for the knee regressor only the features related to channels of Biceps Femoris, Semitendinosus, Rectus Femoris, Vastus Medialis and Lateralis are selected; while for the ankle regressor only the features related to the channels of Tibialis Anterior, Gastrocnemius Medialis and Lateralis are taken into account. It is reminded that the GRNN regressor is trained with the same subset of 6 feature used for the training of the classifiers, while the MLR uses only the LOG(VAR) feature for the selected channels.

Moreover, for each DOF and for both GRNN and MLR models, two types of regressor are trained: a class-specialized regressor and a general regressor.

- The **class-specialized regressor** contains 7 different models, one for each class in this study, and the prediction of each model is specific for a movement. The training and testing of this regressor is performed with a Leave-One-Out cross validation (LOOCV), using 10 trials (the same used for the training of the classifiers) in total, 9 for the training and 1 for the test. Similarly to the classifier case the model that has the best performances (highest R^2 value) in terms of prediction for each movement class in a cycle of the test phase is chosen for performing the validation phase.
- The **general regressor**, instead, consists of a unique model and is able to make a prediction for all the movements. This regressor is trained using all the 10 trials.

4.9 Validation phase

In this phase the aim is to compare the performances of a system composed by a classifier in chain with the class-specialized regressor and a system based only on a not specialized regressor.

For the class-specialized regressor, the prediction of the validation angle is made in this way: first the classifier recognize the movement and, basing on the predicted class, triggers the correspondent model in the specialized regressor to make the angle prediction from the EMG. Since we have 2 classifier models and 2 regression model, for each DOF a total of 4 different combinations are tested (SVM-MLR, KNN-MLR, SVM-GRNN, KNN-GRNN) in this study.

Two different procedures of validation are proposed:

- **First Method:** in the first validation method, two new trials for each movement are taken into account. After the classification procedure, the angle of both DOFs are predicted with the specialized regressor and then with the not specialized regressor.
- **Second Method:** in the second validation method, the subject is asked to perform a sequence of movements in order to simulate a daily scenario. The selected sequence is : rest stand - sitting - standing - sitting - rest sitting - standing - (stair ascending / stair descending) x2 - gait. To identify the movement epochs within the the signal and to label the tasks for the classification, a first rough segmentation is manually performed by the operator and then refined using the same algorithms described in section 4.2, Once the final segmentation of the tasks is found, the classification takes place and then the predictions of angles with the specialized regressor and the not specialized regressor is performed.

5 Results and Discussion

5.1 Performance Metrics Definitions

5.1.1 Classifier Performances Evaluation Metrics

A common way of reporting classification results in a multiclass supervised setting, is to compile a *Confusion Matrix*, also referred to as a *Contingency table* or *Accumulation matrix*. Each column of the matrix represents the instances in a predicted class while each row represents the instances in an actual class (or viceversa). Each entry of the diagonal of the confusion matrix is the number of elements that are correctly classified by a classifier, while the other entries represent the misclassification errors between class i^{th} and class j^{th} .

		estimated			
		$\xi_{i,1}$	$\xi_{i,2}$	\dots	$\xi_{i,C}$
true	$\xi_{1,j}$	$\xi_{1,1}$	$\xi_{1,2}$	\dots	$\xi_{1,C}$
	$\xi_{2,j}$	$\xi_{2,1}$	$\xi_{2,2}$	\dots	$\xi_{2,C}$
	\vdots	\vdots		\ddots	
	$\xi_{C,j}$	$\xi_{C,1}$	$\xi_{C,2}$	\dots	$\xi_{C,C}$

Figure 38: Example of multiclass confusion matrix. Taken from [19]

From this matrix, two performance metrics can be calculated considering a problem of C classes:

- **Class Accuracy:** Expressed in percentage, represent the number of correct classification for the i^{th} class. It can be defined as the ratio between the number of correct classification for class i and the total number of elements within that class:

$$Accuracy_i = \frac{\xi_{i,i}}{\sum_{i=1}^C \xi_{i,j}}$$

- **Average or Overall Accuracy:** Expressed in percentage, represent the total number of correct classification. It can be defined as the ratio between the trace of the matrix and the total number of elements that are classified:

$$Accuracy = \frac{\sum_{i=1}^C \xi_{i,i}}{\sum_{i=1}^C \sum_{j=1}^C \xi_{i,j}}$$

5.1.2 Regressor Performances Evaluation Metrics

The goodness of fit describes how well a model fits a set of observations. Measures of goodness of fit typically summarize the discrepancy between observed values and the values expected under the model in question. In this case we are interested to study how well a regressor can predict an angle basing on EMG features. Two metrics are used in this study:

- **Coefficient of Determination (R^2):** is a measure used in statistical analysis that assesses how well a model explains and predicts future outcomes. It is indicative of the level of explained variability in the data set. The coefficient of determination, also commonly known as "R-squared" is used as a guideline to measure the accuracy of the model. Given $y = [y_1, \dots, y_n]$ as the vector containing the observed values and $\hat{y} = [\hat{y}_1, \dots, \hat{y}_n]$ the vector containing the predicted values, the coefficient of determination is defined as:

$$R^2 = 1 - \frac{\sum_{j=1}^n (y_j - \hat{y}_j)^2}{\sum_{j=1}^n (y_j - \bar{y})^2}$$

and represents the ratio of variations explained by the model to the total variations present in the observed data. In our case, R^2 values are evaluated separately for knee joint and ankle joint angle predictions.

- **Root Mean Square Error (RMSE):** is a frequently used measure of the difference between values predicted by a model and the values actually observed from the environment that is being modelled. These individual differences are also called

residuals, and the RMSE serves to aggregate them into a single measure of predictive power.

The RMSE of a model prediction (\hat{y}) with respect to the observed value (y) is defined as the square root of the mean squared error:

$$RMSE = \sqrt{\frac{\sum_{j=1}^n (y_j - \hat{y}_j)^2}{n}}$$

Nonetheless, a non dimensional form of RMSE (NRMSE) is useful when we have to compare variables with different units, or like in this case, movements with different Ranges of Motion (ROM). For that reason, a normalization approach is used:

$$NRMSE = \frac{RMSE}{(max(y) - min(y))}$$

where $(max(y) - min(y))$ is indeed the ROM of the movement.

For the ankle joint the considered Range Of Motion is $[-50^\circ, 30^\circ]$ while for the knee joint is $[90^\circ, 180^\circ]$.

5.2 Classifiers Cross-Validation

In this section the results derived from the 10 cycles of the Leave-One-Out Cross-Validation are presented for all the 8 selected subjects. A boxplot graph is shown with the distribution of the accuracy rate for each of the 7 classes along the 10 cycles and a bar diagram with average value of accuracy and range intervals. This two type of graphs are shown for both SVM and KNN.

5.2.1 Knn LOOCV results

It is clear from Figure 39 that the median value of accuracy for each of the 7 classes is always greater than **93%** for almost all the subjects and this indicates a good stability of the classifier due to a good choice of its parameters. We can see also some outliers with classification accuracy below 80% : this can be motivated by a not properly correct execution of the exercise by a specific subject.

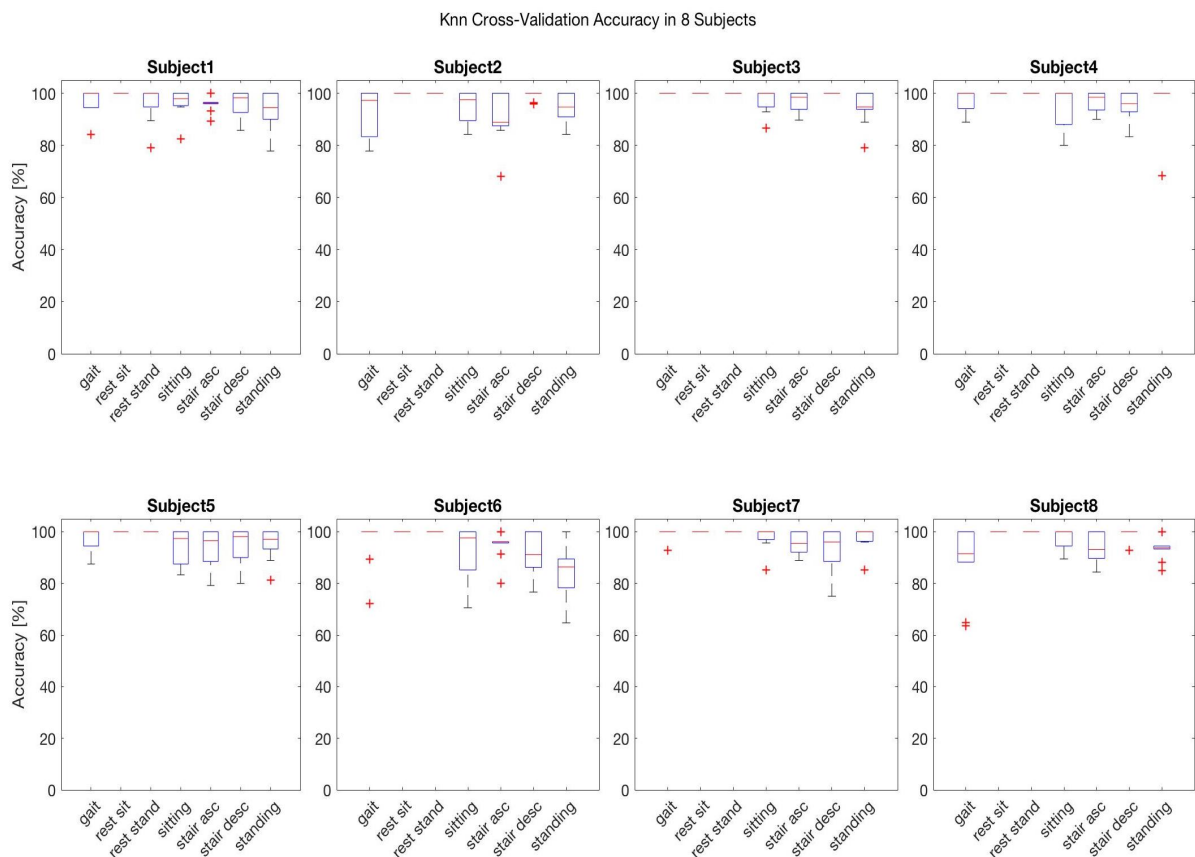


Figure 39: Boxplot containing Knn Cross-Validation Accuracy values evaluated for each class in test subjects

From the bar diagram in Figure 40 instead, we can have an overview on the average performances of the classifier. The average performances of the classifier are always above **94%** with peaks of 100% of accuracy. Choosing the classifier model with the highest average accuracy on all 7 classes in a cycle of the cross-validation allows to keep only the well performed trials as training set and to eliminate the worst.

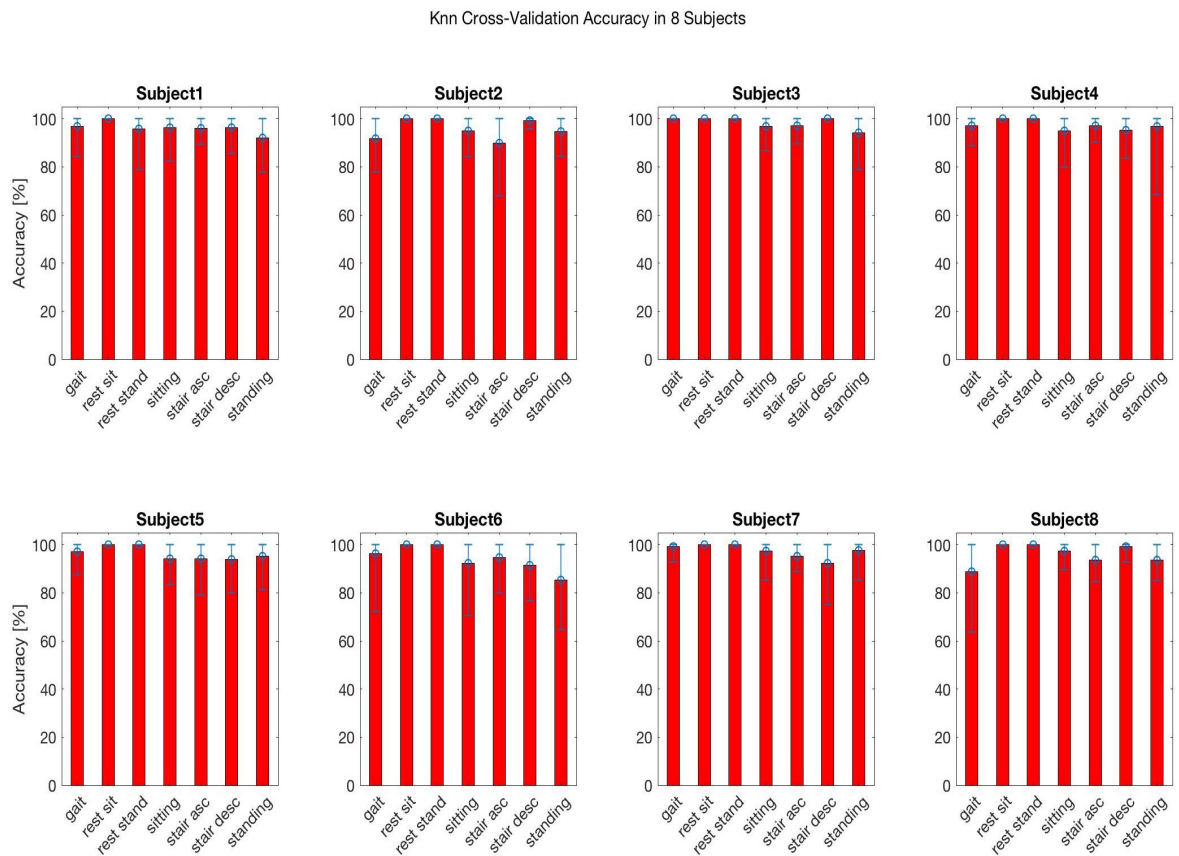


Figure 40: Boxplot containing Knn Cross-Validation Accuracy values evaluated for each class in test subjects

With this two type of representation, we are able to analyse only the overall performances of the classifier but it is not possible to see how the misclassification errors are distributed and which are the classes that are mainly confused. In order to achieve that, the confusion matrices for exemplificative subjects 1, 3, 5 and 7 are presented (Figure 41). These matrices are the sum of all the 10 confusion matrices derived from each cycle of the cross-validation, in the way that it is possible to see the overall misclassification errors.

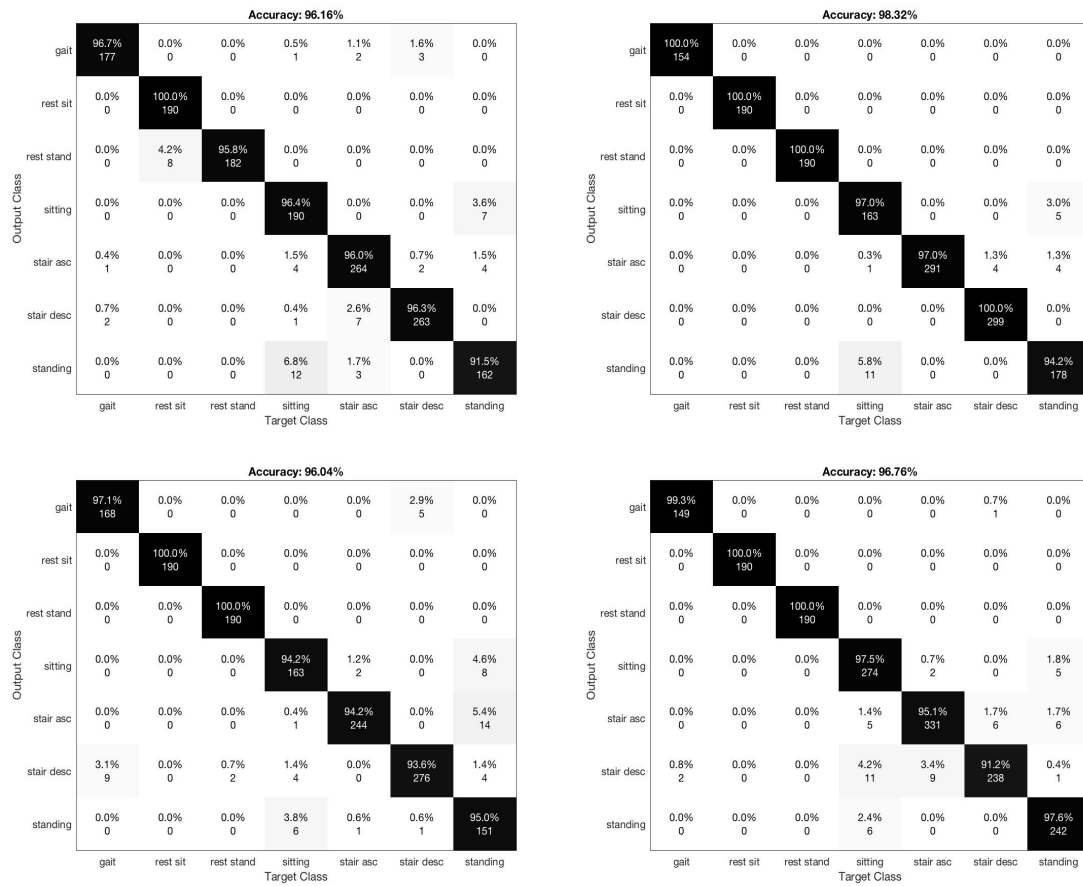


Figure 41: Confusion Matrices of Subject 1 (top left), 3 (top right), 5 (bottom left) and 7 (bottom right). The average Accuracy of the KNN classifier is indicated on the top of the matrix

By analyzing these three confusion matrices, there is the confirmation that the overall performances of the classifier are robust and widely acceptable. It is worth noting, however, that the most of the classification errors are between Standing and Sitting class and Stair Ascending with Standing class. This seems to be reasonable because in this movement, the involved muscles follow the same scheme of activation: the sitting movement can be seen as the inverse of the standing movement from the point of view of muscular patterns. Also for the stair ascending movement, if only the dominant leg is studied, the muscular pattern seems to be similar with respect to the standing movement. Nevertheless, this misclassification errors are reasonably in small amount, and the average performance of the classifier still can be considered as satisfying.

5.2.2 SVM LOOCV results

From Figure 42 it can be noted that the median value of accuracy for each of the 7 classes is always greater than **92%** for almost all the subjects. The accuracy of the SVM classifier, in this phase of study results to be very similar to the KNN one with also the presence of outliers of accuracy below 80% and in some cases also below 60%. Since these are only outliers, the motivation of this could be found in a not correct execution of one trial in the dataset.

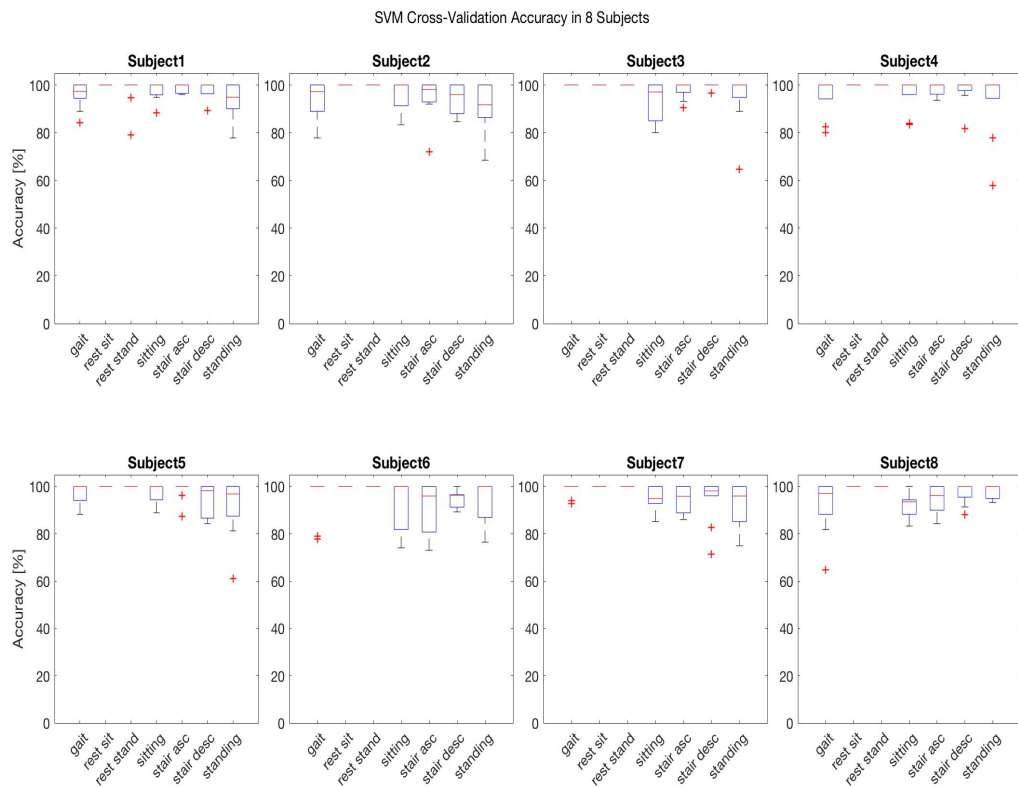


Figure 42: Boxplot containing Knn Cross-Validation Accuracy values evaluated for each class in test subjects

Similarly, we can find an overview of the average performances of the SVM classifier along the cycles of LOOCV and it is possible to see in Figure 43 that the results of the classification seems to be reasonably reliable and stable for each class and for each subject. There are peaks of 100% of accuracy also in this case in all the studied subjects, and this is a signal of a correct choice of the SVM parameters and robustness of the classifier.

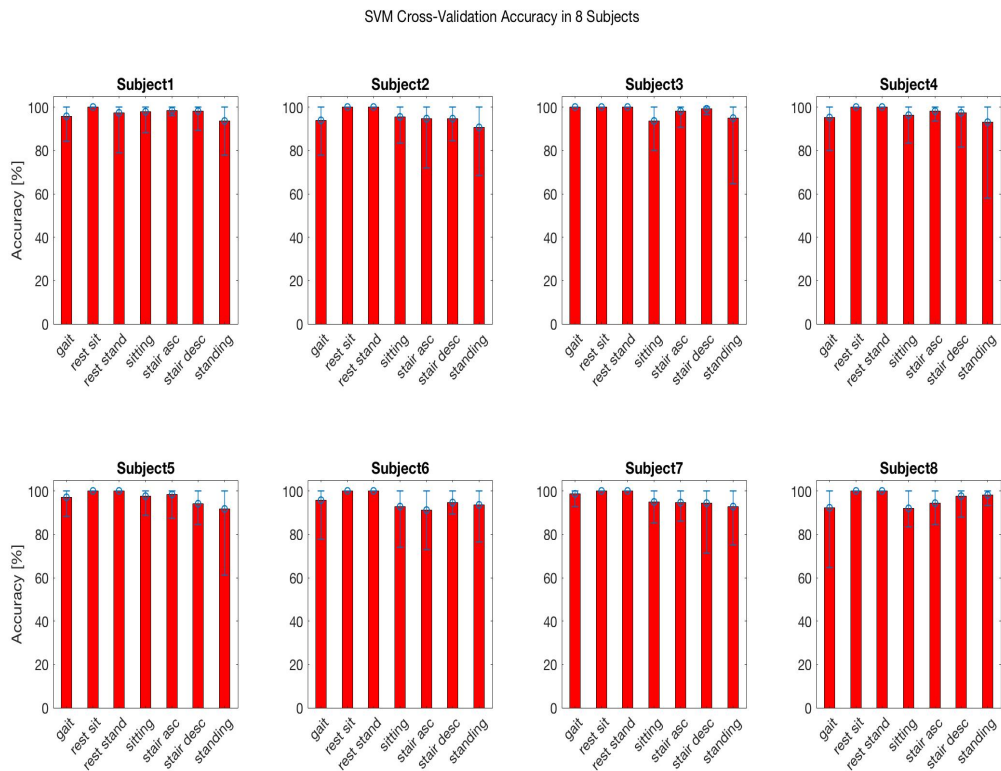


Figure 43: Boxplot containing Knn Cross-Validation Accuracy values evaluated for each class in test subjects

Similarly to the KNN case, the confusion matrices for subjects 1,3 and 5 are presented for demonstration purposes (Figure 44). Also in this case these matrices are the sum of all the 10 confusion matrices derived from each cycle of the cross-validation, in the way that it is possible to see the overall misclassification errors.

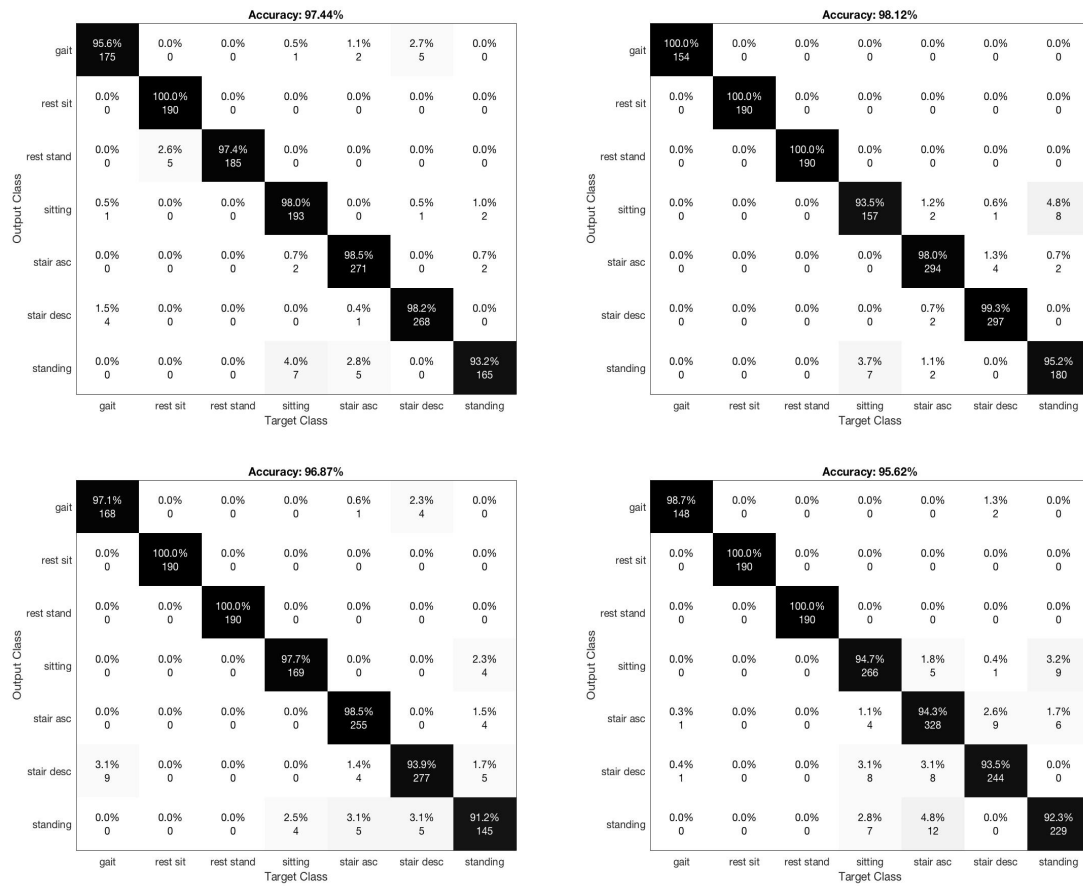


Figure 44: Confusion Matrices of Subject 1 (top left), 3 (top right), 5 (bottom left) and 7 (bottom right). The average Accuracy of the SVM classifier is indicated on the top of the matrix

Analyzing these three confusion matrices, there is the confirmation that the overall performances of the SVM classifier are robust. We can see that also in this case the most of the classification errors are between Standing and Sitting class and Stair Ascending with Standing class, even if on a smaller scale. Nevertheless, this misclassification errors are reasonably in small amount, and the average performance of the classifier still can be considered as satisfying.

5.3 Regressors Cross-Validation

In this section the results derived from the 10 cycles of the Leave-One-Out Cross-Validation for the two regressor models are presented considering all the 8 selected subjects. It is chosen to show a boxplot graph, for both R^2 and $NRMSE$ values in order to analyze the performances of prediction for each of the 7 classes.

5.3.1 GRNN LOOCV results for ankle joint

From Figure 45 it is possible to see that the performances of prediction in terms of R^2 value with the the Neural Network are not robust, they are distributed in all the range and their trend differs from subject to subject. However, very good reconstructions with $R^2 \geq 0.8$ are present: this can be motivated by the fact that in the cyclic repetitions of the movements, the subject doesn't follow the same angular patterns and so the regressor is not always able to perfectly predict the angular trend with the chosen emg features.

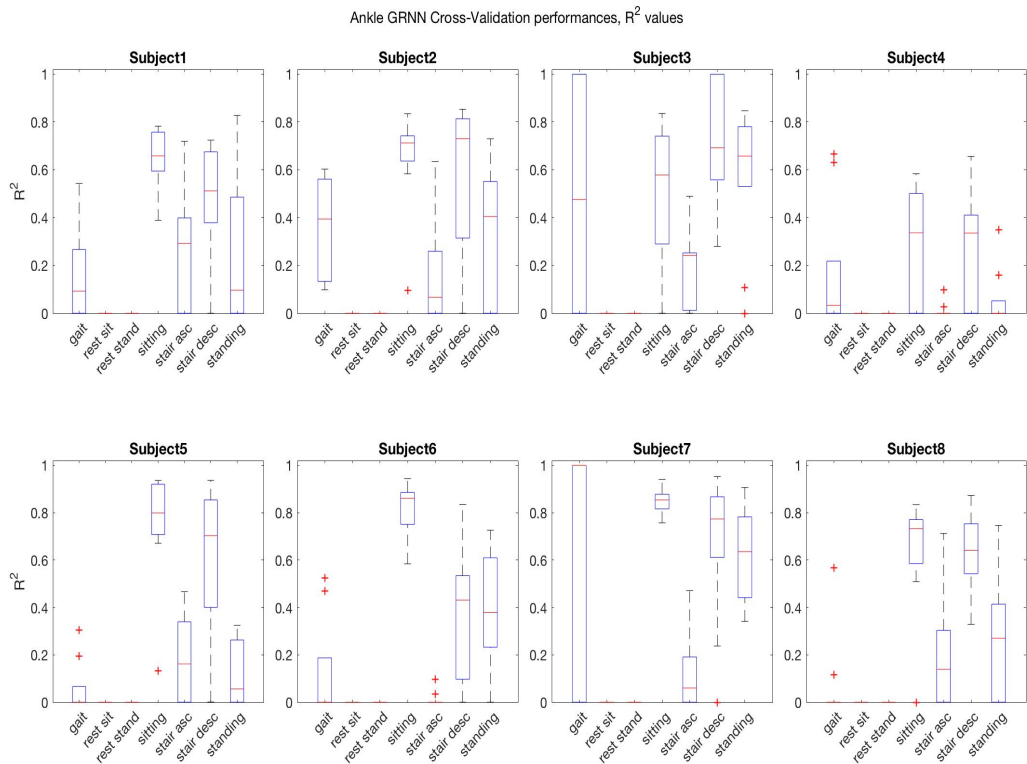


Figure 45: Boxplot containing GRNN Cross-Validation R^2 values evaluated for each class in test subjects for Ankle joint

We can see that the class that has the overall worst performances and cannot be well reconstructed is the *Stair ascending* class and for subject 5 and 8 also the *Gait* movement. These are two complex movements and probably the muscle activation in each cycle could be not maintained similar or the chosen features used to predict this movement are not explicative and robust in every trial.

It is also worth noting that for the rest movement the R^2 value is near to zero: this is because R^2 is not a good metric of performance for movement with constant trend because it is a value that consider the variability of the observed data. From that point of view it is considered to present also the NRMSE values, because with this indicator we can have an idea of how much the predictor is erring with respect of the Range Of Motion of the considered joint. In fact, from Figure 46 we can see that for all the classes and for all the subjects the NRMSE values are below 0.3, and this is an indicator that even if the prediction is not accurate, the error is inferior to the 30% of the Range of Motion the ankle joint.

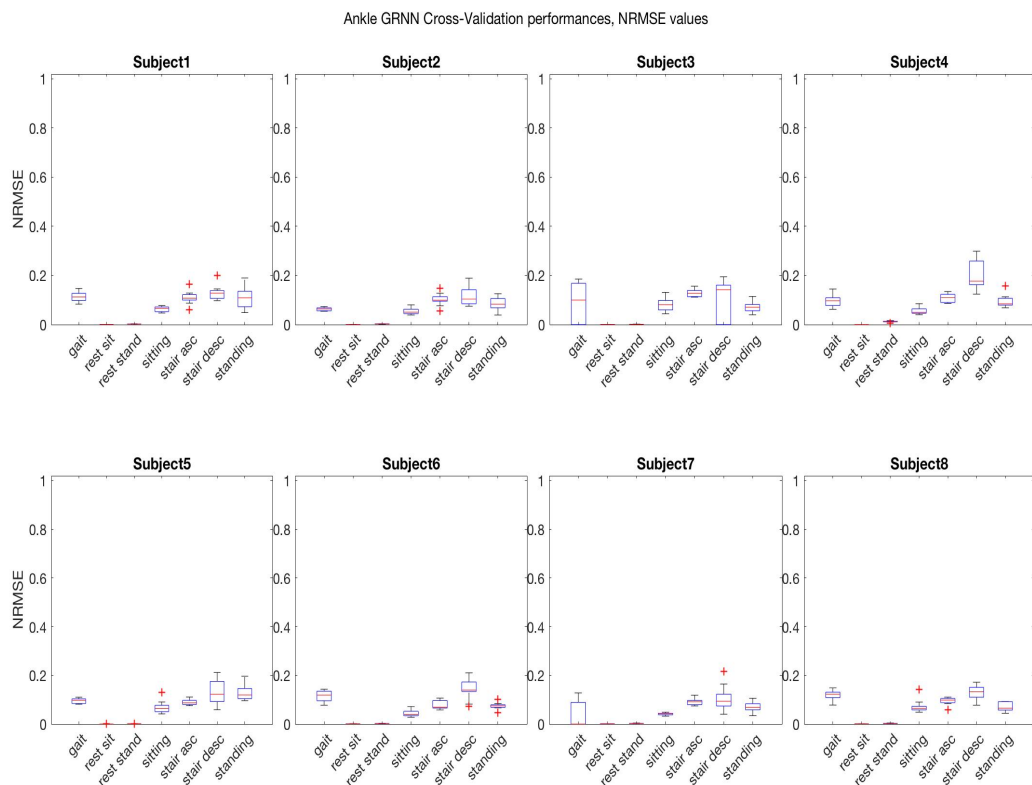


Figure 46: Boxplot containing GRNN Cross-Validation NRMSE values evaluated for each class in test subjects for Ankle joint

In order to be reasonably sure that the model of GRNN is able to make a prediction also in the validation phase, only the models that has the best performances, for each class in a cycle of cross-validation, are selected and merged in a unique class-specialized model. In this way, only the reliable predictions are considered and only the most significative trials are included in the training of the regressor.

5.3.2 GRNN LOOCV results for knee joint

From Figure 47 it is possible to see that the performances of prediction in terms of R^2 value with the the Neural Network are not robust, they are distributed in all the range and their trend differs from subject to subject, like in the case of Ankle joint.

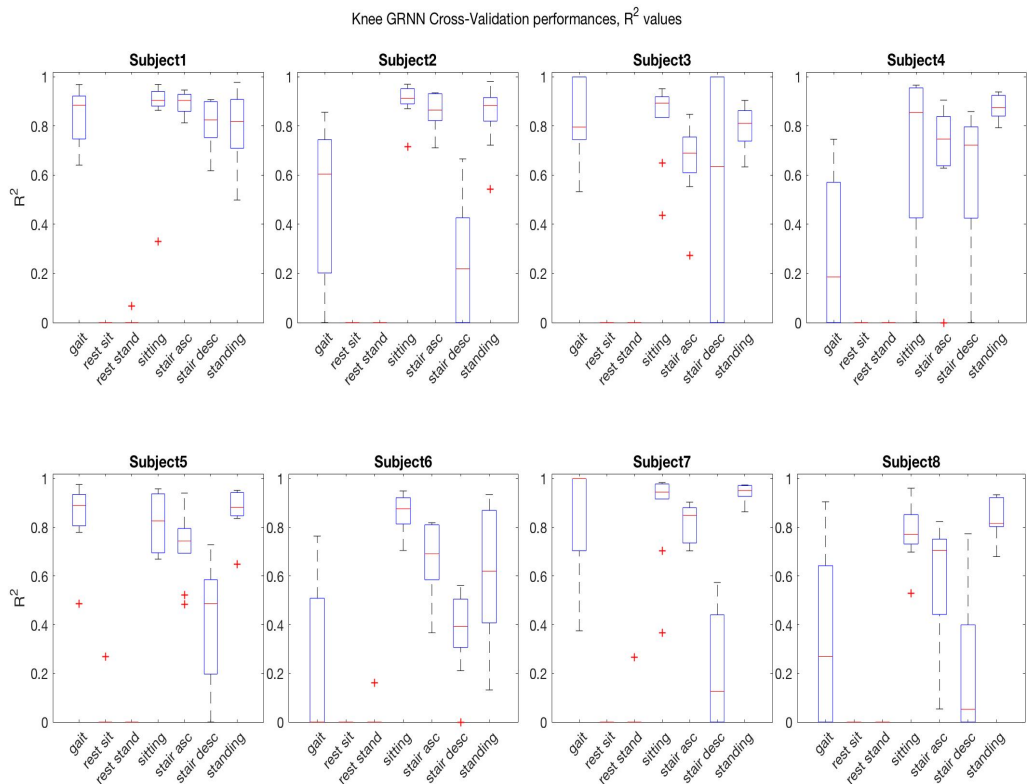


Figure 47: Boxplot containing GRNN Cross-Validation R^2 values evaluated for each class in test subjects for Knee joint

The results in this case seem to have higher median values and an overall better performances with respect to ankle angles reconstructions. One hypothesis to explain this outcome is that this improvement in the prediction can be due to a higher number of

muscles, involved in knee flexion and extension (5 muscles) compared to ankle flexion and extension (3 muscles): this leads to a dimensionally higher feature vector (1x30 for knee versus 1x18 for ankle) associated to each window of EMG and it can be the reason for a more accurate prediction made by the network.

From the boxplot representing the distribution of NRMSE values in Figure 48 we can see that for all the classes and for all the subjects the median of NRMSE values, is below 0.25 even though the R^2 values are not always good. This is an indicator that even if the prediction is not accurate, the error is inferior to the 25% of the Range of Motion the knee joint.

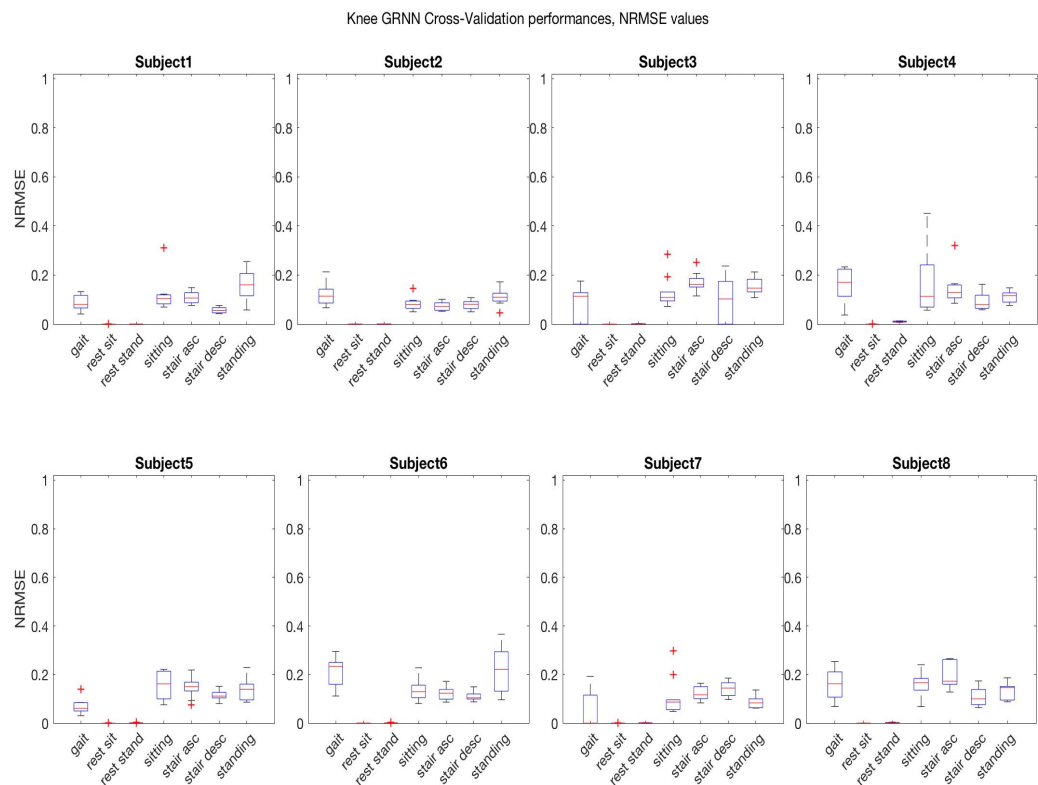


Figure 48: Boxplot containing GRNN Cross-Validation NRMSE values evaluated for each class in test subjects for Knee joint

Also in this case, only the model of GRNN for each class that had the best performances in a cycle of the cross-validation are taken into account to perform the validation phase in order to exclude the worst trials from the training set and to keep only the most robust ones.

5.3.3 MLR LOOCV results for ankle joint

The performances of MLR prediction for ankle joint are comparable to the GRNN ones. The distribution of the performances in terms of R^2 values has large variability both between different subjects and between the different classes for a specific subject (Figure 49). This is an indicator that not always the Regressor is able to accurately reconstruct the angle with only the LOG(VAR) feature.

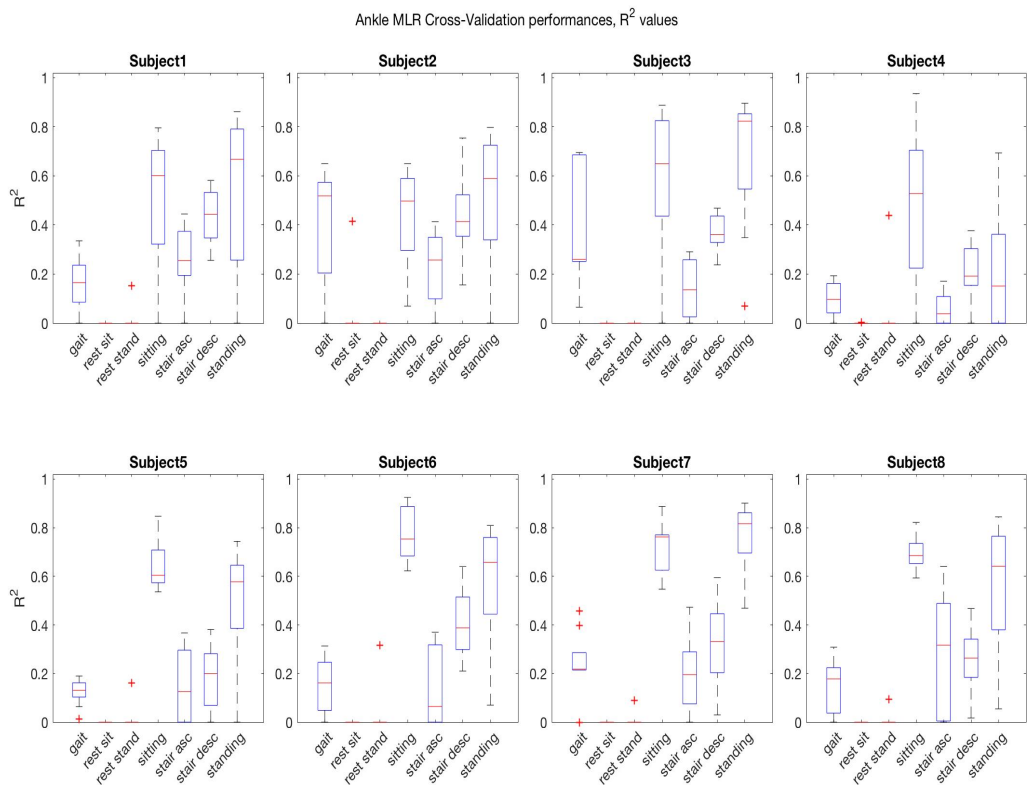


Figure 49: Boxplot containing MLR Cross-Validation R^2 values evaluated for each class in test subjects for Ankle joint

However, it is also possible to note the presence of very good reconstructions with $R^2 \geq 0.8$ for classes *Sitting* and *Standing* while for the *Gait* movement there is an overall difficulty to accurately predict the joint angle with median values of R^2 that span from about 0.2 and 0.5. For this specific type of movement, the GRNN model presents better performances with respect to MLR.

For the same reasons described above, also in this case the boxplot representing the NRMSE values distribution is presented.

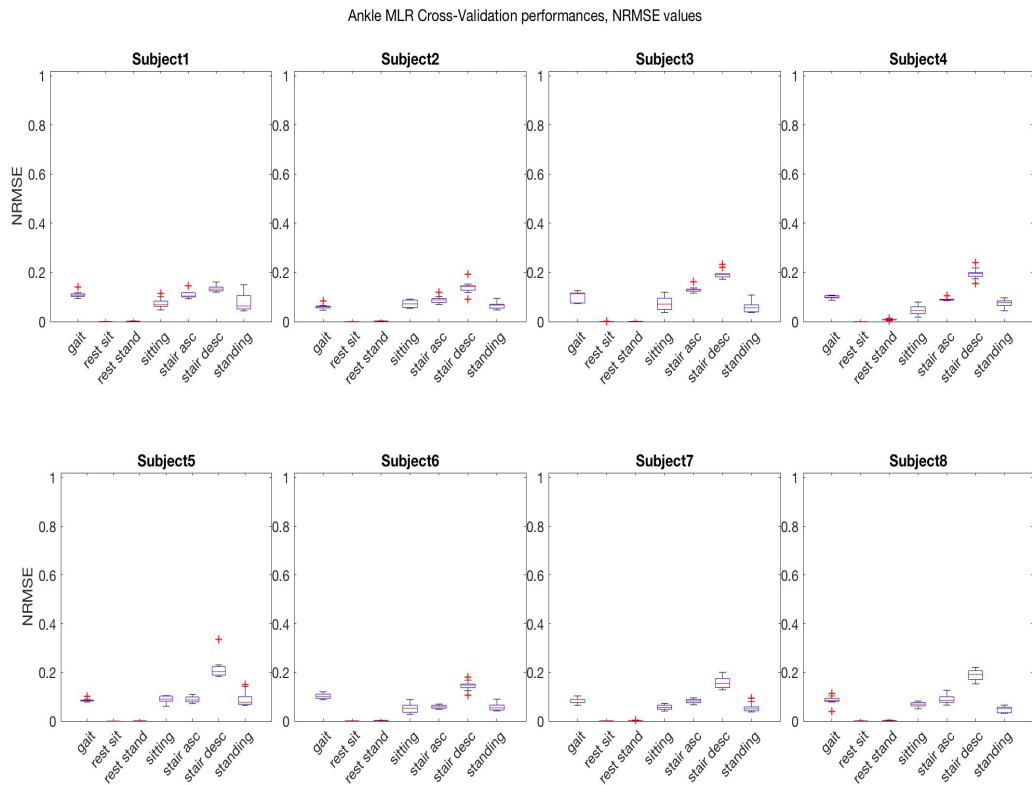


Figure 50: Boxplot containing MLR Cross-Validation *NRMSE* values evaluated for each class in test subjects for Ankle joint

It is worth noting that the results are comparable to the GRNN case. The NRMSE values present small variability both between the subjects and between each class of movement. All the values are contained in the range [0.1-0.25] like the GRNN case and so the error of prediction is maintained below the 25% of the Range of Motion of the Ankle joint. Also for the MLR, the Weight matrix associated to a specific movement that gives the best performances is saved and then merged into a unique class-specialized model.

5.3.4 MLR LOOCV results for knee joint

The performances of MLR prediction for knee joint are comparable to the GRNN ones. The distribution of the performances in terms of R^2 values has large variability both between different subjects and between the different classes for a specific subject (Figure 51).

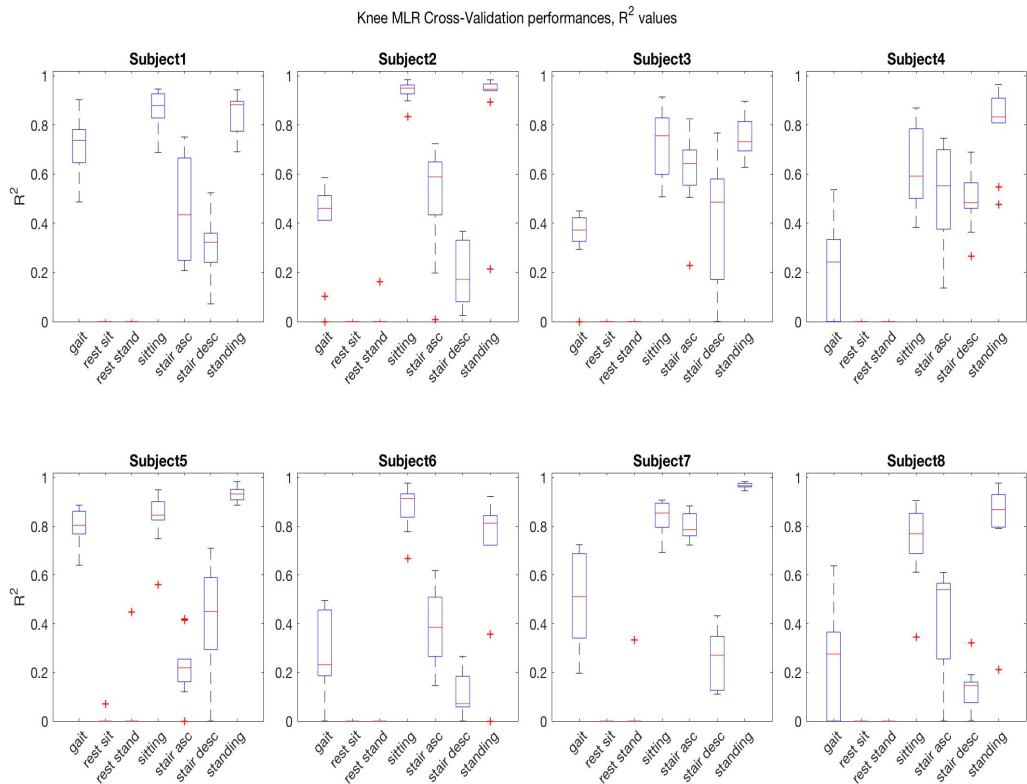


Figure 51: Boxplot containing MLR Cross-Validation R^2 values evaluated for each class in test subjects for Knee joint

It is possible to note the presence of very good reconstructions with $R^2 \geq 0.8$ for classes *Sitting* and *Standing*, but also *Stair Ascending* movement presents good performances in prediction for the most of the subjects. The most difficult tasks to predict seem to be the *Stair descending* as we can see in subjects 5,6 and 8. This results are similar to the GRNN case, even if for the latter the best performances have an absolute overall higher value on the 7 subjects.

Also in this case the knee joint angle prediction results seem to have higher median values with respect to ankle angles reconstructions. The hypothesis is the same as it is

previously explained for the GRNN case: the higher number of dimensionality of features and channels associated to the knee joint leads to a better representation of its activity with respect to the ankle one (1x5 feature vector for the knee against 1x3 feature vector for the ankle).

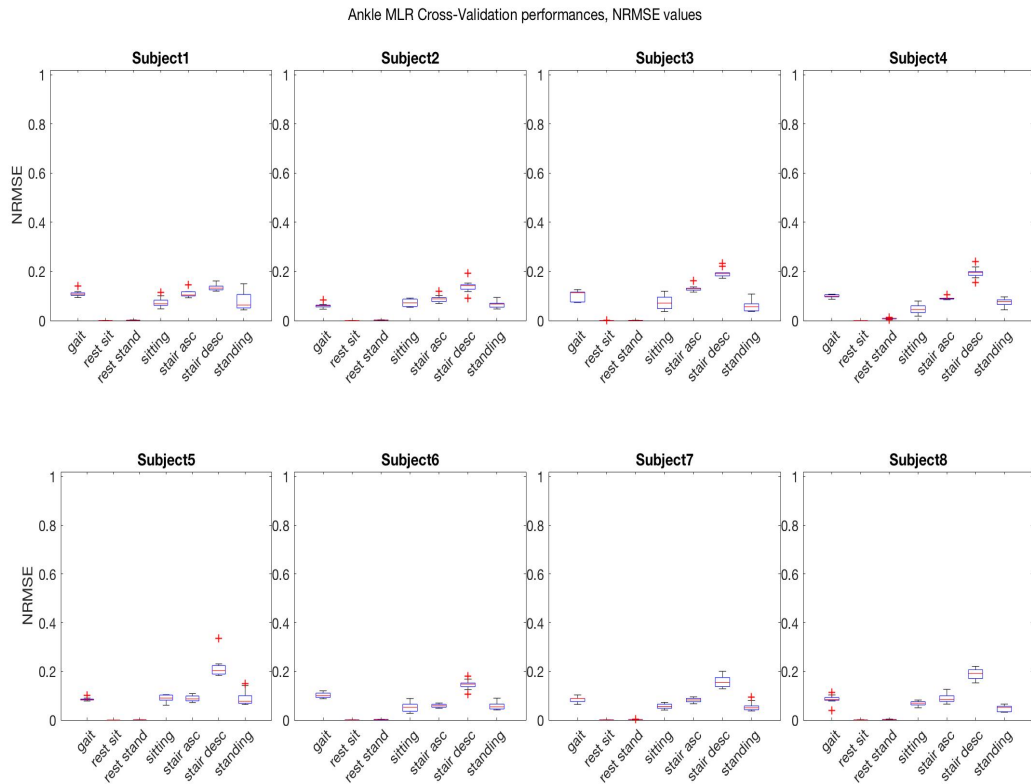


Figure 52: Boxplot containing MLR Cross-Validation *NRMSE* values evaluated for each class in test subjects for Knee joint

The *NRMSE* values present small variability both between the subjects and between each class of movement. All the values are contained in the range [0.1-0.25] like the GRNN case and so the error of prediction is maintained below the 25% of the Range of Motion of the Knee joint.

5.4 Validation - First method

In this section the results coming from the first validation method are presented. It is reminded that in this phase two previously segmented trials, that are not used for the cross-validation phase, are firstly classified by the two classifiers and the output (the class prediction) is used to trigger the class-specialized regressor in order to perform the prediction. Four different combination of classifier-regressor are tested (SVM-GRNN, KNN-GRNN, SVM-MLR, KNN-MLR) and their performances in prediction on the concatenated movements are compared to the performances of the general regressors (GRNN-MLR). This phase is repeated for the two degrees of freedom. A statistical analysis with one-way ANOVA and a post-hoc Tukey-Kramer test is then performed in order to study the statistical significance of the results.

5.4.1 Classification

First of all, the results of the classification are presented for both the KNN and SVM classifiers with a bar diagram in which is highlighted the accuracy for each class and the average accuracy on all 7 classes (Figure 53 and Figure 54).

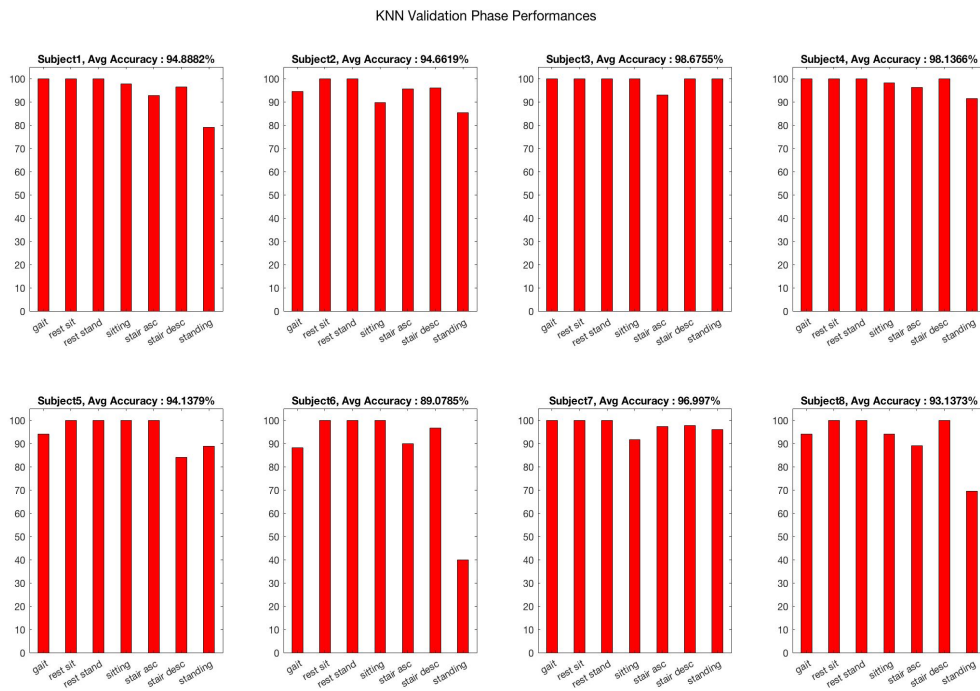


Figure 53: Bar diagram with KNN validation accuracy values for each class in 8 subjects

The performances for KNN results (Figure 53) are reasonably satisfying: except for subject 6, the average classification accuracy is over 93% and also for all classes the accuracy is about 90%. By analyzing more deeply the results, it can be noted that the class that has the lowest accuracy rate is *Standing* and, also in this case, the error of misclassification is due to a confusion with the *Standing* movement.

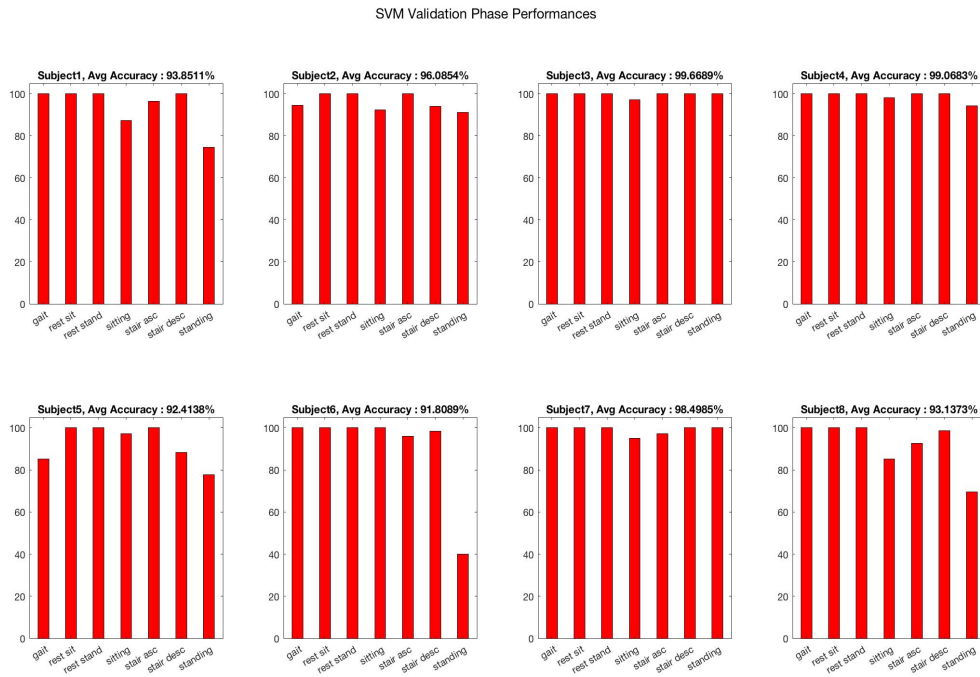


Figure 54: Bar diagram with KNN validation accuracy values for each class in 8 subjects

For what concerns SVM, the results are comparable with the KNN classifier. The average accuracy is high (over 92%) for all the subjects and the specific accuracy for each class follow the same trend of the KNN case. This result demonstrates a good classification robustness for both the classifiers.

5.4.2 Ankle angle predictions

The trend of the performances of prediction in terms of R^2 and NRMSE values with all the models among the 8 subjects is reported respectively in Figures 55 and 56.

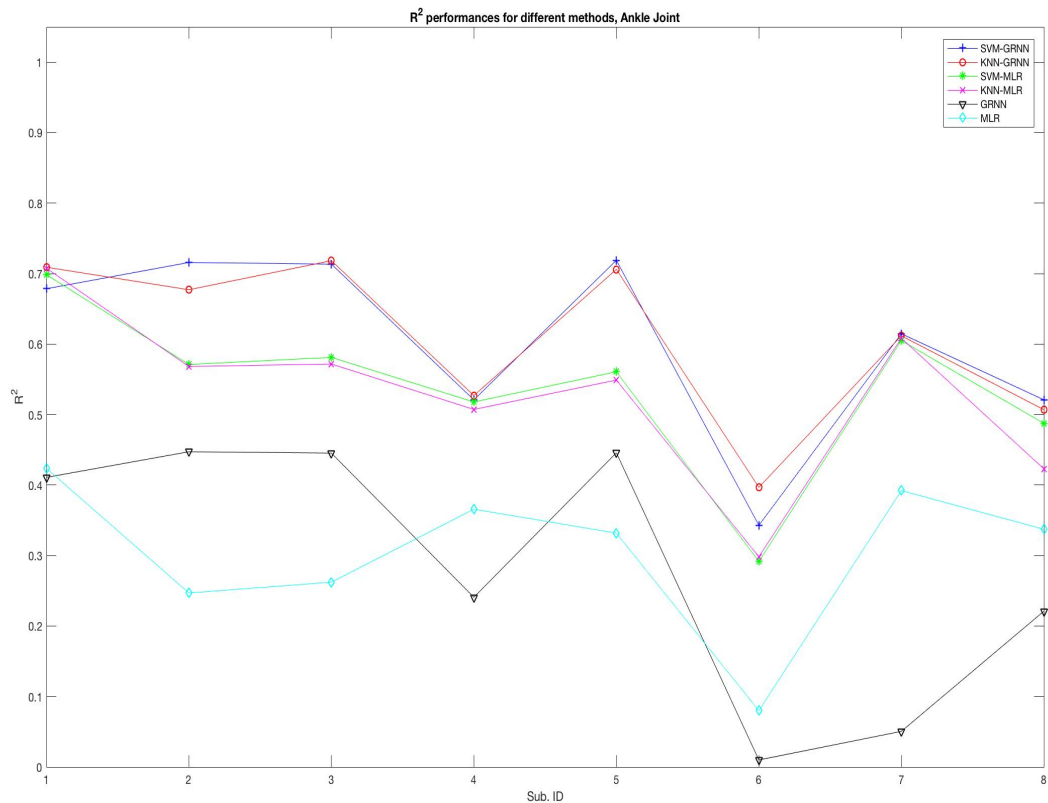


Figure 55: R^2 value trend for different models in 8 subjects, Ankle Joint

From Figure 55 it is evident that all the combined models demonstrate better performances with respect to the two general regressors. The improvement derived from the use of the combined approach in this case can be quantified in an increase of the R^2 values of about 0.27 in average for all the subjects.

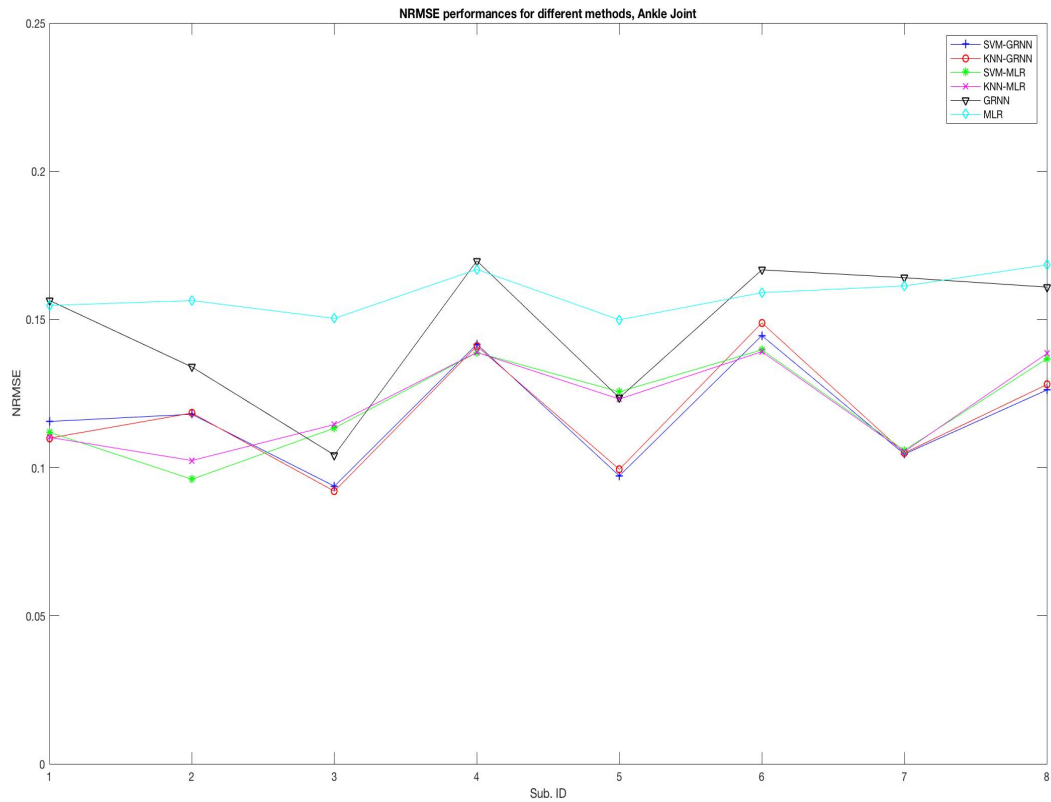


Figure 56: NRMSE value trend for different models in 8 subjects, Ankle Joint

This improving is less evident analysing the NRMSE, but it is possible to note that also in this case we have an overall decreasing (about 0.05 in average) of NRMSE values by using the combined approach.

For the sake of clarity, the reconstructed angle signals with all the different approaches relative to subject 7 are presented below (Figure 57).

From this figure we can see how the prediction with the combined models have an important improvement, in particular with SVM-GRNN and KNN-GRNN methods, where also the morphology of the signal is conserved. With the SVM-MLR and KNN-MLR there is also an improvement in terms of R^2 and NRMSE value with respect to GRNN and MLR models where the reconstruction is much more noisy. In fact both GRNN and MLR are not able to accurately reconstruct the gait movement, an error that is corrected with the combined approach. It is also clear that MLR models are not able to reach the angle peak points.

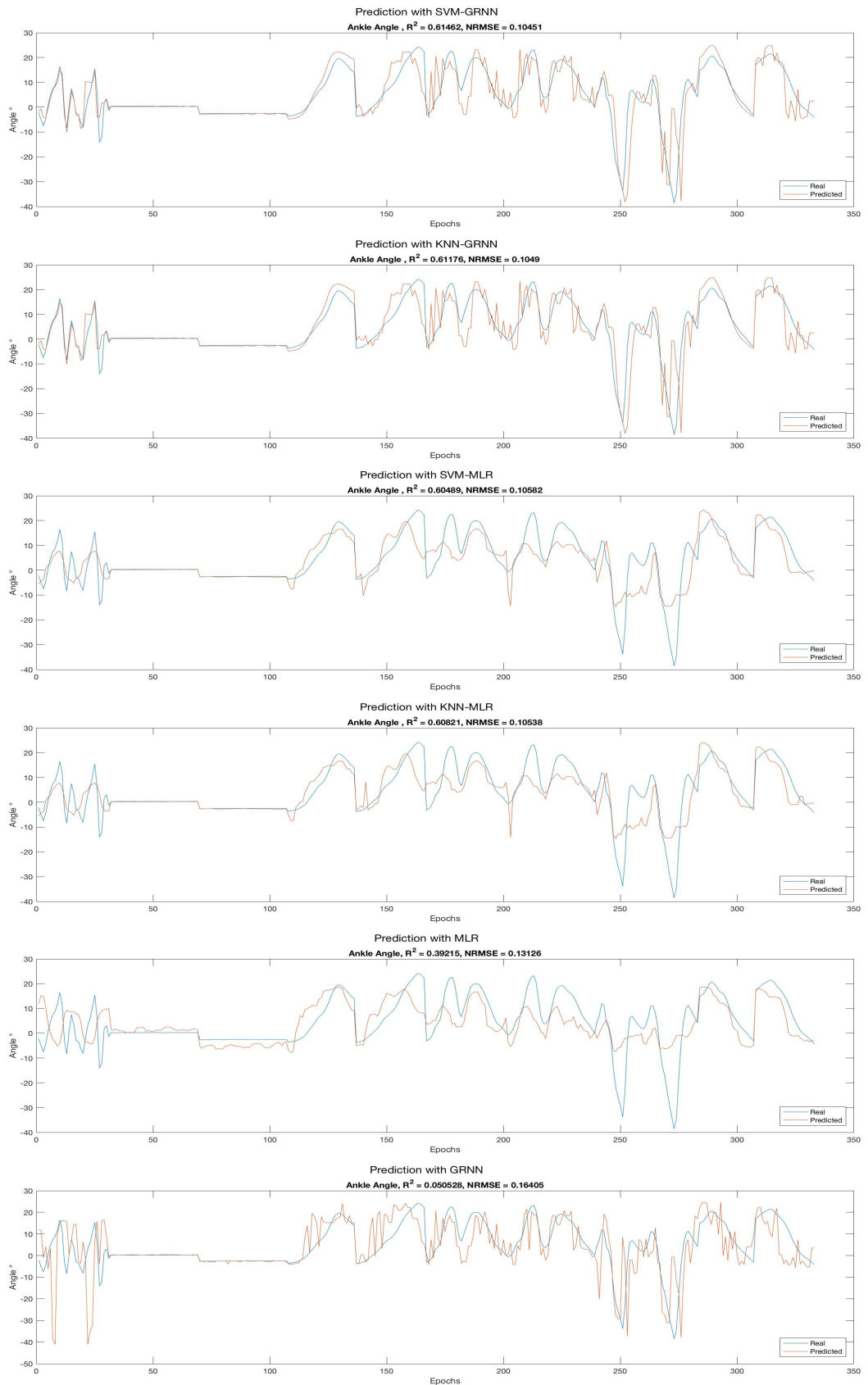


Figure 57: Ankle angle reconstruction in subjects 7 with different models. From top to bottom: SVM-GRNN, KNN-GRNN, SVM-MLR, KNN-MLR, MLR and GRNN

STATISTICAL ANALYSIS

What is qualitatively seen in the previous sections, it has been quantitatively confirmed by the statistical analysis performed with a one-way ANOVA using R^2 values. The result of the test is that, comparing all the six methods, the null hypothesis is refused ($p < 0.05$) and then the difference between the groups means are significant. In order to see the differences between the combined and standard approach, a Tukey-Kramer multiple comparison post-hoc test was performed (Table 3).

Multiple comparison test	GRNN	MLR
SVM-GRNN	$p < 0.01$	$p < 0.01$
KNN-GRNN	$p < 0.01$	$p < 0.01$
SVM-MLR	$p < 0.01$	$p < 0.05$
KNN-MLR	$p < 0.05$	$p < 0.05$

Table 3: First Method, Ankle joint: Tukey-Kramer multiple comparison test. p-values of the pairwise comparison between combined methods and general regressors

This test revealed that all the combined models are significantly better ($p < 0.05$) than both GRNN and MLR models, and this confirms the thesis that using the combined approach can lead to better results in terms of prediction accuracy. The table below (Table 4) mean and standard deviation of the R^2 values on the 8 subjects are reported in order to have the possibility of comparison among the methods.

R^2	SVM-GRNN	KNN-GRNN	SVM-MLR	KNN-MLR	GRNN	MLRR
Mean	0.6032	0.6066	0.5392	0.5291	0.2839	0.3050
STD	0.1338	0.1184	0.1179	0.1235	0.1814	0.1089

Table 4: First Method, Ankle joint: R^2 Mean and Standard deviation values of the six methods predictions

From this table it is possible to see that SVM-GRNN and KNN-GRNN are substantially equivalent and are the most performing methods for ankle angle reconstruction. Statistical analysis performed with NRMSE confirms the same results.

5.4.3 Knee angle predictions

The trend of the performances of prediction in terms of R^2 and NRMSE values with all the models among the 8 subjects is reported respectively in Figures 58 and 59.

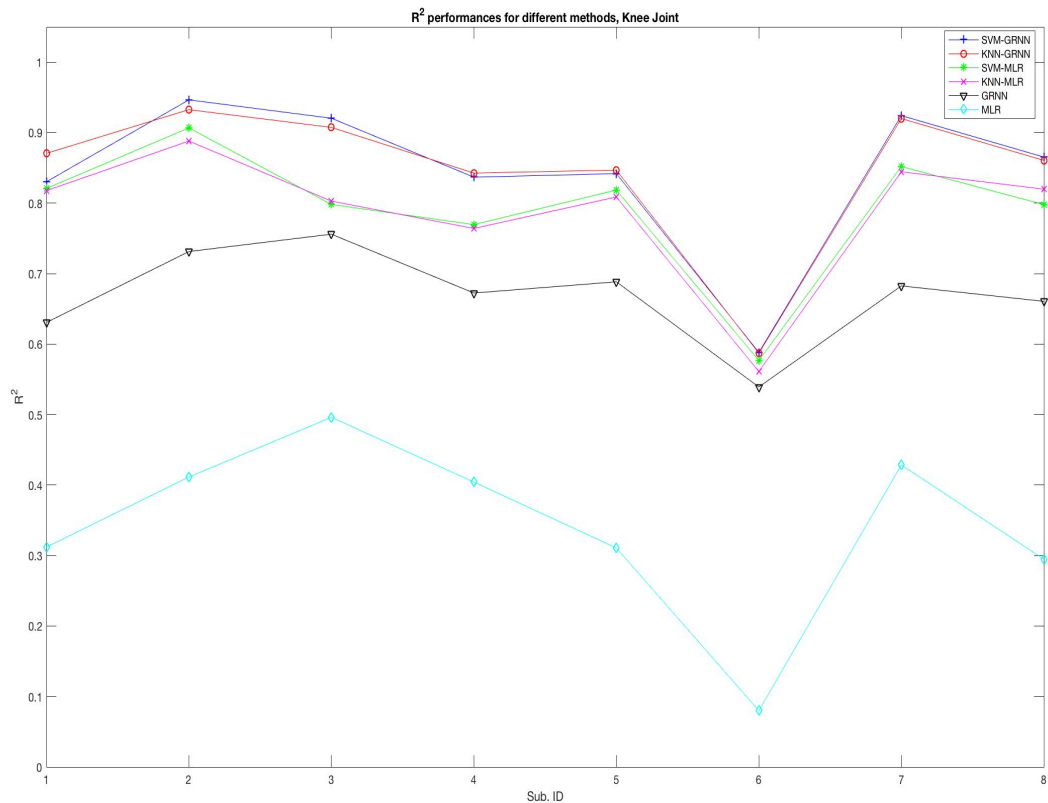


Figure 58: R^2 value trend for different models in 8 subjects, Ankle Joint

From Figure 58 it is evident that, also in this case, all the combined models demonstrate better performances with respect to the two general regressors. The improvement derived from the use of the combined approach in this case can be quantified in an increase of the R^2 values of about 0.31 in average for all the subjects.

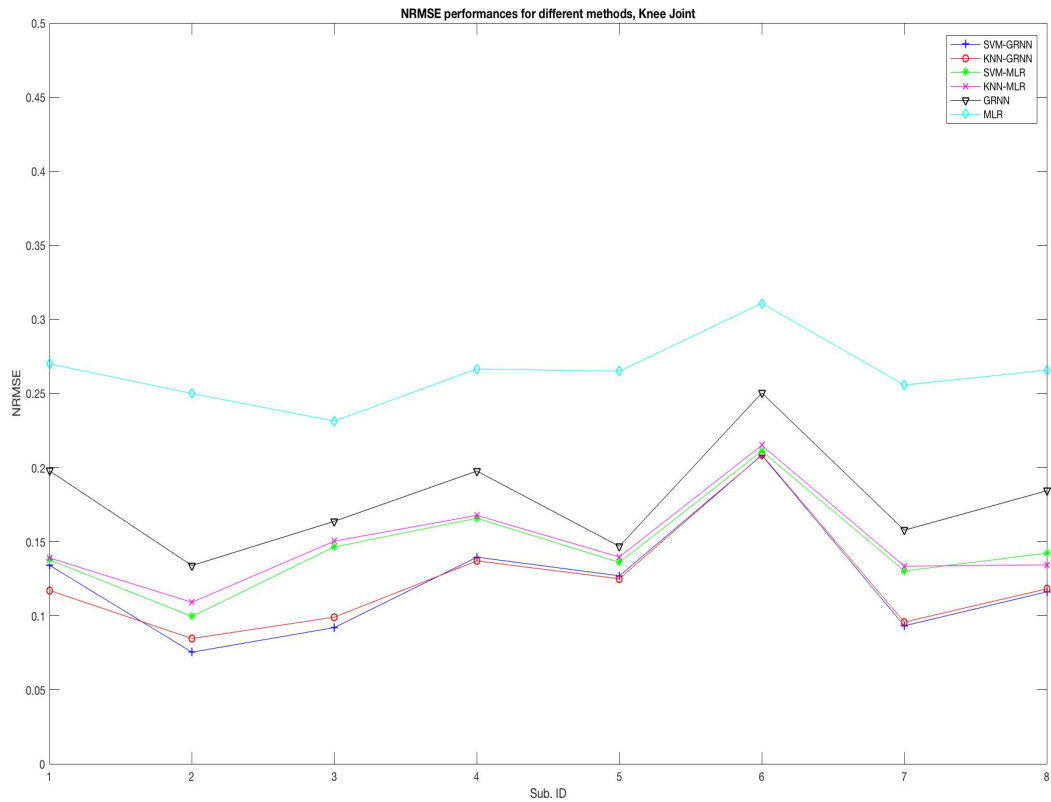


Figure 59: NRMSE value trend for different models in 8 subjects, Ankle Joint

This improvement is evident also by analyzing NRMSE trends, and it is possible to note that also in this case we have an overall decreasing (about 0.08 in average) of NRMSE values by using the combined approach.

For the sake of clarity, the reconstructed angle signals with all the different approaches relative to subject 7 are presented below (Figure 60).

From this figure we can see how the prediction with the combined models have an ingent improvement, in particular with SVM-GRNN and KNN-GRNN methods. With the SVM-MLR and KNN-MLR there is also an improvement in terms of R^2 and NRMSE values with respect to GRNN and MLR models where the reconstruction is much more noisy. The improvement in this case is more evident with respect to ankle joint, and it is possible to see that the error in prediction made with the general regressors are corrected with the combined approach: the prediction is smoother and it is more reliable to the measured angles.

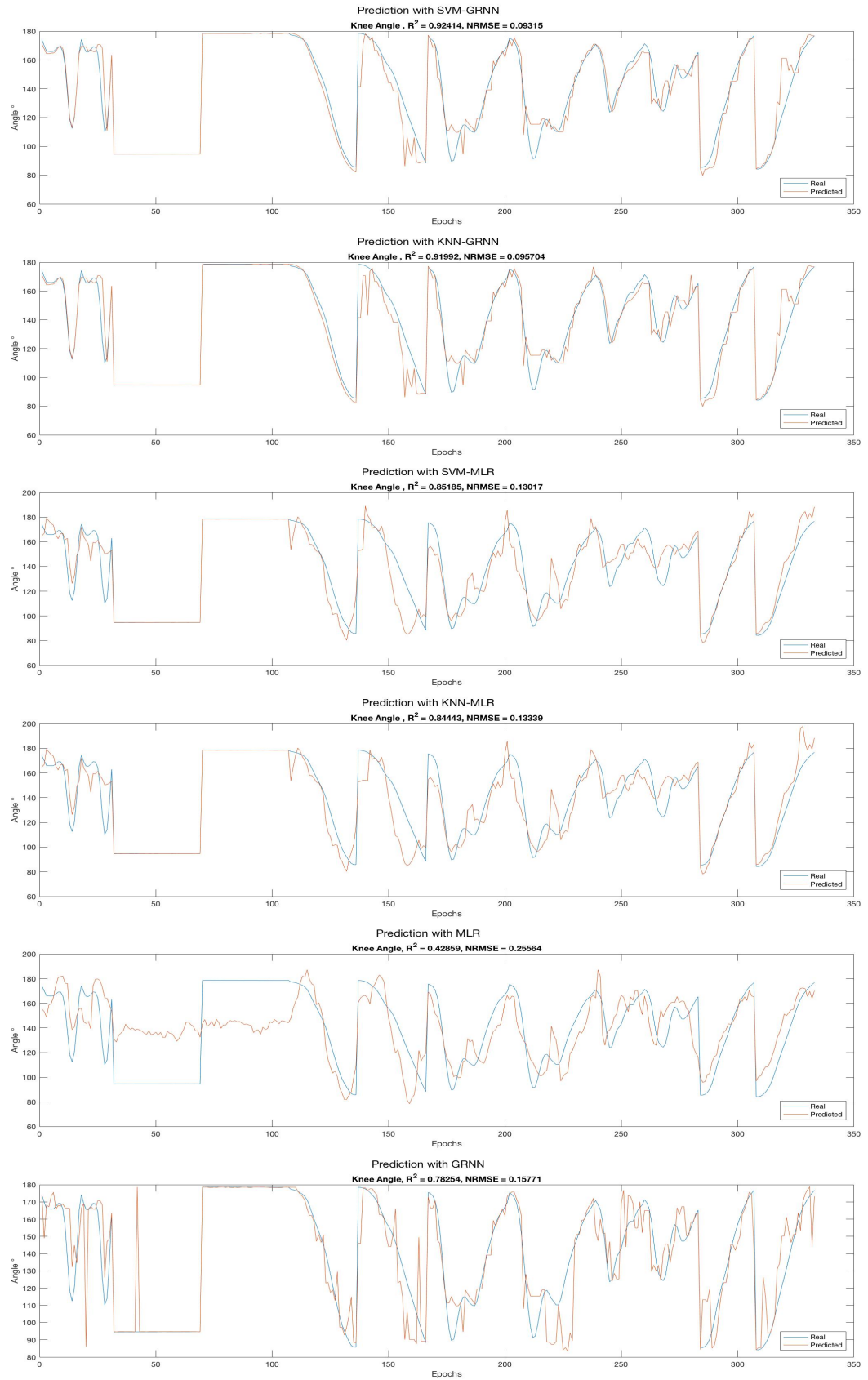


Figure 60: Knee angle reconstruction in subjects 7 with different models. From top to bottom: SVM-GRNN, KNN-GRNN, SVM-MLR, KNN-MLR, MLR and GRNN

STATISTICAL ANALYSIS

It has been quantitatively confirmed by the statistical analysis performed with a one-way ANOVA using R^2 values that, comparing all the six methods, the null hypothesis is refused ($p < 0.05$) and then the difference between the groups means are significant. In order to see the differences between the combined and standard approach, a Tukey-Kramer multiple comparison post-hoc test was performed (Table 5).

Multiple comparison test	GRNN	MLR
SVM-GRNN	$p < 0.05$	$p < 0.01$
KNN-GRNN	$p < 0.05$	$p < 0.01$
SVM-MLR	0.1917	$p < 0.01$
KNN-MLR	0.2228	$p < 0.01$

Table 5: First Method, Knee joint: Tukey-Kramer multiple comparison test. p-values of the pairwise comparison between combined methods and general regressors

This test revealed that SVM-GRNN and KNN-GRNN are significantly better ($p < 0.05$) than both GRNN and MLR models, and this confirms the thesis that using the combined approach can lead to better results in terms of prediction accuracy. SVM-MLR and KNN-MLR instead are significantly better ($p < 0.05$) than MLR model, while the statistical difference with the GRNN model is not significant in this test even if the average R^2 values (see Table 6) for these two models on all the 8 subjects (0.7925 for SVM-MLR and 0.7883 for KNN-MLR) are higher than the GRNN one (0.6701).

R^2	SVM-GRNN	KNN-GRNN	SVM-MLR	KNN-MLR	GRNN	MLRR
Mean	0.8442	0.8459	0.7925	0.7883	0.6701	0.3422
STD	0.1127	0.1099	0.0965	0.0984	0.0659	0.1269

Table 6: First Method, Knee joint: R^2 Mean and Standard deviation values of the six methods predictions

Also in this case it is possible to state that SVM-GRNN and KNN-GRNN are equivalent and significantly are the best models for knee angle prediction in this study. Statistical analysis performed with NRMSE confirms the same results.

5.5 Validation - Second method

In this section the results coming from the second validation method are presented. It is reminded that in this phase the movements are performed by the subject in a unique task, then all the trials are segmented in order to eliminate the transition phases and then concatenated. Firstly the classification by the two classifiers is performed and then the output (the class prediction) is used to trigger the class-specialized regressor in order to perform the prediction. Four different combination of classifier-regressor are tested (SVM-GRNN, KNN-GRNN, SVM-MLR, KNN-MLR) and their performances in prediction on the concatenated movements are compared to the performances of the general regressors (GRNN-MLR). This phase is repeated for the two degrees of freedom. A statistical analysis with one-way ANOVA and a post-hoc Tukey-Kramer test is then performed in order to study the statistical significance of the results.

5.5.1 Classification

The results of the classification are presented for both the KNN and SVM classifiers (Figure 61 and Figure 62).

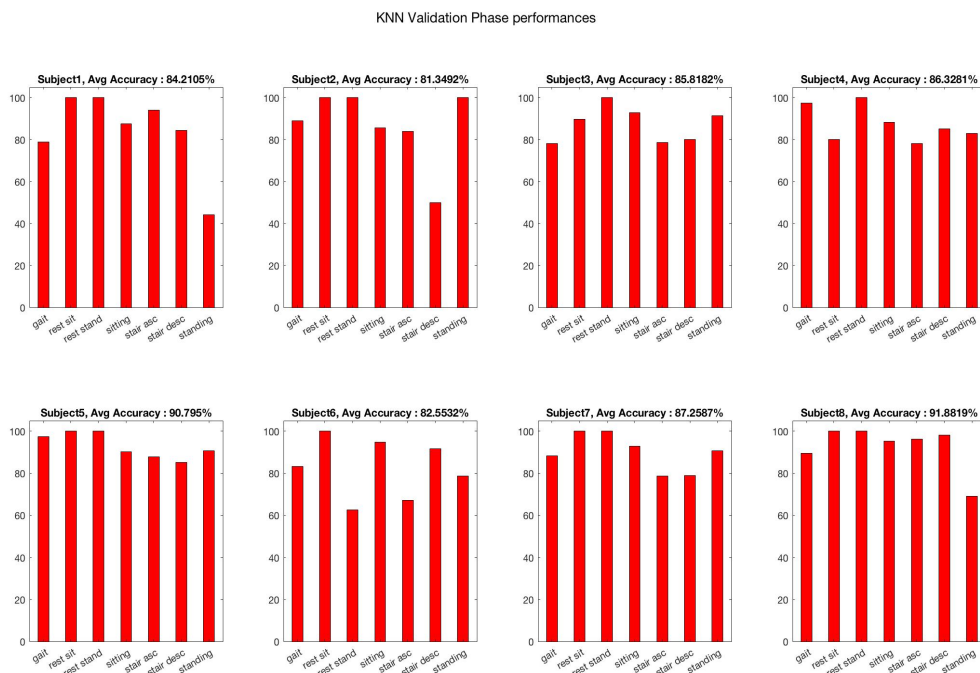


Figure 61: Bar diagram with KNN validation accuracy values for each class in 8 subjects

The performances for KNN results (Figure 53) less robust than the first method ones: except for subject 5 and 8 with an average classification accuracy over 90%, for the other subjects the average accuracy is in the range 81%-87%, a result that can be still considered acceptable because not all the classes are misclassified. Analyzing more deeply, it can be noted that the classes that has the lowest accuracy rate are *Standing* and *Stair Ascending*. The most of the misclassification errors are between this two classes and in some cases (Subject 6) between the *Rest* tasks: this can be due to a subject that is not in total relax, but probably there is residual activation coming from the previous movement because the tasks are performed consequently.

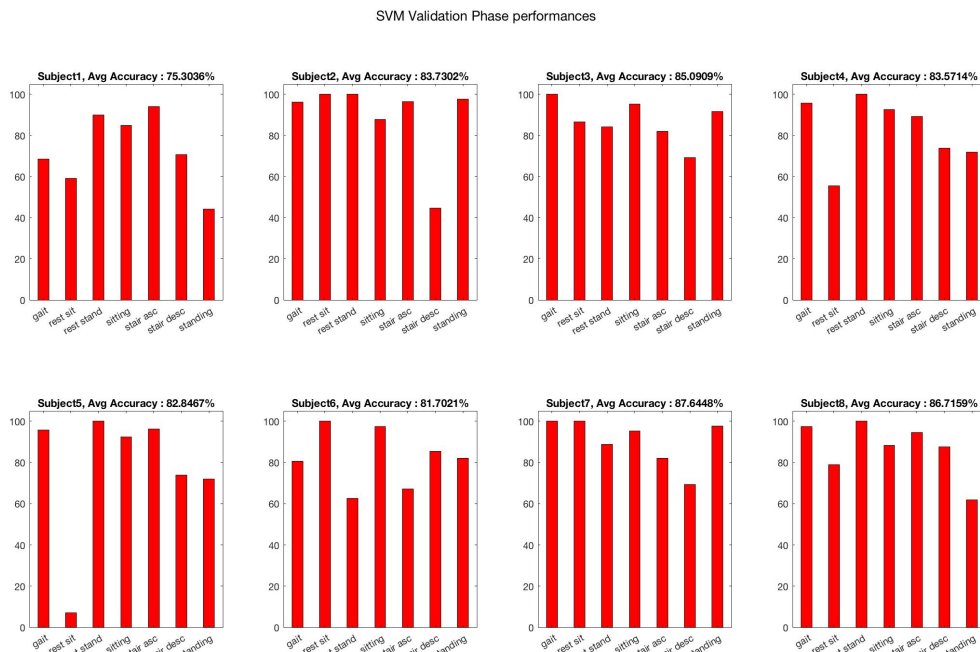


Figure 62: Bar diagram with KNN validation accuracy values for each class in 8 subjects

For what concerns SVM, it is possible to note that this type of classifier is less stable for a dynamic task with respect to KNN. The average accuracies are lower than KNN ones for each subject, and spans in the range 81%-87%. There are some classes that are less misclassified, like *Gait* and *Sitting* with peaks of class accuracy over 93%. The most of misclassification errors comes from the same classes of KNN case, and can be explained by the modality of execution of the task, which is different from the modality of training.

5.5.2 Ankle angle predictions

The trend of the performances of prediction in terms of R^2 and NRMSE values with all the models among the 8 subjects is reported respectively in Figures 63 and 64.

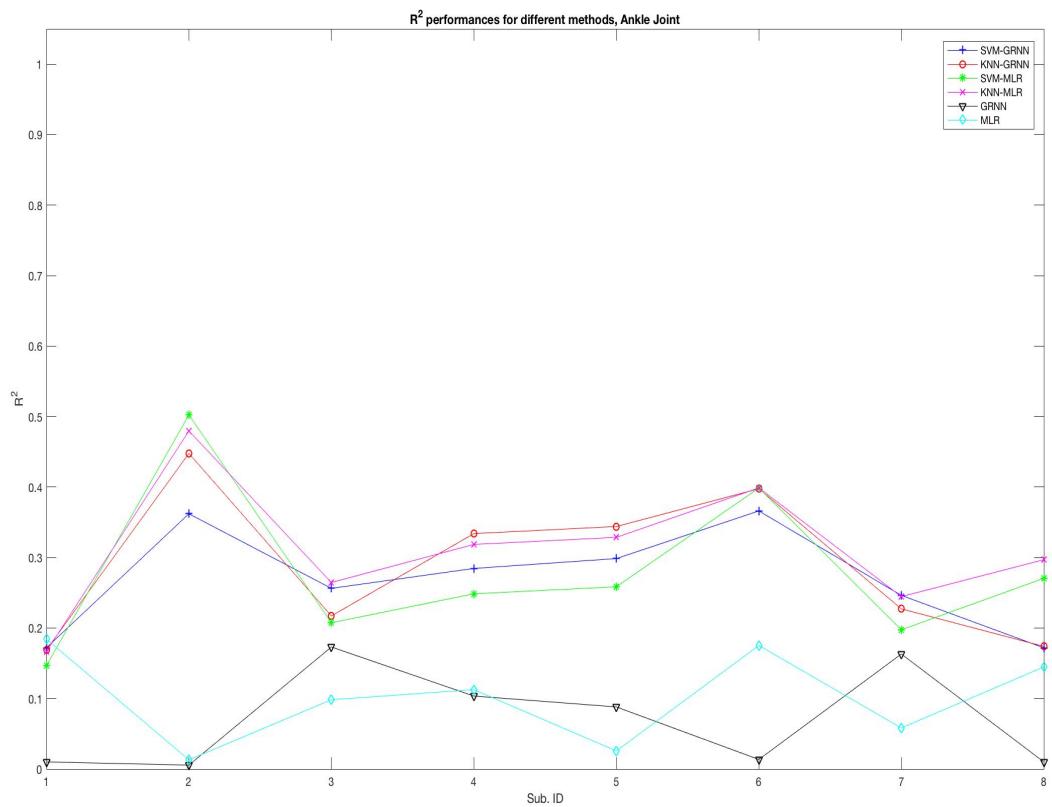


Figure 63: R^2 value trend for different models in 8 subjects, Ankle Joint

From Figure 55 it is evident that, also in this case, all the combined models demonstrate better performances with respect to the two general regressors, even if the overall quality of prediction is decreased with respect to the first validation method.

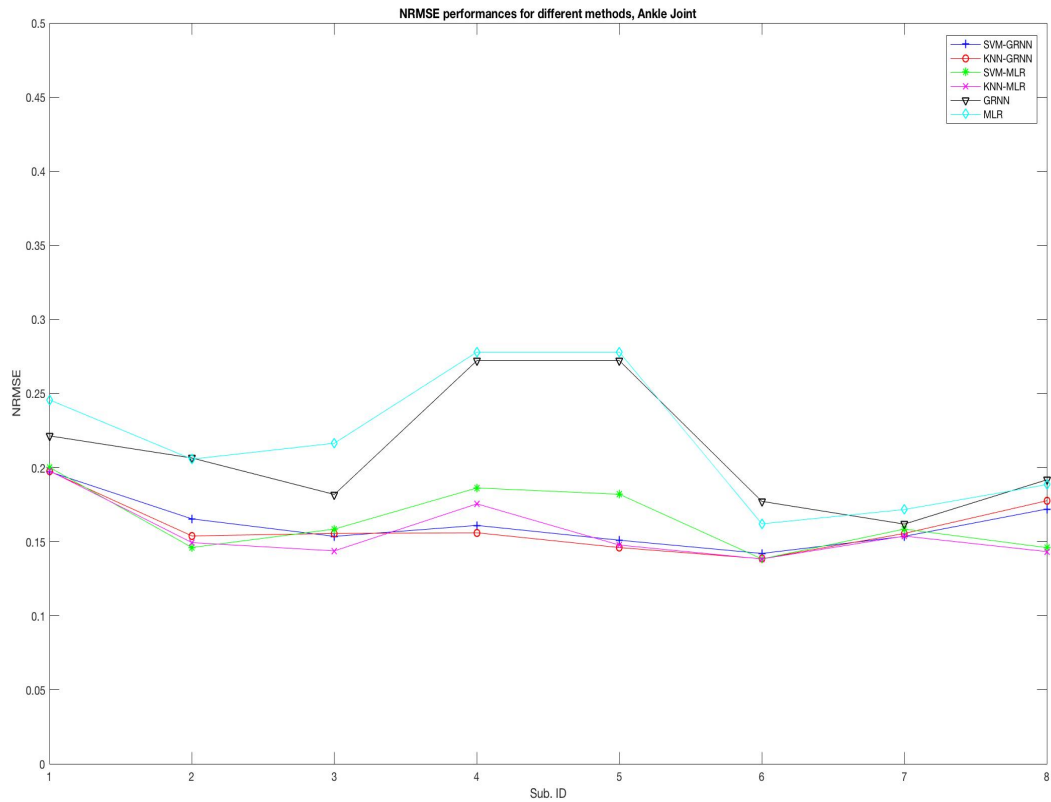


Figure 64: NRMSE value trend for different models in 8 subjects, Ankle Joint

This improvement is also evident analyzing the NRMSE, and it is possible to note that in this case we have an overall decreasing of NRMSE values by using the combined approach, in particular with subjects 4 and 5.

For the sake of clarity, the reconstructed angle signals with all the different approaches relative to subject 7 are presented below (Figure 65).

From this figure we can see that the quality of reconstruction is not as good as the previous case of validation (Figure 57), but it is possible to note that the prediction with the combined models have in any case a slight improvement, in particular with SVM-GRNN and KNN-GRNN methods. With the SVM-MLR and KNN-MLR there is also an improvement in terms of R^2 and NRMSE value with respect to GRNN and MLR models even if the reconstruction is not robust to the morphology of the angle signal.

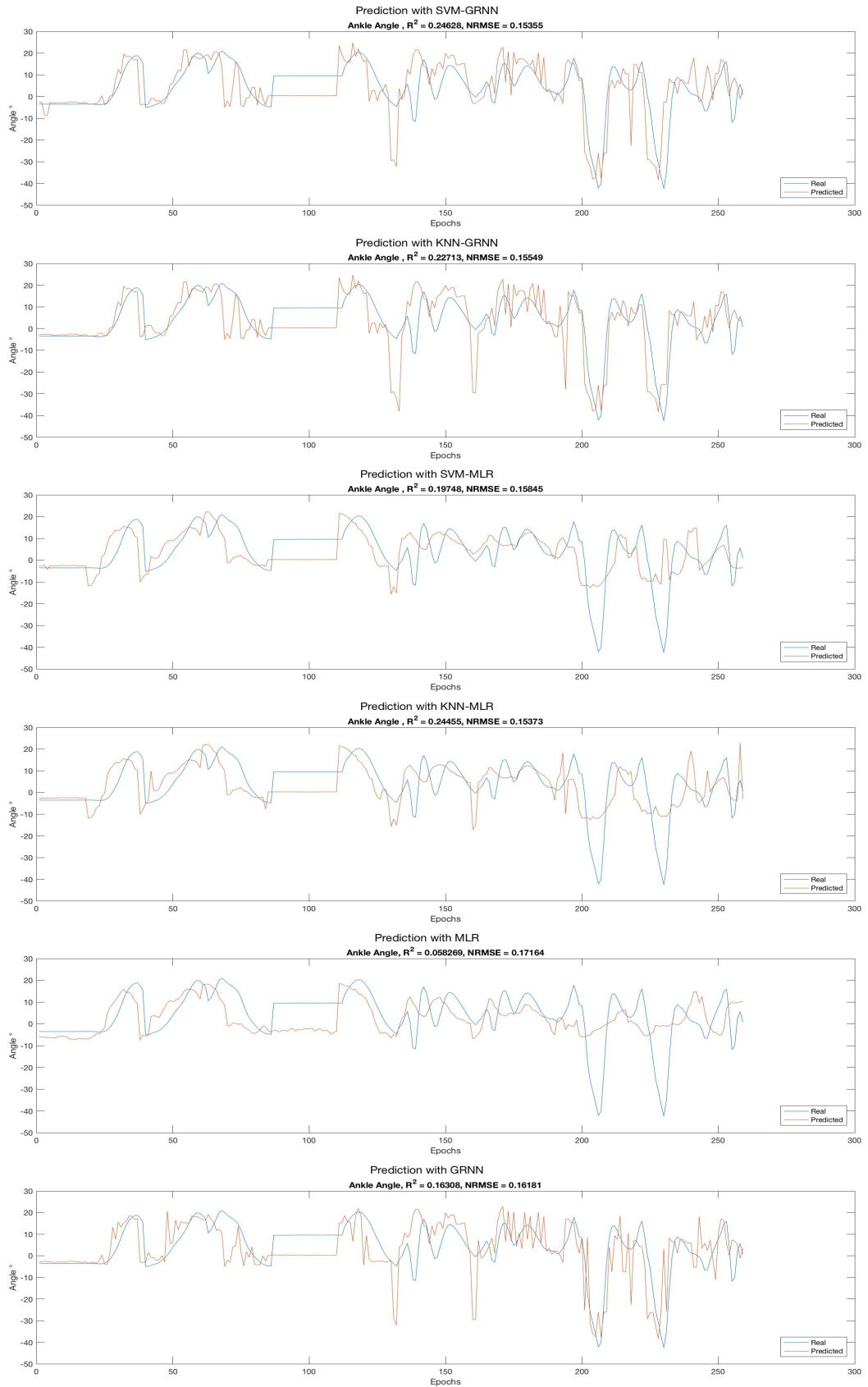


Figure 65: Ankle angle reconstruction in subjects 7 with different models. From top to bottom: SVM-GRNN, KNN-GRNN, SVM-MLR, KNN-MLR, MLR and GRNN

STATISTICAL ANALYSIS

It has been quantitatively confirmed by the statistical analysis performed with a one-way ANOVA using R^2 values that, comparing all the six methods, the null hypothesis is refused ($p < 0.05$) and then the difference between the groups means are significant. In order to see the differences between the combined and standard approach, a Tukey-Kramer multiple comparison post-hoc test was performed (Table 7).

Multiple comparison test	GRNN	MLR
SVM-GRNN	$p < 0.01$	$p < 0.05$
KNN-GRNN	$p < 0.01$	$p < 0.05$
SVM-MLR	$p < 0.01$	$p < 0.05$
KNN-MLR	$p < 0.01$	$p < 0.01$

Table 7: Second Method, Ankle joint: Tukey-Kramer multiple comparison test. p -values of the pairwise comparison between combined methods and general regressors

This test revealed that all the combined methods are significantly better ($p < 0.05$) than both GRNN and MLR models. In Table 8, R^2 mean and standard deviation values of the six models are reported.

R^2	SVM-GRNN	KNN-GRNN	SVM-MLR	KNN-MLR	GRNN	MLRR
Mean	0.2697	0.2888	0.2788	0.3123	0.0708	0.1015
STD	0.0744	0.1060	0.1164	0.0957	0.0710	0.0652

Table 8: Second Method, Ankle joint: R^2 Mean and Standard deviation values of the six methods predictions

In this case, as it has been said before, the quality of reconstruction is not satisfying in any case, but it is possible to state that all the combined methods are equivalent and outperform the two non specialized regressors. Statistical analysis performed with NRMSE confirms the same results.

5.5.3 Knee angle predictions

The trend of the performances of prediction in terms of R^2 and NRMSE values with all the models among the 8 subjects is reported respectively in Figures 66 and 67.

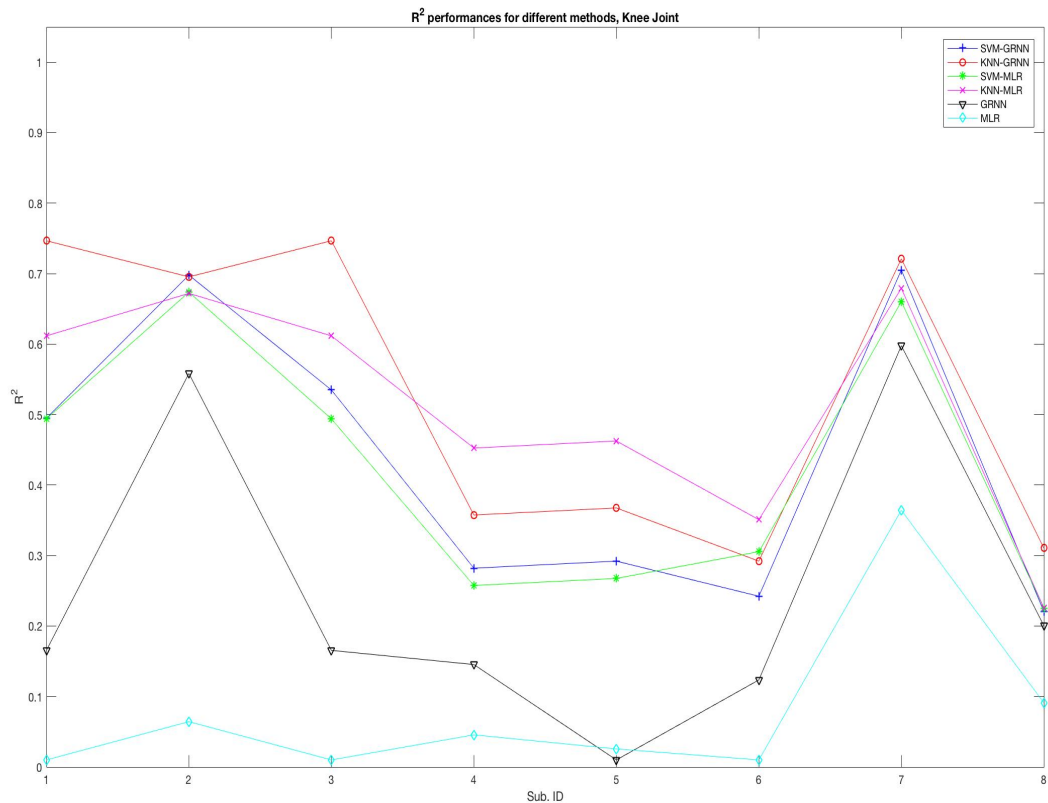


Figure 66: R^2 value trend for different models in 8 subjects, Ankle Joint

From Figure 66 it is evident that all the combined models demonstrate better performances with respect to the two general regressors. Also in this case we can note a decreasing in the accuracy of prediction with respect to the first validation method, due to the same reasons previously explained.

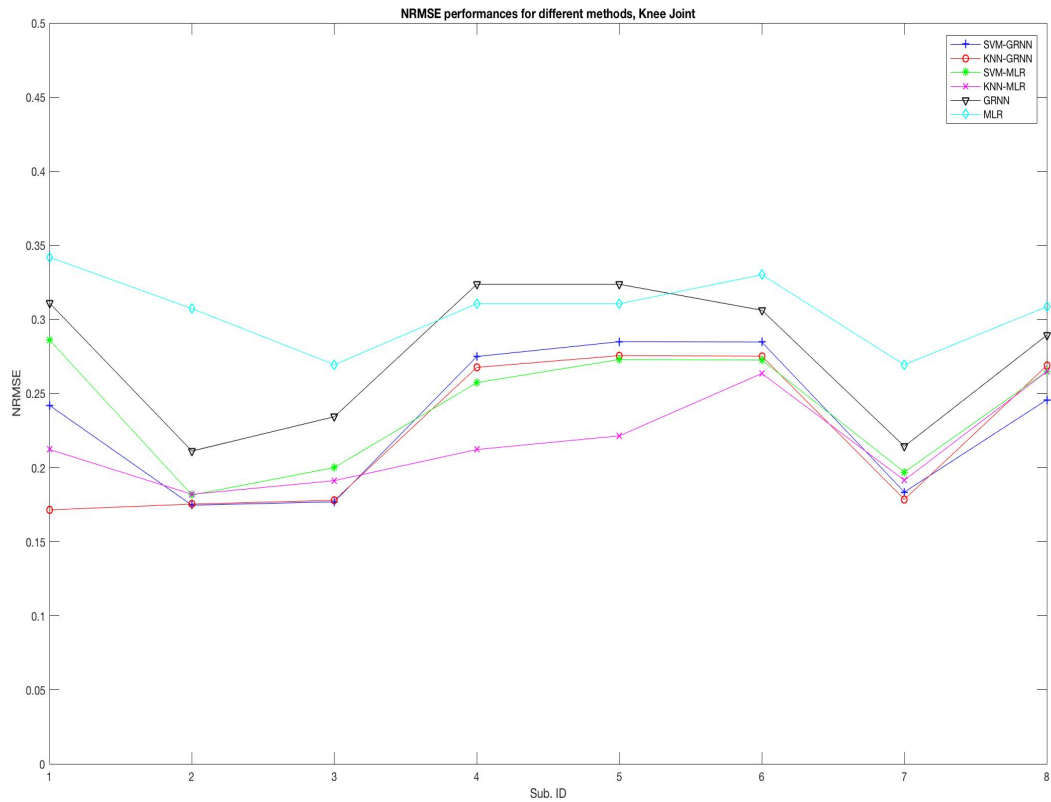


Figure 67: NRMSE value trend for different models in 8 subjects, Ankle Joint

This improvement is evident also by analyzing NRMSE trends, and it is possible to note that also in this case we have an overall decreasing of NRMSE values on all 8 subjects by using the combined approach.

For the sake of clarity, the reconstructed angle signals with all the different approaches relative to subject 7 are presented below (Figure 68).

From this figure we can see how the prediction with the combined models have an ingent improvement, in particular with SVM-GRNN and KNN-GRNN methods. With the SVM-MLR and KNN-MLR there is also an improvement in terms of R^2 and NRMSE values with respect to GRNN and MLR models where the reconstruction is much more noisy. In particular, it is interesting to note that there is an improvement in the prediction even if the classifier accuracy is lower. This is an evidence that this kind of approach has obviously a dependence from the classifier but it seems to be robust to misclassifications.

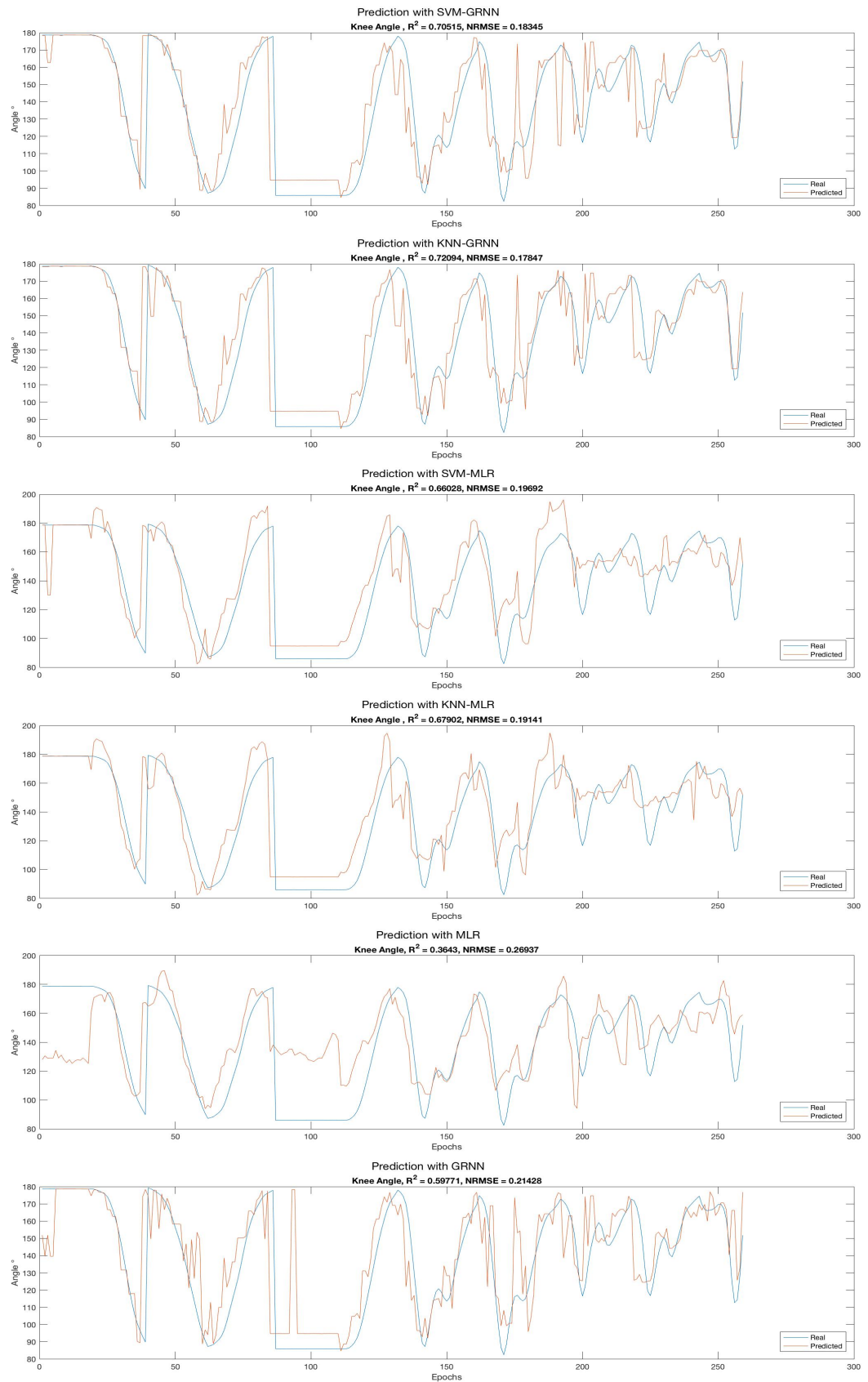


Figure 68: Knee angle reconstruction in subjects 7 with different models. From top to bottom: SVM-GRNN, KNN-GRNN, SVM-MLR, KNN-MLR, MLR and GRNN

STATISTICAL ANALYSIS

From one-way ANOVA using R^2 values, comparing all the six methods, the null hypothesis is refused ($p < 0.05$) and then the difference between the groups means are significant. In order to see the differences between the combined and standard approach, a Tukey-Kramer multiple comparison post-hoc test was performed (Table 9).

Multiple comparison test	GRNN	MLR
SVM-GRNN	0.3430	$p < 0.01$
KNN-GRNN	$p < 0.05$	$p < 0.01$
SVM-MLR	0.4190	$p < 0.01$
KNN-MLR	0.0711	$p < 0.01$

Table 9: Second Method, Knee joint: Tukey-Kramer multiple comparison test. p -values of the pairwise comparison between combined methods and general regressors

This test revealed that only KNN-GRNN is significantly better ($p < 0.05$) than both GRNN and MLR models, while all the combined models result significantly better than only MLR. However, from Table 10 it possible to see that in this study on 8 subjects, all the combined methods outperform the general regressors in terms of average R^2 values.

R^2	SVM-GRNN	KNN-GRNN	SVM-MLR	KNN-MLR	GRNN	MLRR
Mean	0.4337	0.5296	0.4222	0.5082	0.2458	0.0776
STD	0.2009	0.2133	0.1827	0.1635	0.2128	0.1195

Table 10: Second Method, Knee joint: R^2 Mean and Standard deviation values of the six methods predictions

From this table it is evident that the KNN-GRNN model is the one that has the best performances, and it is also the same that reveals statistical significance of the improvement. This confirms that the combined approach results more performing than the standard one. Statistical analysis performed with NRMSE confirms the same results.

5.6 Processing Time Analysis

In order to study the application of a combined approach for real-time control of an active prostheses or exoskeleton, a further analysis is performed in order to study if the processing time spent for a prediction is suitable for an online application. The time delay to extract a prediction from a window (epoch) is composed by: a delay for feature extraction, a delay for classification and a delay to make the prediction with the regressor. The results are summarized in Table 11.

(Time referred to analysis with MacBook Pro Retina with Intel Core i5 2.7 Ghz processor and 8Gb DDR3 RAM, using Matlab).

Delay (ms)	SVM-GRNN	KNN-GRNN	SVM-MLR	KNN-MLR
Feature extraction	2.5875	2.5875	2.6511	2.6511
Classification	0.087	0.0783	0.087	0.0783
Prediction	6.4977	6.4977	0.0436	0.0436
Total	9.1722	9.1635	2.7817	2.773

Table 11: Processing delays for angle prediction from an EMG epoch.

All the delays are below 10ms and this makes the combined approach suitable for real-time applications.

6 Conclusions and Future Work

6.1 Conclusion

An sEMG based control strategy that exploits combined information from pattern recognition and proportional myoelectric control methods for a lower limb exoskeleton control has been developed and test.

An experimental protocol has been developed for the recording of EMG signals and joint angle signal in a laboratory. This protocol contains guidelines to assure that recorded data sets are usable in the further work on pattern recognition and proportional control in order to have measures repeatability. The EMG signals are recorded using DuePro system with adhesive disposable bipolar electrodes, while for the angle signal two Biometrics Electrogoniometers are used in association with a DueBio probe in order to record ankle signal from knee and ankle joint. 7 different movements of activities of daily living (ADL) are taken into account: *gait, sitting down, standing up, stair ascending, stair descending, rest (standing position) and rest (sitting position)*. In order to study this movements, 8 lower limbs muscles are selected: TA, GL and GM that are mainly responsible to actuate the ankle joint movements while RF, VL, VM, BF and ST are associated to knee joint activity. The electrodes are positioned on this muscles following the SENIAM guidelines. The electrogoniometers placement instead is performed following the Biometrics Operating Manual. Eight able-bodied male subjects participated for the data collection procedure.

Four different combined model were tested: SVM-GRNN, KNN-GRNN, SVM-MLR and KNN-MLR. The performances of these models are then compared to two standard techniques of regression, i.e. GRNN and MLR.

The EMG signal in each trial is segmented using 250ms windows with 75% of overlap and a subset of six features (RMS, ZC, IEMG, WA, NT, WL) is used to characterize each window. This way constructed feature vector is used as input for SVM, KNN and GRNN models, while for the MLR only the LOG(VAR) feature is used.

Basically, two processes were conducted: a training and testing phase in order to find the best classifier and regressor models and a validation phase in order to analyze the performances of the different systems. After a tuning process to find the best classifier parameters for each subject, a Leave One Out Cross-Validation is performed on 10 trials of

the different movements and the classifier model that has the highest average accuracy on a cycle of the Cross-Validation is selected for performing the validation phase. This process is repeated for both KNN and SVM classifiers. Similarly, for the two models of regressors a LOOCV on the same 10 trials is performed and the model that has the highest R^2 value for each class reconstruction in a cycle of the cross-validation is selected for performing the validation phase. This process is repeated for both ankle and knee joints. The general regressors are instead trained using all the 10 trials.

The first validation method consisted on comparing the performances of the combined and standard models using two previously segmented trials for each movement. In this phase both the KNN and SVM classifiers has shown good accuracy in recognizing the movement (about 93% average accuracy on 8 subjects). For both ankle and knee joints the quality of angle prediction is improved ($p < 0.05$) using a the combined approach, in particular the best performances are registered with SVM-GRNN ($R^2 = 0.8442 \pm 0.1127$ and $NRMSE = 0.1232 \pm 0.0411$ for knee joint and $R^2 = 0.6032 \pm 0.1338$ and $NRMSE = 0.1176 \pm 0.0190$ for ankle joint) and KNN-GRNN ($R^2 = 0.8459 \pm 0.1127$ and $NRMSE = 0.1231 \pm 0.0385$ for knee joint and $R^2 = 0.6066 \pm 0.1184$ and $NRMSE = 0.1178 \pm 0.0201$ for ankle joint).

In the second validation method, the subject is asked to perform a sequence of movements in order to simulate a daily scenario. In this phase there is the evidence of a decreasing in the performances for both the classification and the prediction of the angles due to the different modality of movement execution. In particular it has been noted that the KNN classifier is slightly more robust than SVM in predicting a movement in a dynamic condition.

Nevertheless, also in this case the combined approach has better prediction performances ($p < 0.05$) with respect to the standard one, in particular KNN-GRNN model has demonstrated the highest quality of prediction ($R^2 = 0.5296 \pm 0.2133$ and $NRMSE = 0.2237 \pm 0.0514$ for knee joint and $R^2 = 0.2888 \pm 0.1060$ and $NRMSE = 0.1600 \pm 0.0188$ for ankle joint).

6.2 Future work

This section explains the interesting topics for future work on this field of study and the possibilities for making a real application for rehabilitation exoskeleton.

- **Improvement of the quality of regression.** From this study there is the evidence that the combined approach gives better performances than the standard one. Nevertheless, the results in terms of quality of prediction are not optimal and there is the need to improve the regression accuracy. One solution can be found in a different modality of training (like online or adaptive learning). One other important concern is the feature selection: it could also be an hypothesis that the extracted features are not the best in order to maximize the regressor performances. For that reason a work on feature extraction and selection for regressors models is suggested.
- **Improvement of the quality of the classifiers prediction in dynamic sequences of movements.** From the second validation method result, it has been shown that the classifiers had a slight decreasing in prediction accuracy due to the different condition of execution of movements. For that reason it is suggested to study more deeply the robustness of classification when the test set is taken in different conditions with respect to the training set. Also in this case an online learning approach is suggested.
- **Study of the transition phases between movements.** For a real-time application it is important to find a strategy in order to process the transition phases among different movements, giving the classifier robustness to changing signals and changing activation. One suggestion could be to study a post-processing of the class predictions based on the *majority vote*.
- **Implementation of the real-time control.** After all the improvements of the control strategy, the aim is then to implement the real-time control and first trying to control a virtual model before testing on an exoskeleton.
- **Exoskeleton control.** The first stage of the study is indeed the final control of the exoskeleton motors. It is also important to study the effect of the extracted control signal on the PID controllers of the exoskeleton and to find the better way to maximize the robustness of the system.

- **Application on not able-bodied subjects.** It is important to find out if this study could be suitable for subjects with reduced muscular activity (like post-stroke patients). In this way this strategy could be used for rehabilitation purposes.

References

- [1] L3-neurons. [Online]. Available: <https://droso4schools.wordpress.com/l3-neurons/>
- [2] Motor unit. [Online]. Available: <https://medical-dictionary.thefreedictionary.com/motor+unit>
- [3] J. Basmajian and C. De Luca, "Muscles alive — their functions revealed by electromyography," *The Anatomical Record*, vol. 147, no. 3, pp. 440–441. [Online]. Available: <https://onlinelibrary.wiley.com/doi/abs/10.1002/ar.1091470317>
- [4] D. Stashuk, "Emg signal decomposition: how can it be accomplished and used?" *Journal of Electromyography and Kinesiology*, vol. 11, no. 3, pp. 151 – 173, 2001. [Online]. Available: <http://www.sciencedirect.com/science/article/pii/S105064110000050X>
- [5] P. Geethanjali, "Myoelectric control of prosthetic hands: state-of-the-art review," *Medical Devices (Auckland, N.Z.)*, vol. 9, pp. 247–255, 2016.
- [6] M. S. S. AL-QURAIISHI, "Classification of ankle joint movements based on surface electromyography signal," Master's thesis, Universiti Putra Malaysia, 2015.
- [7] C. G. Riberholt, "Lokomat: Clinical training and experience in a neurorehabilitation hospital," in *Replace, Repair, Restore, Relieve – Bridging Clinical and Engineering Solutions in Neurorehabilitation*, W. Jensen, O. K. Andersen, and M. Akay, Eds. Cham: Springer International Publishing, 2014, pp. 137–138.
- [8] J. Veneman, R. Kruidhof, E. Hekman, R. Ekkelenkamp, E. van Asseldonk, and H. van der Kooij, "Design and evaluation of the lopes exoskeleton robot for interactive gait rehabilitation," *IEEE transactions on neural systems and rehabilitation engineering*, vol. 15, no. 3, pp. 379–386, 2007.
- [9] S. K. Banala, S. K. Agrawal, and J. P. Scholz, "Active leg exoskeleton (alex) for gait rehabilitation of motor-impaired patients," in *2007 IEEE 10th International Conference on Rehabilitation Robotics*, June 2007, pp. 401–407.

-
- [10] M. Bortole, A. Venkatakrishnan, F. Zhu, J. C. Moreno, G. E. Francisco, J. L. Pons, and J. L. Contreras-Vidal, "The h2 robotic exoskeleton for gait rehabilitation after stroke: early findings from a clinical study," *Journal of NeuroEngineering and Rehabilitation*, vol. 12, no. 1, p. 54, Jun 2015. [Online]. Available: <https://doi.org/10.1186/s12984-015-0048-y>
- [11] A. Wall, J. Borg, and S. Palmcrantz, "Clinical application of the hybrid assistive limb (hal) for gait training—a systematic review," *Frontiers in Systems Neuroscience*, vol. 9, p. 48, 2015. [Online]. Available: <https://www.frontiersin.org/article/10.3389/fnsys.2015.00048>
- [12] K. Englehart and B. Hudgins, "A robust, real-time control scheme for multifunction myoelectric control," *IEEE Trans Biomed Eng*, vol. 50, no. 7, pp. 848–854, Jul 2003.
- [13] C. J. C. Burges, "A tutorial on support vector machines for pattern recognition," *Data Min. Knowl. Discov.*, vol. 2, no. 2, pp. 121–167, Jun. 1998. [Online]. Available: <https://doi.org/10.1023/A:1009715923555>
- [14] F. Gran, "Pattern recognition using svm," Master's thesis, Matematikcentrum LTH, 2002.
- [15] (2018) k-nearest neighbors algorithm. [Online]. Available: https://en.wikipedia.org/wiki/K-nearest_neighbors_algorithm
- [16] (2018) Linear regression. [Online]. Available: https://en.wikipedia.org/wiki/Linear_regression
- [17] G. James, D. Witten, T. Hastie, and R. Tibshirani, *An Introduction to Statistical Learning: With Applications in R*. Springer Publishing Company, Incorporated, 2014.
- [18] J. L. G. Rosa, *Artificial Neural Networks*. IntechOpen, 2016.
- [19] R. P. Duin and T. C. Landgrebe, "Efficient multiclass roc approximation by decomposition via confusion matrix perturbation analysis," *IEEE Transactions on Pattern Analysis and Machine Intelligence*, vol. 30, pp. 810–822, 07 2007. [Online]. Available: [doi.ieeecomputersociety.org/10.1109/TPAMI.2007.70740](https://doi.org/10.1109/TPAMI.2007.70740)

-
- [20] B. Freriks and H. Hermens, "European Recommendations for Surface Electromyography: Results of the SENIAM Project," *Roessingh Research and Development*, 2000.
- [21] V. L. Feigin, C. M. Lawes, D. A. Bennett, S. L. Barker-Collo, and V. Parag, "Worldwide stroke incidence and early case fatality reported in 56 population-based studies: a systematic review," *The Lancet Neurology*, vol. 8, no. 4, pp. 355–369, 2018/07/13 2009.
- [22] R. Merletti and P. Parker, *Electromyography: Physiology, Engineering and Noninvasive Applications*. John Wiley & Sons, 2004.
- [23] F. Buchthal and H. Schmalbruch, "Motor unit of mammalian muscle." *Physiological Reviews*, vol. 60, no. 1, pp. 90–142, 1980, PMID: 6766557. [Online]. Available: <https://doi.org/10.1152/physrev.1980.60.1.90>
- [24] H. Elwood and M. L. M., *Functional Organization of Motoneuron Pool and its Inputs*. American Cancer Society, 2011, pp. 423–507. [Online]. Available: <https://onlinelibrary.wiley.com/doi/abs/10.1002/cphy.cp010211>
- [25] R. Merletti and D. Farina, "Analysis of intramuscular electromyogram signals," *Philosophical Transactions of the Royal Society A: Mathematical, Physical and Engineering Sciences*, vol. 367, no. 1887, pp. 357–368, 2009.
- [26] H. He and K. Kiguchi, "A study on emg-based control of exoskeleton robots for human lower-limb motion assist," in *2007 6th International Special Topic Conference on Information Technology Applications in Biomedicine*, Nov 2007, pp. 292–295.
- [27] M. Oskoei and H. Hu, "Myoelectric control systems - a survey," vol. 2, 10 2007.
- [28] J. He, D. Zhang, X. Sheng, and X. Zhu, "Effects of long-term myoelectric signals on pattern recognition," in *Intelligent Robotics and Applications*, J. Lee, M. C. Lee, H. Liu, and J.-H. Ryu, Eds. Berlin, Heidelberg: Springer Berlin Heidelberg, 2013, pp. 396–404.
- [29] H. V. A. Hakonen, Maria; Piitulainen, "Current state of digital signal processing in myoelectric interfaces and related applications," pp. 334–359, 2015. [Online]. Available: <http://urn.fi/URN:NBN:fi:aalto-201503112032>

-
- [30] B. S. Rupal, S. Rafique, A. Singla, E. Singla, M. Isaksson, and G. S. Virk, "Lower-limb exoskeletons: Research trends and regulatory guidelines in medical and non-medical applications," *International Journal of Advanced Robotic Systems*, vol. 14, no. 6, p. 1729881417743554, 2017.
- [31] G. A. Lichtwark, K. Bougoulias, and A. M. Wilson, "Muscle fascicle and series elastic element length changes along the length of the human gastrocnemius during walking and running," *J Biomech*, vol. 40, no. 1, pp. 157–164, 2007.
- [32] X. Xi, M. Tang, S. M. Miran, and Z. Luo, "Evaluation of Feature Extraction and Recognition for Activity Monitoring and Fall Detection Based on Wearable sEMG Sensors," *Sensors (Basel)*, vol. 17, no. 6, May 2017.
- [33] L. H. Smith, L. J. Hargrove, B. A. Lock, and T. A. Kuiken, "Determining the optimal window length for pattern recognition-based myoelectric control: balancing the competing effects of classification error and controller delay," *IEEE Trans Neural Syst Rehabil Eng*, vol. 19, no. 2, pp. 186–192, Apr 2011.
- [34] A. Phinyomark, P. Phukpattaranont, and C. Limsakul, "Feature reduction and selection for EMG signal classification," *Expert Systems with Applications*, 2012.
- [35] R. Boostani and M. H. Moradi, "Evaluation of the forearm EMG signal features for the control of a prosthetic hand," *Physiol Meas*, vol. 24, no. 2, pp. 309–319, May 2003.
- [36] B. Hudgins, P. Parker, and R. N. Scott, "A new strategy for multifunction myoelectric control," *IEEE Trans Biomed Eng*, vol. 40, no. 1, pp. 82–94, Jan 1993.
- [37] R. Merletti, "Standards for reporting EMG data," *Journal of Electromyography and Kinesiology*, 1996.
- [38] J. M. Hahne, F. Biessmann, N. Jiang, H. Rehbaum, D. Farina, F. C. Meinecke, K. R. Muller, and L. C. Parra, "Linear and nonlinear regression techniques for simultaneous and proportional myoelectric control," *IEEE Trans Neural Syst Rehabil Eng*, vol. 22, no. 2, pp. 269–279, Mar 2014.
- [39] C.-W. Hsu, C.-C. Chang, and C.-J. Lin, "A Practical Guide to Support Vector Classification," *National Taiwan University*, 2016.

-
- [40] H. Byun and S.-W. Lee, “Applications of support vector machines for pattern recognition: A survey,” in *Proceedings of the First International Workshop on Pattern Recognition with Support Vector Machines*, ser. SVM '02. London, UK, UK: Springer-Verlag, 2002, pp. 213–236. [Online]. Available: <http://dl.acm.org/citation.cfm?id=647230.719394>
- [41] Kressel and Ulrich, *Advances in Kernel Methods*. Cambridge, MA, USA: MIT Press, 1999, ch. Pairwise Classification and Support Vector Machines, pp. 255–268. [Online]. Available: <http://dl.acm.org/citation.cfm?id=299094.299108>
- [42] Y. Ma and G. Guo, *Support Vector Machines Applications*. Springer Publishing Company, Incorporated, 2014.
- [43] C.-C. Chang and C.-J. Lin, “Libsvm: A library for support vector machines,” *ACM Trans. Intell. Syst. Technol.*, vol. 2, no. 3, pp. 27:1–27:27, May 2011. [Online]. Available: <http://doi.acm.org/10.1145/1961189.1961199>
- [44] A. C. Rencher and W. F. Christensen, *Methods of Multivariate Analysis.*, 3rd ed., ser. Wiley series in probability and statistics. Hoboken, New Jersey :: Wiley,, [2012], includes Appendix, Index and Reference.
- [45] D. Specht, “A General Regression Neural Network,” *IEEE transactions on Neural Networks*, 1991.